AD-757 220

SIGNAL PROCESSING STUDY OF IMPULSE
EXCITED OBJECTS IN SPACE

V. C. Martins, et al

Braddock, Dunn and McDonald, Incorporated

Prepared for:

Rome Air Development Center

January 1973
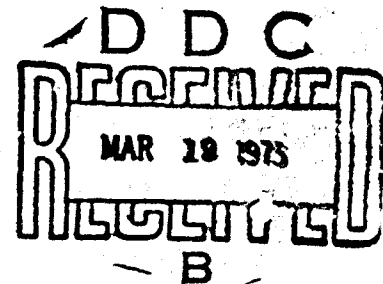
AD757220

RADC-TR-72-347
Final Technical Report
January 1973

SIGNAL PROCESSING STUDY OF IMPULSE EXCITED OBJECTS IN SPACE

Braddock, Dunn and McDonald, Inc.

Approved for public release;
distribution unlimited.

DDC

R E C E I V E D
MAR 19 1973

— B —

Rome Air Development Center
Air Force Systems Command
Griffiss Air Force Base, New York

243

DOCUMENT CONTROL DATA - R & D

(Security classification of title, body of abstract and indexing annotation must be entered when the overall report is classified)

1 ORIGINATING ACTIVITY (Corporate author)	2a. REPORT SECURITY CLASSIFICATION
Braddock, Dunn and McDonald, Inc. 8027 Leesburg Pike McLean, Virginia 22101	UNCLASSIFIED
	2b. GROUP N/A

3 REPORT TITLE

SIGNAL PROCESSING STUDY OF IMPULSE EXCITED OBJECTS IN SPACE

4 DESCRIPTIVE NOTES (Type of report and inclusive dates)

Final Report   June 1971 - September 1972

5 AUTHOR(S) (First name, middle initial, last name)

V.C. Martins
J. VanMeter

6 REPORT DATE	7a. TOTAL NO. OF PAGES	7b. NO. OF REFS
January 1973	230 243	14

8a. CONTRACT OR GRANT NO.	9a. ORIGINATOR'S REPORT NUMBER(S)
F30602-71-C-0158 Job Order No. 45060186	BDM/W-TR72-094
	9b. OTHER REPORT NO(S) (Any other numbers that may be assigned this report) RADC-TR-72-347

10 DISTRIBUTION STATEMENT

Approved for public release; distribution unlimited.

11. SUPPLEMENTARY NOTES	12. SPONSORING MILITARY ACTIVITY
RADC PROJECT ENGINEER: Paul VanEtten (OCTS) AC 315 330-4306	Rome Air Development Center (OCTS) Griffiss Air Force Base, New York 13441

13. ABSTRACT

This report contains the results of an investigation of optimum techniques for detecting and discriminating backscattered electromagnetic radiation associated with the impulse radar concept. The study reported herein is divided into three areas of investigation. The first of these is a study of backscatter in which several waveform variations for the sphere, rectangular plate, and thin rod geometries were developed in an effort to determine mathematically tractable expressions for the scattered energy from typical geometrical shapes. This section consists essentially of a definition of the tools which are used in the bulk of the report. The second part of this program involved the development of several optimal-like filter configurations based upon a knowledge of the characteristics of the waveforms of interest. Employing the waveforms developed in the first section of the study, each filter was studied for its enhancement of the output-to-input signal-to-clutter ratio as a function of the target to clutter size ratio. The double integrated-matched filter configuration, which was found to be an optimum one for the conditions of interest, was also investigated for its enhancement of target-to-clutter ratios with a typical rain environment. Finally, the geometry identification problem was investigated in the third section. A system was postulated for determining the class of an impinging waveform related to a geometry of arbitrary size. Several methods for measuring closeness between functions including correlation and area differences were investigated, along with the need for weighting.

14. KEY WORDS	LINK A		LINK B		LINK C	
	ROLE	WT	ROLE	WT	ROLE	WT
Impulse Response						
Radar Cross Section						

SIGNAL PROCESSING STUDY OF IMPULSE EXCITED OBJECTS IN SPACE

V. C. Martins
J. VanMeter

Braddock, Dunn and McDonald, Inc.

i

FOREWORD

This final technical report represents the results of an investigation by Braddock, Dunn and McDonald, Incorporated, 8027 Leesburg Pike, McLean, Virginia, under Contract F30602-71-C-0158, Job Order Number 45060186, for Rome Air Development Center, Griffiss Air Force Base, New York. Contractor's identification number is BDM/W-TR72-094. Mr. Paul Van Etten (OCTS) is the RADC Project Engineer in charge.

This work was performed over the period from June 1971 to September 1972.

This report has been reviewed by the RADC Information Office (OI) and is releasable to the National Technical Information Service (NTIS).

This technical report has been reviewed and is approved.

Approved: PAUL VANETTEN
Project Engineer

Approved: ARTHUR J. FROHLCH
Chief, Techniques Branch
Surveillance & Control Division

FOR THE COMMANDER:

FRED I. DIAMOND
Chief, Plans Office

ii

TABLE OF CONTENTS

TABLE OF CONTENTS (CONT'D)

LIST OF ILLUSTRATIONS

LIST OF ILLUSTRATIONS (CONT'D)

LIST OF ILLUSTRATIONS (CONT'D)

CHAPTER I

INTRODUCTION

The objective of this report was to develop optimum signal processing techniques for discriminating between target and clutter objects in space that have been excited by impulse-like electromagnetic waves in order to further the relatively new field of impulse radars. The targets and clutter specified for this study were to be of relatively simple geometries, and to be fixed in space, but randomly distributed. The study is divided into three major areas of investigation.

The first of these is a study of backscatter in which several waveform variations for the sphere, rectangular plate and thin rod geometries were developed in an effort to determine mathematically tractable expressions for the scattered energy from typical geometrical shapes. This study also revealed that by combining simple methods the composite waveshape from many objects of various geometry may be used to approximate a complex one. This section consists essentially of a definition of the tools which are used in the bulk of the report.

The second part of this program involved the development of several optimal-like filter configurations based upon a knowledge of the characteristics of the waveforms of interest. Employing the waveforms developed in the first section of the study, each filter was studied for its enhancement of the output-to-input signal to clutter ratio as a function of the target to clutter size ratio. It was found for the case of a target body much larger than the clutter that a system encompassing a double integrator followed by a matched filter configuration produces the greatest enhancement of the power signal to clutter ratio. The enhancement of this ratio is proportional to the fourth

power of the target to clutter size ratio.

The effect of rain as a clutter medium is studied, along with this optimal filter configuration, in an attempt to relate the clutter study to a realistic situation. It is shown that a golf ball sized metallic sphere in space can produce a power signal to clutter ratio of 20 dB for an impulse radar of 1.5 degrees beam width in the midst of heavy rain (the clutter) at a distance of 146 kilometers with proper range gating and the optimal filter developed herein. This calculation is based upon a large power source and an infinite bandwidth system in order to obtain an upper limit of the optimum filter's performance.

Finally, the geometry identification problem was investigated in the third section. A system was postulated for determining the class of an impinging waveform related to a geometry of arbitrary size. Several methods for measuring closeness between functions, including correlation and area differences were investigated, along with the need for weighting. The decision template concept is shown to be the best technique for waveform identification when the impinging backscattered waveshape is a well known, non-corrupted waveform.

The reader may obtain an overview of the study results by referring to Chapter V.

CHAPTER II

PREDICTION OF IMPULSE RADAR EXCITED BACKSCATTER WAVESHAPES

A. OPENING STATEMENT

In this section a relatively simple technique will be shown which allows the prediction of impulse excited time waveshapes of targets in a short period of time and with a very limited number of calculations. Of particular interest here are the responses to a perfectly conducting unit sphere, the flat plate, and the thin rod.

The reasons for including a study of this type in a discussion of a radar design philosophy are numerous. First, a simplified version of a signature allows for an interpretation of signature formation in terms of the geometry and physics of a given situation. Secondly, a more simplified signature allows for parameterization of variables to include size considerations in the interpretation of a signature. Finally, the prediction of signature allows the estimation of signatures of targets whose experimentally determined data is not available, as well as allowing the designer to more easily evaluate a proposed system design without resorting to long and expensive computer aided solutions.

In the ideal situation the radar cross-section could be determined through an investigation of the physics of the target and radar system and a solution of the electromagnetic equations of the body with its accompanying boundary conditions. The resulting differential equation forms can be solved through conventional techniques such as separation of variables in a few situations, namely those where one of the sixteen orthogonal coordinate

3

systems simplifies the specification of boundary conditions. In other cases, the differential equations can only be solved through some type of numerical approximation technique. On the other hand, the integral form can be used in some cases to simplify the solution of these complex formulations. Specifically, the equations' solutions would yield a complete description of the total equivalent surface currents which could be used to determine the so called reflected fields at the receiving antenna.

In general, however, exact solutions are not available because most objects of interest are much too complex to result in easily simplified or readily solved electromagnetic equations. For this reason, the use of predicted approximate solutions to the scatter cross-section is the most practical and really the only available approach aside from inspecting experimentally determined data.

There are a number of approximating techniques which are used to determine the radar cross-sections of objects which are larger in size than a few wavelengths in dimension. One of these approaches is the technique of geometric optics, which utilizes the laws of reflection and refraction applied to the incident electromagnetic field treated in the form of rays to determine the reflected field. This technique is similar to the one used with visible light in the mirror problem in that its major shortcoming is that it treats the radiation as particulate and thus fails to bring out the wave nature and associated characteristics such as polarization, of the problem. Since the wavelike nature of the interrogating waveform gives rise to some of the characteristics which are important in predicting the reflected waveform,

for example the creeping wave on the target's surface, this first approximation is unacceptable.

Another approximation is one called the physical optics approach. Here the wavelike nature of the interrogator is included. The basic concept here is that the local current density at each isolated point of the illuminated portion of the target is assumed to be equal to one which would flow at that point on an infinite sized tangent plane. The assumption here which is invalid is that the current density in the shadow region is zero. Also in question is an assumption that neglects the effects of possible mutual influence between adjacent currents on the target surface.

Still another approach is one called geometrical diffraction theory. This technique uses some of the elements of physical optics as well as geometrical optics with its ray theory to provide the necessary considerations of wavelength, phases, polarization, and interference as well as ray reflection to provide the reflected waveform. The concept of scattering centers becomes introduced through this technique and it indicates that they become localized at or near points of geometric discontinuities.

B. THE CLASSICALLY DETERMINED SPHERE CROSS-SECTION

The sphere is one of the geometries which will become useful later in the discussion, partly because of its simplicity but more importantly because of the fact that some of the clutter models can be built in the form of assemblies of small spheres. Another reason for looking at the sphere is that its backscatter cross-section is well known, since it is one of a few geometries which lend themselves to separation of variables and exact solutions.

5

A large body of work presently exists in the literature for consideration and comparison for this particular geometry. The current distribution on the surface is well known and therefore this geometry is an appropriate one for using as a standard for approximating techniques. The sphere is unique in that its scattering is independent of aspect angle; i.e., viewed from any angle the response is the same.

In Figure 1 is shown the radar cross-section of a sphere, normalized to πa^2, the sphere's projected area as seen by the observer. This plot is the result of an exact solution; i.e., it was determined on the basis of a solution of the differential equations arising from Maxwell's equations for the surface of the sphere (see Reference 1).

There are three distinct regions in the radar cross-section for a perfectly conducting sphere, which vary with the circumference/wavelength ratio. In the low-frequency region, which is called the Rayleigh region, the radar cross-section varies as the inverse of the fourth power of the wavelength of the incident radiation. Here the frequency is such that the circumference is less than one wavelength. All objects whose greatest dimensions are smaller than the wavelength of the incident radiation will exhibit a behavior similar to that of the Rayleigh region of the sphere.

The second region, the Mie or resonance region ($1 < 2\pi a/\lambda < 10$) is a region of transition characterized by a damped oscillation about the $\sigma/\pi a^2 = 1$ value. The oscillatory behavior is thought to be due to interference between a specular component and a component due to waves which are exponentially damped as they "creep" around the shadowed portion of the sphere and circumnavigate it to be

6
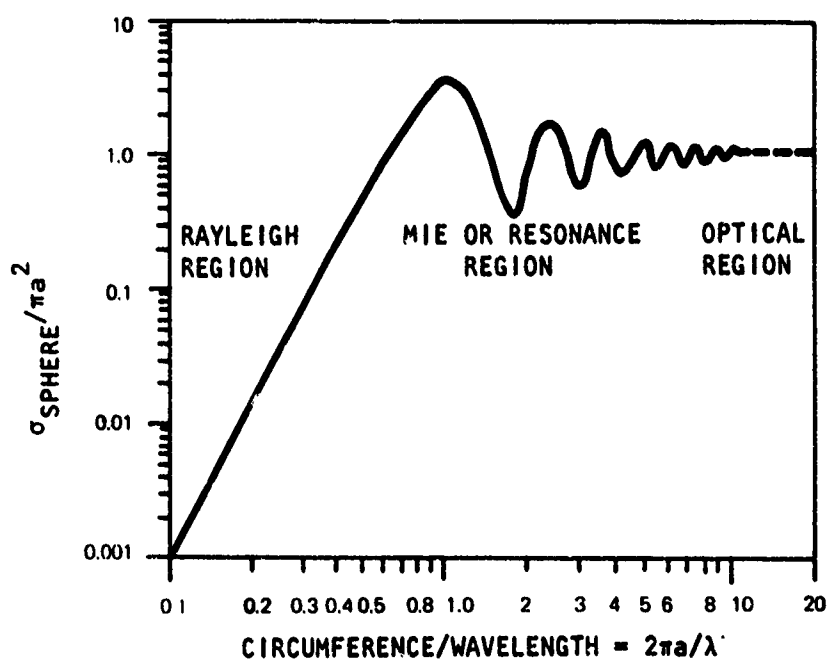
Figure 1. Radar Cross Section of a Sphere: a = radius, λ = wavelength

relaunched in the direction of the radar receiving antenna. In the high frequency or optical ($2\pi a/\lambda > 10$) region, the cross-section finally settles down to a value of $\sigma/\pi a^2 = 1$, which is the visual projected area of the subject sphere. As will be shown later, the high frequency limit agrees in the determinations of all methods - physical optics, impulse approximation, or in the exact theory as determined through the Maxwell equation solution.

C. THE KENNAUGH-COSGRIFF IMPULSE RESPONSE APPROXIMATION

1. Introduction

At this point, the approach has been to indicate the results of data which has been generated from an exact solution of the differential equations governing the current density residing on the surface of the sphere (see References 1 and 2).

Now we turn to the objective of this section of the report, the development of an approximation to the response to an impinging delta function. The chief value of the impulse response is that it can add insight to the relationship between the target shape and radar reflectivity. The customary approach in developing solutions to electromagnetic scattering problems is to assume a monochromatic source with a suitable constraint on the ratio of impinging wavelength to the physical dimensions. When this ratio is small the solution is merely a perturbation of the geometrical or physical optics solution. On the other hand, when the ratio is large the solution is very similar in form to that predicted by the Rayleigh region scattering model. Usually most approximations yield reasonable results in the high and low frequency regions but fail to account adequately for the cross-section in the resonance or Mie region.

A solution for the impulse response to a scatterer allows a determination of the response to any monochromatic interrogator, or for any interrogating waveform. The approximating solution of Kennaugh and Cosgriff is chosen such that the cross-section is matched to both the limiting case of zero and infinite source frequency, and constraining conditions are met such that the resonance region is fairly well determined.

2. Linear System Analysis

One of the concepts which will help in understanding the radar impulse response approximation is that of a linear system. The system will be assumed to be time invariant, i.e., the scatterer is assumed to not move, either translationally or rotationally. Input and output electric field intensities will be defined for two points in space and will be signified by $e_i(t)$ and $e_o(t)$ respectively. If the direction and polarization of the incident plane wave are restricted, the scatter transfer function $\Delta_s(j\omega) = \frac{E_o(j\omega)}{E_i(j\omega)}$ is that of a one-dimensional linear system. Further restricting the input to an impulse or delta function $\delta(t) = e_i(t)$ will yield the impulse function output $\delta_s(t)$.

Since the process is assumed to be a linear one, the output response to an arbitrary input function $e_i(t)$ may be determined through a convolution of the impulse output response and the arbitrary input function:

$$e_o(t) = \int_0^t e_i(\tau)\, \delta_s(t-\tau)\, d\tau \tag{1}$$

Therefore, once the impulse response has been determined, the response to any arbitrary input function can be easily reached through this integral transformation. It should be made clear that the transfer function $\Delta_s(j\omega)$ and $\delta_s(t)$ are a Fourier transform pair.

9

3. Low Frequency Approximation - The Rayleigh Region

Let the system transfer function be approximated by a series in $(j\omega)$ with constants a_n. This series can be written:

$$\Delta_s(j\omega) = a_o + a_1(j\omega) + a_2(j\omega)^2 + \ldots \quad . \tag{2}$$

For the low frequency estimate to $\Delta_s(j\omega)$, the Rayleigh law of scattering postulates that the first two constants are zero and the third proportional to the volume of the scatterer. This results in the following moment conditions on $\delta_s(t)$ (see Reference 3):

$$\int_0^\infty \delta_s(t) \, dt = 0$$

$$\int_0^\infty t \, \delta_s(t) \, dt = 0$$

$$\int_0^\infty t^2 \, \delta_s(t) \, dt = 2a_2$$

$$\bullet$$
$$\bullet$$
$$\bullet$$

$$\int_0^\infty t^n \, \delta_s(t) \, dt = (-1)^n n! a_n \tag{3}$$

The first relation is equivalent to the statement that for the impulse response to any arbitrary shape, the DC level or average area under the time-waveshape area is zero. The constant a_2 is a constant which can be determined from a knowledge of the scattering from static electromagnetic fields and is called the Rayleigh coefficient. With the use of only the first three relationships

good approximations to $\delta_s(t)$ can be made, but in some special cases the higher order terms can be used and are available.

4. High Frequency Approximation - The Optical Region

A simple yet useful approximation to scattering by a body in the high frequency region is the physical optics approximation. In this approximation, the local current density at each point on the illuminated portion of the body is assumed to be equal to that which would flow at the same point on an infinite tangent plane. Specifically, it is assumed that at each point on only the illuminated side of the surface, the current density is equal to $2\underline{n} \times \underline{H}$, where $\underline{n}$ is a vector normal to the surface, and $\underline{H}$ is the impinging magnetic field intensity. On the shadowed side the surface current density is assumed to be zero (see Reference 4).

The electric field response which has been determined to be scattered at large distances in the source direction as a result of illumination by an impulse has been found to be of the form

$$\delta_s(t) = \frac{1}{4\pi} \frac{d^2 A(z)}{dz^2} \qquad (4)$$

where $z = \frac{ct}{2}$ and $A(z)$ is the silhouette area of the target as delineated by the incident wave, which is assumed to move over the surface of the target at a velocity equal to one-half that of the free-space velocity, c.

In Figure 2, the physical optics impulse response to three geometries, the sphere, spheroid, and off axis square plate are indicated. The impulses in the responses of the cases of the sphere and spheroid result from the discontinuity in the change of the rate of change of the radar cross-section at the first point of incidence. In all three cases the response was derived with the use of expression (3) exclusively.

11

a) SHPERE — NORMALIZED IMPULSE RESPONSE

b) SPHEROID — NORMALIZED IMPULSE RESPONSE

c) SQUARE PLATE

$\frac{\delta(t)}{e_i}$, IMPULSE EXCITATION
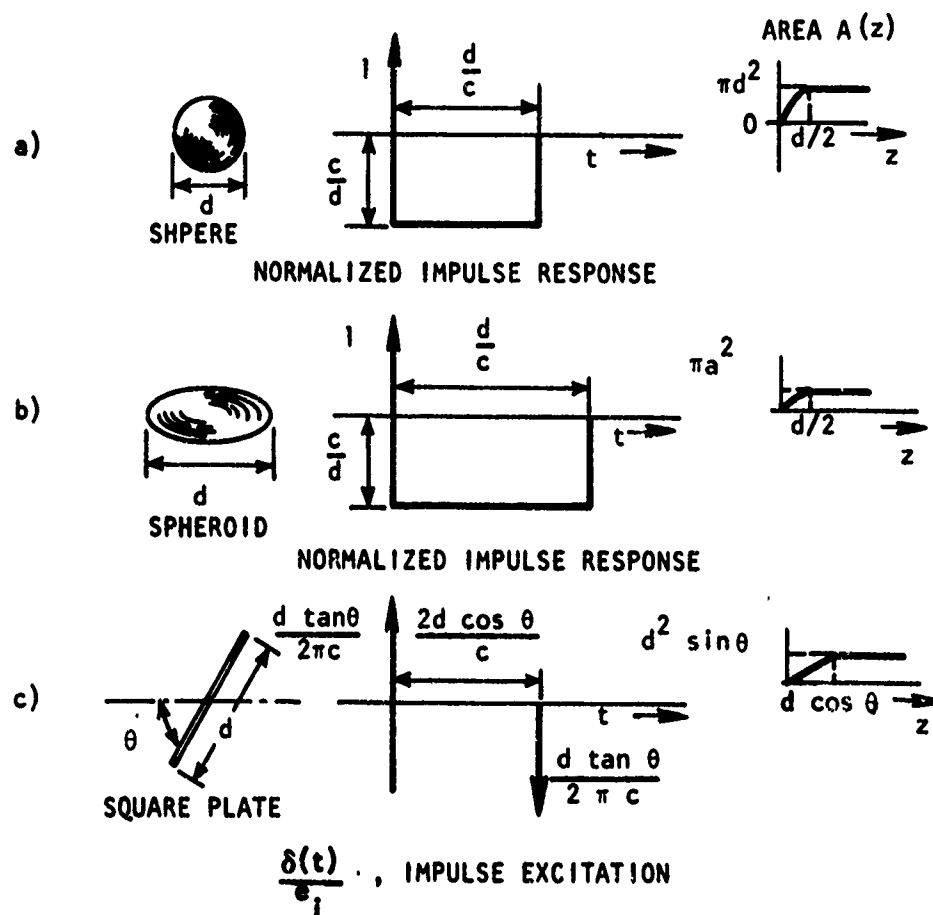
BDM-W-72-094

Figure 2. Impulse Response of Scatterers According to Physical Optics

12

Figure 3 indicates the cross-section of the conducting sphere determined through the physical optics approximation as displayed in Figure 2 for comparison with the more exact electromagnetic solution.

Note that the envelope size and shape in the high frequency region is approximately correct, but the oscillatory frequency is not correct. In the Rayleigh region the physical optics approximation is far from being representative of the exact solution.

5. Higher Level Approximations

The approach which has been suggested in the literature for higher level approximations is to alter the time function determined in the physical optics solution in such a manner as to yield the Rayleigh condition. This is done by adding additional time function data to the information indicated in Figure 2, for example, subject to the Rayleigh constraints of expression 3. Usually only the first three moment conditions are used to form this approximation (see Reference 4).

A number of appropriate functions can be postulated which not only are based upon the physical optics solution but also satisfy the Rayleigh condition.

The simplest extension or correction to the spherical impulse response approximation is the step correction indicated in Figure 4. An investigation of the physical optics solution indicates that it meets the constraint imposed by the first Rayleigh moment condition, i.e., its DC or average value is indeed always zero. Thus, the constraint which must be met by the corrector is that its components have a zero DC level, and that the total waveform satisfy the additional moment conditions specified in expression 3.

13
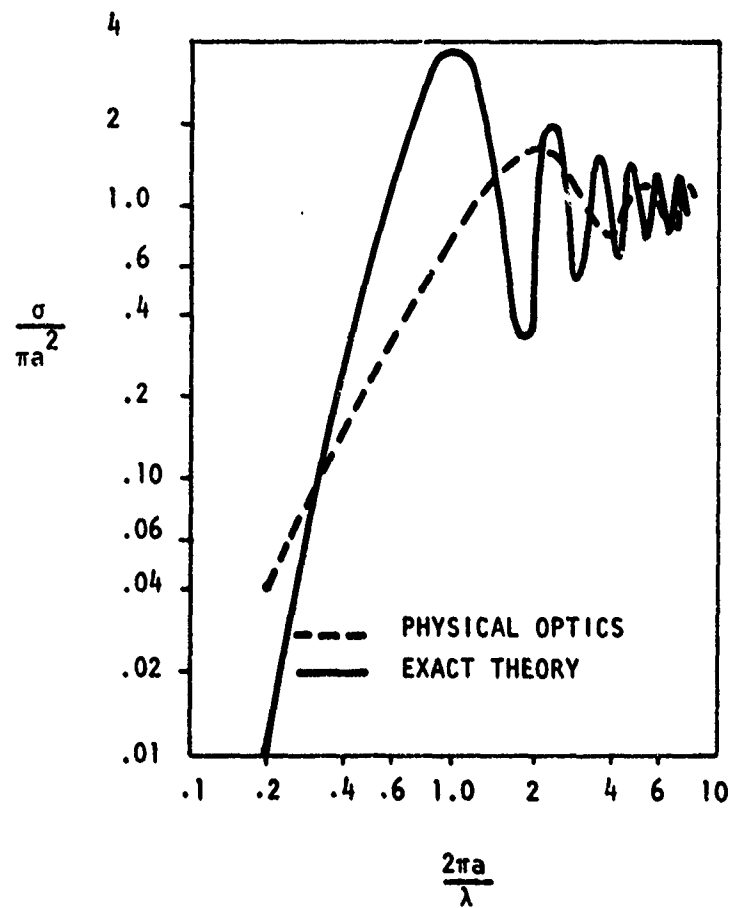
Figure 3. Back-scattering From a Conducting Sphere
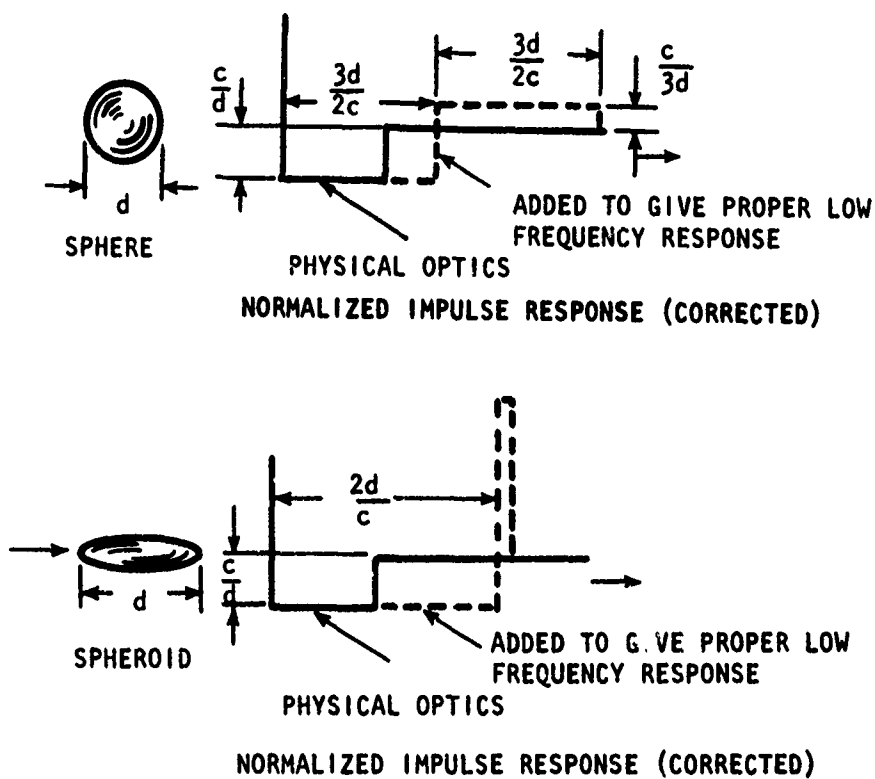
BDM–W–72–094

14

Figure 4. The Step Correction to the Physical
Optics Solution for the Sphere and
Spheroid

Figure 5 shows the radar cross-section which results from this approximation. It can be seen here that both the high frequency and particularly the Rayleigh region are reasonably well approximated by this waveshape. The behavior in the resonance region is not particularly well defined, however.

Another method for correction can be studied by applying a polynomial form instead of the step which, like the step correction starts at the final value of the physical optics time response. Again, the moment equations are met by choosing the polynomial coefficients appropriately. Indicated in Figure 6 are the polynomial corrections to the physical optics solutions for the sphere and spheroid.

In Figure 7 the cross-section for the polynomial correction to the impulse spherical response is shown to be reasonably good except for a shift in the resonant region. In the low and high frequency regions, the approximation is quite good.

Kennaugh and Moffatt indicate a more complex solution to the spherical impulse scattering problem, which is indicated in Figure 8. This approach is based upon experimental data and a model which uses a finite number of harmonically related plane waves which are superimposed to produce a composite backscatter $\delta_s(t)$. In the figure, tabulated values of the backscatter waveform at given values corresponding to a sphere radius to wavelength ratio of 0.04 to 19.0 in steps of 0.04 were used in a calculation including 475 harmonics. In addition, the step and ramp responses to the unit conducting sphere are included for comparison. These waveforms will be used in the further development of our simplified backscatter models to act as standards (see Reference 5).
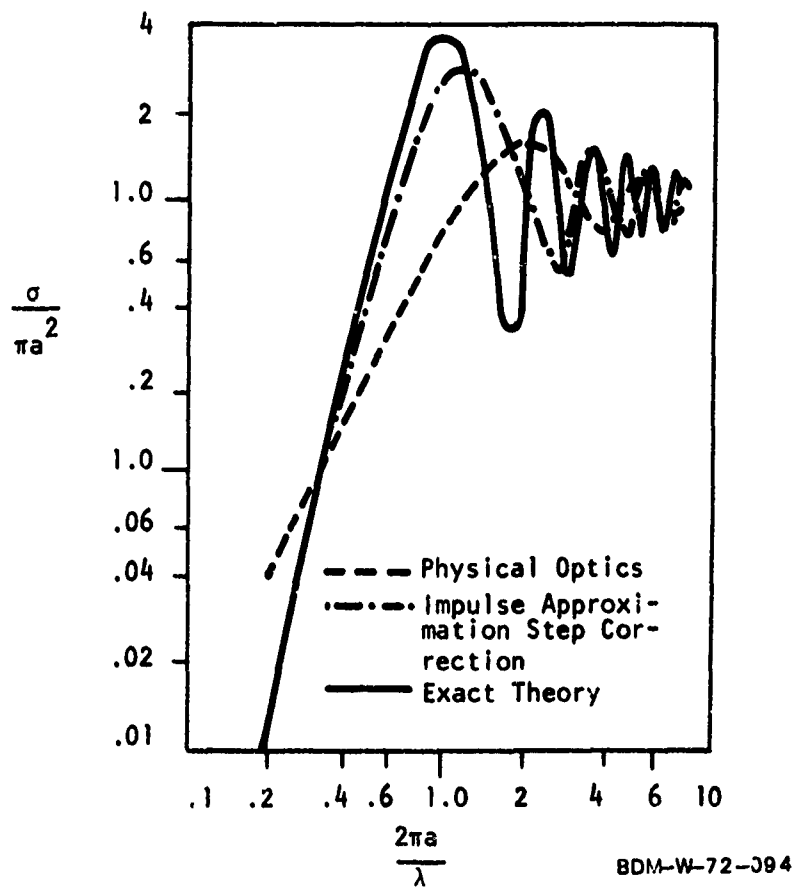
Figure 5. Radar Cross-Section for Back-Scattering from a Conducting Sphere, Including the Step Corrector Approximation
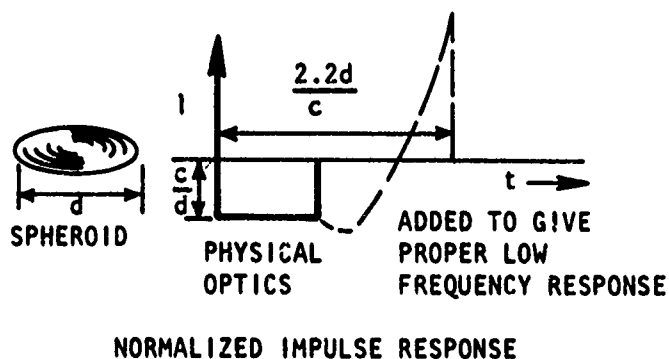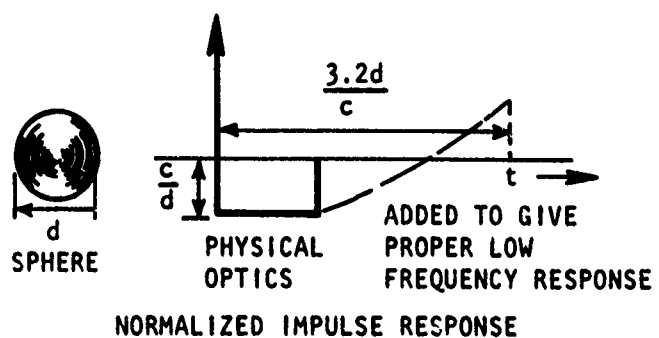
Figure 6. Polynomial Correction to Approximation for Impulse Response

BDM-W-72-094
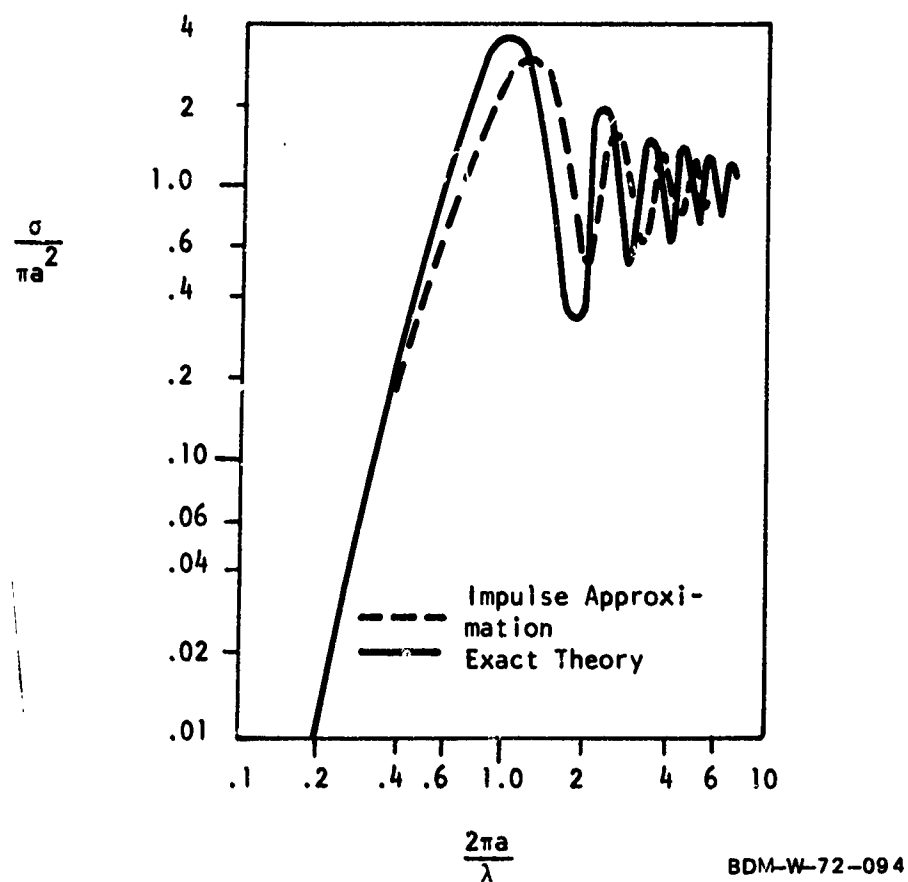
Figure 7. Radar Cross-Section For a Conducting Sphere;
Including Polynomial Correction Term
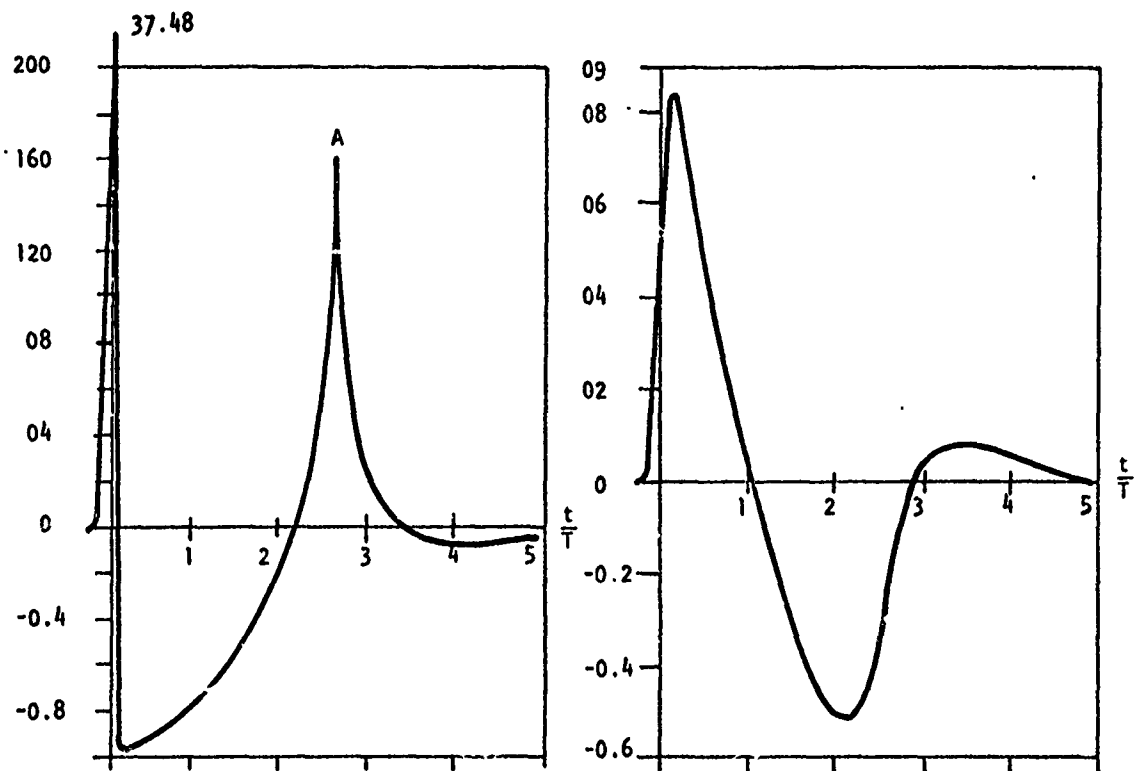
a. Normalized Short Pulse Backscatter Response of a Conducting Sphere

b. Normalized Step Backscatter Response of Conducting Sphere
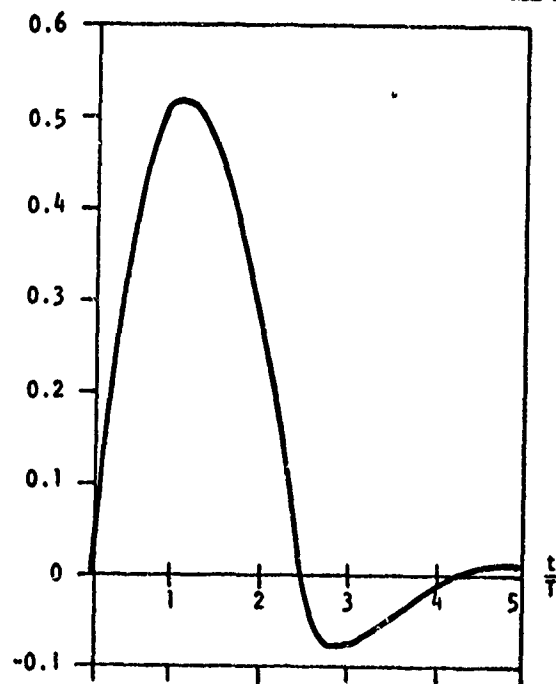
c. Normalized Ramp Backscatter Response of Conducting Sphere

BDM-W-72-094

Figure 8.   Impulse, Step, And Ramp, Sphere Scattering Responses (Kennaugh and Moffatt, Ref. 5)

20

6. Mathematically Tenable Model for the Sphere

Based upon the models and work presented thus far, a model for the impulse excited spherical backscatter waveform which is mathematically simpler is desired. Specifically, a response waveform is desired which takes on a form which is easily written either in the time or frequency domain. Still constraining this model waveform however, are the Rayleigh condition and the high frequency region response, the latter of which is satisfied by the physical optics approach.

(a) The response postulated in Figure 9 serves as a trial waveform for this approach. This waveform was postulated because its shape approximates that of the more rigorous solution indicated in Figure 8. It was also postulated because it can be relatively easily described mathematically.

By forcing the values of K and τ with respect to T the first Rayleigh condition can be met. Note that the area of the triangle can be made equal to that of the impulse, as well. The equation which describes this impulse response in the frequency domain is

$$\Delta_s(j\omega) = \frac{1}{2} - \frac{1}{j\omega T}\left[1-\epsilon^{-j\omega T}\right] + \frac{K}{(j\omega\tau)2}\left[1-\epsilon^{-j\omega\tau}\right]^2 \epsilon^{-j\omega T} \tag{5}$$

To check for adherence to the Rayleigh moment condition, the limit of $\Delta_s(j\omega)$ can be taken as ω approaches zero. That is, only the ω^2 and higher terms must exist as ω goes to zero. Then,

$$\Delta_s(j\omega) = \left[K-\frac{1}{2}\right] + j\omega\left[\frac{T}{2} - K\left(T+\frac{\tau}{4}\right)\right] + (j\omega)^2\left[\frac{K\tau^2}{6} - \frac{T^2}{6} + \frac{K}{2}\left(T + \frac{\tau}{4}\right)^2\right] \tag{6}$$

$\lim \omega \rightarrow 0$

21
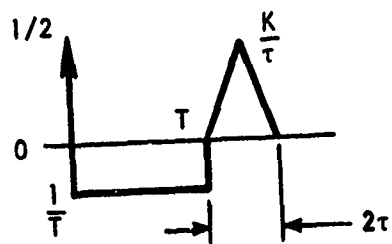
Figure 9.   Sphere Backscatter Trial Response 1

In order to meet the conditions of equations 2 and 3, the first term will disappear if K takes on a value of 1/2, but for any finite pulse width τ the second term cannot be forced to be equal to zero. Hence, this functional form cannot satisfy the Rayleigh condition.

(b) Another form of the backscatter response which can be postulated is that indicated in Figure 10. This response is suggested as an extension of the effort in Section a, since it is the result of letting $\tau = 0$. With this assumption the second term in expression 6 will equal zero, and the three Rayleigh moment conditions will be met.

Letting the value of τ in expression 5 go to zero, the equation which describes the waveform of Figure 10 is given by an expression in the frequency domain which can be written as

$$\Delta_s(j\omega) = \frac{1}{2}\left[1 + \varepsilon^{-j\omega T}\right] - \frac{1}{j\omega T}\left[1 - \varepsilon^{-j\omega T}\right] \tag{7}$$

(c) Another proposed waveshape for mathematical simplification of the backscatter waveshape is indicated in Figure 11.

Expressed in the frequency domain, the expression for this waveshape takes the form:

$$\Delta(j\omega) = \frac{1}{2} - \frac{1}{j\omega T}\left[1 - \varepsilon^{-j\omega T}\right] + \frac{K}{2j\omega\tau}\left[1 - \varepsilon^{-j\omega\tau}\right]\varepsilon^{-j\omega T} \tag{8}$$

Again checking for the Rayleigh conditions by taking the limit,

$$\Delta(j\omega) = \frac{1}{2}[K-1] + j\omega\left[\frac{T}{2}(1-K) - \frac{K\tau}{4}\right] + (j\omega)^2\left[\frac{T^2}{6} + \frac{KT^2}{4} + K\tau\left(\frac{\tau}{6} + \frac{T}{4}\right)\right] \tag{9}$$

$\lim \to 0$

23
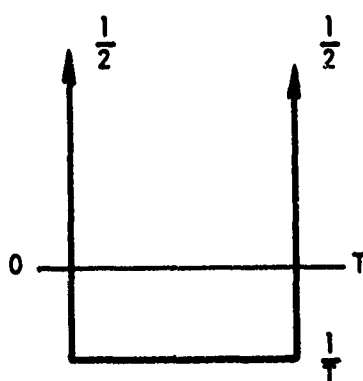
BDM-W-72-094

Figure 10.   Sphere Backscatter Trial Response II

24
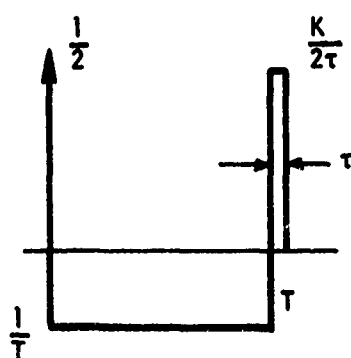
BDM-W-72-094

Figure 11. Sphere Backscatter Trial Response III

25

The first term can be forced to zero by letting K = 1, however, the
second term can also be made to go to zero then only if τ = 0. But
this is identically the case presented in part (b), since the right
positive rectangular pulse becomes an impulse in the limit as τ goes
to zero.

These proposals all indicate that the best approximate waveform
which not only satisfies the Rayleigh and physical optics conditions
but is in addition mathematically simple is the one presented in
part (b).

7. Approximate Sphere Impulse Response - Model A

Still necessary to complete the model developed in part 6, equations 7 and
Figure 10 is the development of its constants, which includes the scattering as
a function of the sphere's dimension and the distance r to the observation point.

Consider first its normalized response. Figure 2 suggests, by comparison
with Figure 10, that the value of T should be d/c (Notice that the impulse and
rectangular response areas would then be the same for each except that the impulse
area is shared between two impulses in Figure 10. Recall that the second impulse
was required to satisfy the Rayleigh condition which Figure 2 does not.) This
value of T, however, is not consistent with wide band scattering as can be
observed from Figure 8a and a consideration of the physical process. The time
to a second peak can be seen from Figure 8a to occur near 2.5 d/c rather than
d/c. This can be verified from the physics by considering the creeping wave
contribution. This contribution occurs at the time it takes the exciting wave
to sweep the sphere's diameter d to excite the sphere's backside at d, and then
travel around the circumference back to the sphere's front side. The total

26

delay from the inception of the excitation is then d/c $(1 + \pi/2)$ or 2.57 d/c.

Figure 10 may then be modified as shown in Figure 12 by increasing the time by 2.5T and reducing the amplitude proportionally in order to maintain equal areas. The entire function was then multiplied by T in order to preserve its un-normalized response.

The multiplier for the waveform of Figure 12, which allows a complete mathematical description of the sphere's impulse response, can be obtained by investigating the sphere's radar cross-section expression. The radar cross-section is defined as:

$$\sigma = 4\pi r^2 \left| \frac{E_o(j\omega)}{E_i(j\omega)} \right|^2 \tag{10}$$

or,

$$\frac{E_o(j\omega)}{E_i(j\omega)} = \left[\frac{\sigma}{4\pi r^2} \right]^{1/2} \tag{11}$$

At optical frequencies the sphere's cross-section is of the form $\sigma = \pi a^2$. (See Figure 1) Then, substituting this value of σ into expression 11 gives

$$\frac{E_o(j\omega)}{E_i(j\omega)} = \left[\frac{\pi a^2}{4 \pi r^2} \right]^{1/2} = \frac{a}{2r} \quad ; \quad \left(\frac{2\pi a}{\lambda} \gg 1 \right) \tag{12}$$

This can be written in terms of the diameter since $d = 2a$ or

$$\frac{E_o(j\omega)}{E_i(j\omega)} = \frac{d}{4r} \quad ; \quad \left(\frac{2\pi a}{\lambda} \gg 1 \right) \tag{13}$$

27

where $T = \dfrac{d}{c}$
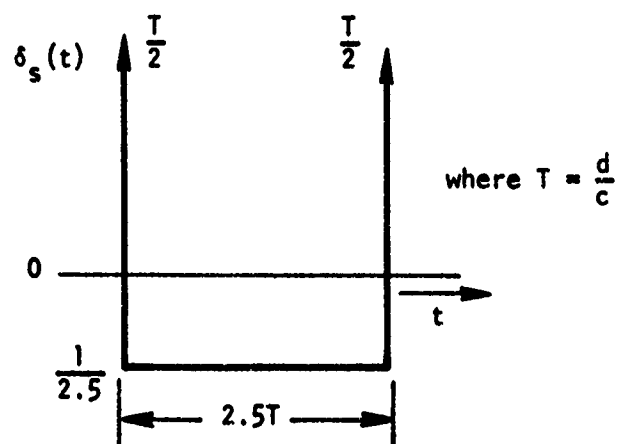
BDM-W-72-094

Figure 12. Normalized Sphere Impulse Response (Simplified Form)

Expression 13 is to be equated to the expression describing the approximate sphere's waveshape (equation 7) at optical frequencies. To make expression 7 apply to Figure 12, T must be multiplied by 2.5 for the creeping wave effect. Also the entire function must be multiplied by KT to un-normalize it. It is the multiplier to be identified to complete the function.

Performing these operations on expression 7 and allowing $2\pi a/\lambda >> 1$, the approximate frequency response magnitude at optical frequencies is

$$\left| \Delta_s(j\omega) \right| = \left| KT \cos(1.25 \, \omega T) \right| \; ; \; \left(\frac{2\pi a}{\lambda} >> 1 \right) \tag{14}$$

Notice that rather than the response being constant as shown in Figure 1, it has zeros at $(2n-1)\pi/2$ intervals. This condition arises due to the addition of the second impulse. Had it been a more dispersed function, this would not ·occur. Fortunately, it will be shown later that these zeros do not alter the value of the model. This will be proven by comparing the results with both experimental and detailed theoretical data.

Now equating expressions 13 and 14, the multiplying factor K takes on the value c/4r. The full expression for the impulse response of a sphere of diameter d can then be written as

$$\delta_s(t) = \frac{c}{4r} \left[\frac{d}{2c} \delta(t) + \frac{d}{2c} \delta\left(t - 2.5 \frac{d}{c}\right) \right.$$
$$\left. - \frac{1}{2.5} u(t) + \frac{1}{2.5} u\left(t - 2.5 \frac{d}{c}\right) \right] \tag{15}$$

Figure 13 shows this response.

The experimental verification of this model will be discussed in the paragraphs to follow.
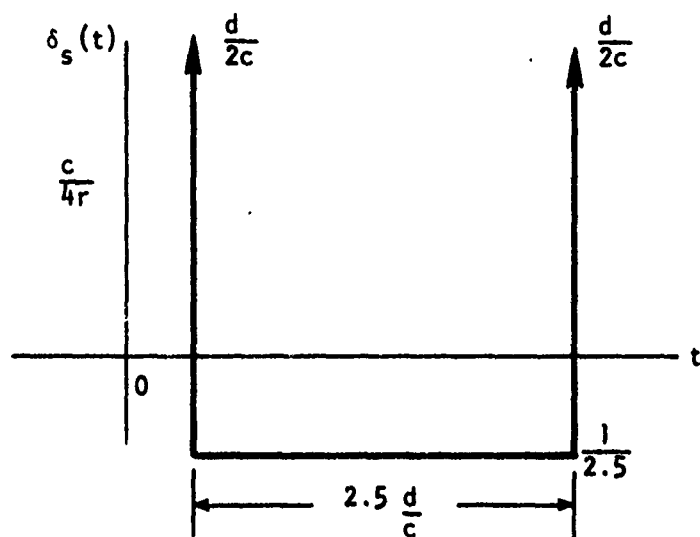
Figure 13.   Absolute Sphere's Impulse Response
(Simplified Form) Model A

BDM-W-72-094

30

8. Experimental Verification of Simplified Model

Sperry Rand, under contract to RADC (see Reference 6), performed scatter-ing experiments from many objects one of which was a sphere. Figure 14 shows the measured incident excitation pulse identified as input pulse, and the scattered response identified as the measured response. Superimposed upon the measured response is the response one can obtain using the normalized model of Figure 13. The response was constructed by convolving the impulse model with the input pulse. This amounted to summing the contributions of two input pulses displaced by the time interval 5 a/c plus the integration of the pulse over that interval.

Notice that the waveshapes over the first alternation are identical after which a variation does occur. If one were to average this measured response's undershoot over the interval, its value would approximate that produced by the model. The same applies to the second pulse's area as compared to the model's. Considering the simplicity of the model this comparison is not bad.

Since much of signal processing encompasses correlation, a measure of the model's performance may be obtained by correlating the model's and the measured responses and comparing their results. The autocorrelation of a function is defined as

$$\phi_{11}(\tau) = \int_{-\infty}^{+\infty} f_1(t) \, f_1(t+\tau) \, dt \tag{16}$$

or

$$\phi_{11}(\tau = 0) = \int_{-\infty}^{+\infty} f_1^2(t) \, dt$$

and it has a maximum value at $\tau = 0$.

31
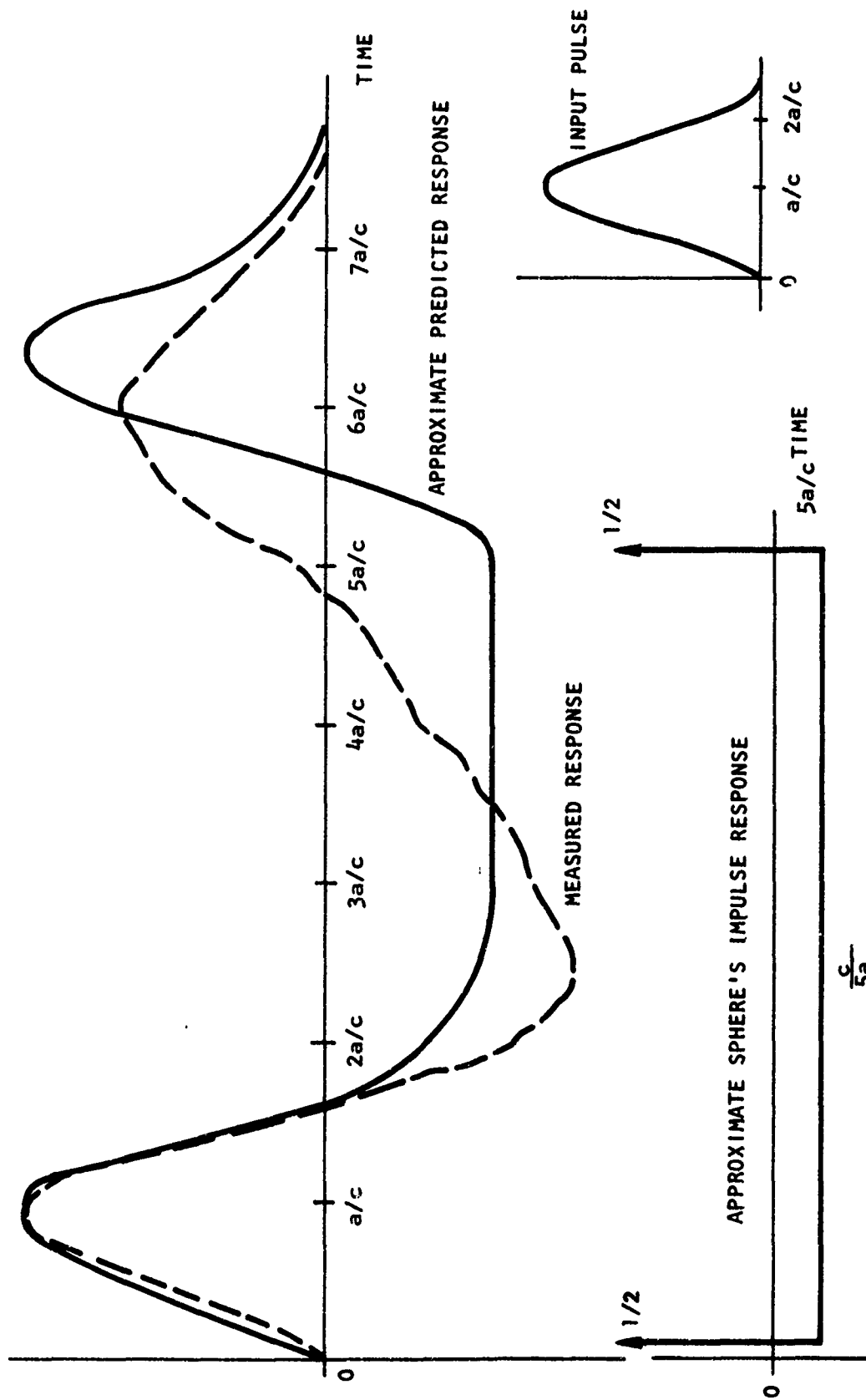
Figure 14. Approximate Predicted and Measured Pulse Responses to a Sphere

BDM-W-72-094

Figures 15 and 16 show the model and measured responses squared $(f_1(t)^2)$, and their integrated values that correspond to $\phi_{11}(0)$. The maximum autocorrelation values are 981.2 units for the model and 872 units for the measured, or an increase of twelve percent over the measured value. This is indeed an acceptable deviation.

Next to be considered is the response that this model will provide for a step or a ramp excitation for purposes of comparing with the detailed theoretical models of Kennaugh and Moffatt.

9. Approximate Models For Step and Ramp Response

At this point a number of methods for describing the impulse response of a conducting sphere have been investigated. It is of interest to further evaluate the waveform of Figure 13 by looking at its response to the step and pulse forms of excitation.

Recall from the earlier discussion that the output response to an arbitrary function may be determined through a convolution of the impulse output response and the arbitrary input function (see expression 1). However, if the excitation is a step function, then the scattered response is the integral of the impulse response. For a ramp excitation, the response is the integral of the step response.

a. Step Response

The step response to the approximate sphere impulse function of Figure 13 is obtained by integrating expression 15. It is listed in expression 17 and sketched in Figure 17.

$$u_s(t) = \frac{c}{4r}\left[\frac{T}{2} u(t) + \frac{T}{2} u(t-2.5T) - \frac{1}{2.5} u(t)\, t + \frac{1}{2.5} u(t-2.5T)\, (t-2.5T)\right] \tag{17}$$

33

$$\Phi_{11}(0) = \int_0^\infty f^2(t)dt = 981.2$$

$f^2(t)$
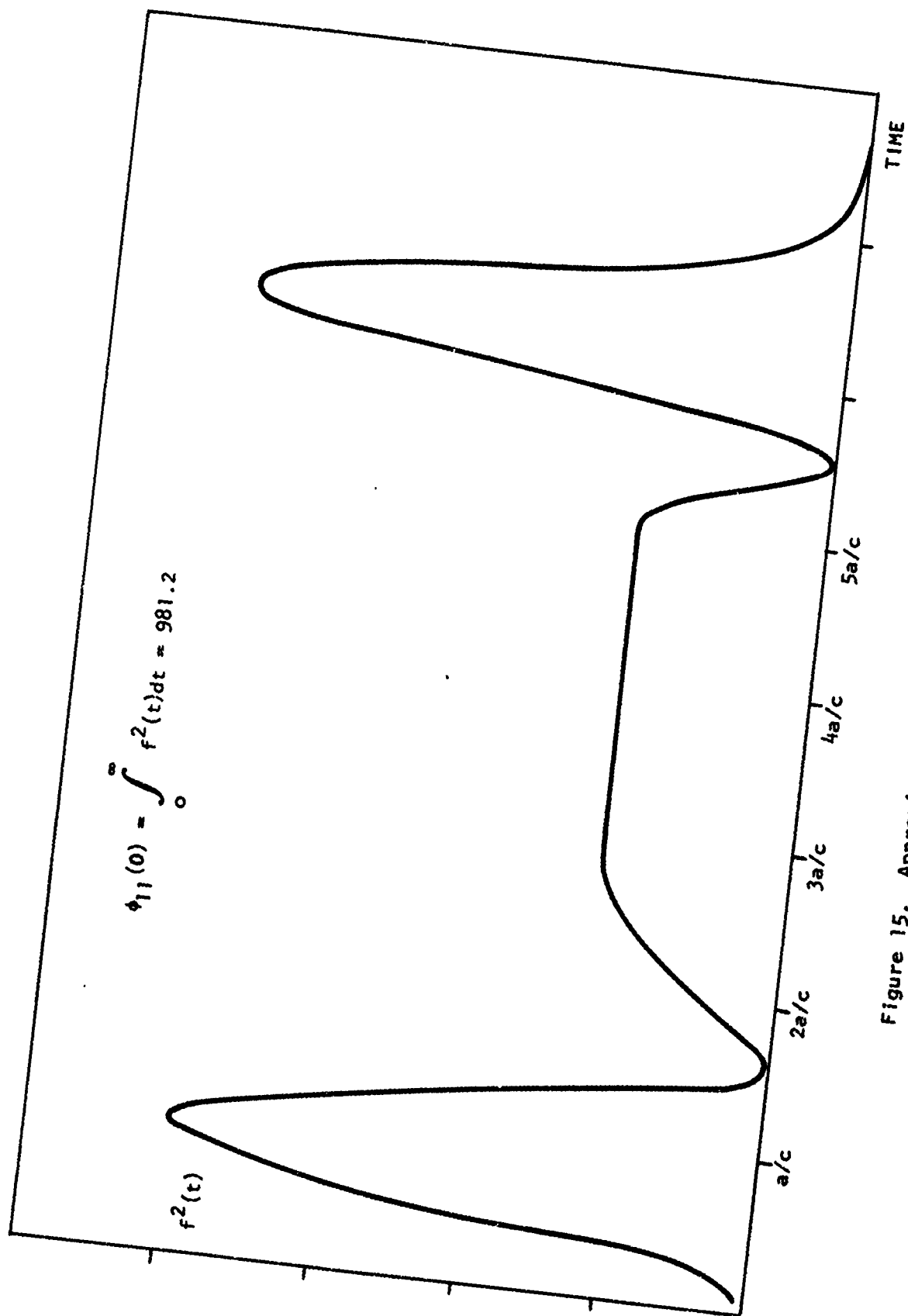
Figure 15. Approximate Sphere's Response Squared

BDM-W-72-094

34

$f^2(t)$

$\phi_{11}(0) = 872$

a/v   2a/v   3a/v   4a/v   5a/v   6a/v   7a/v
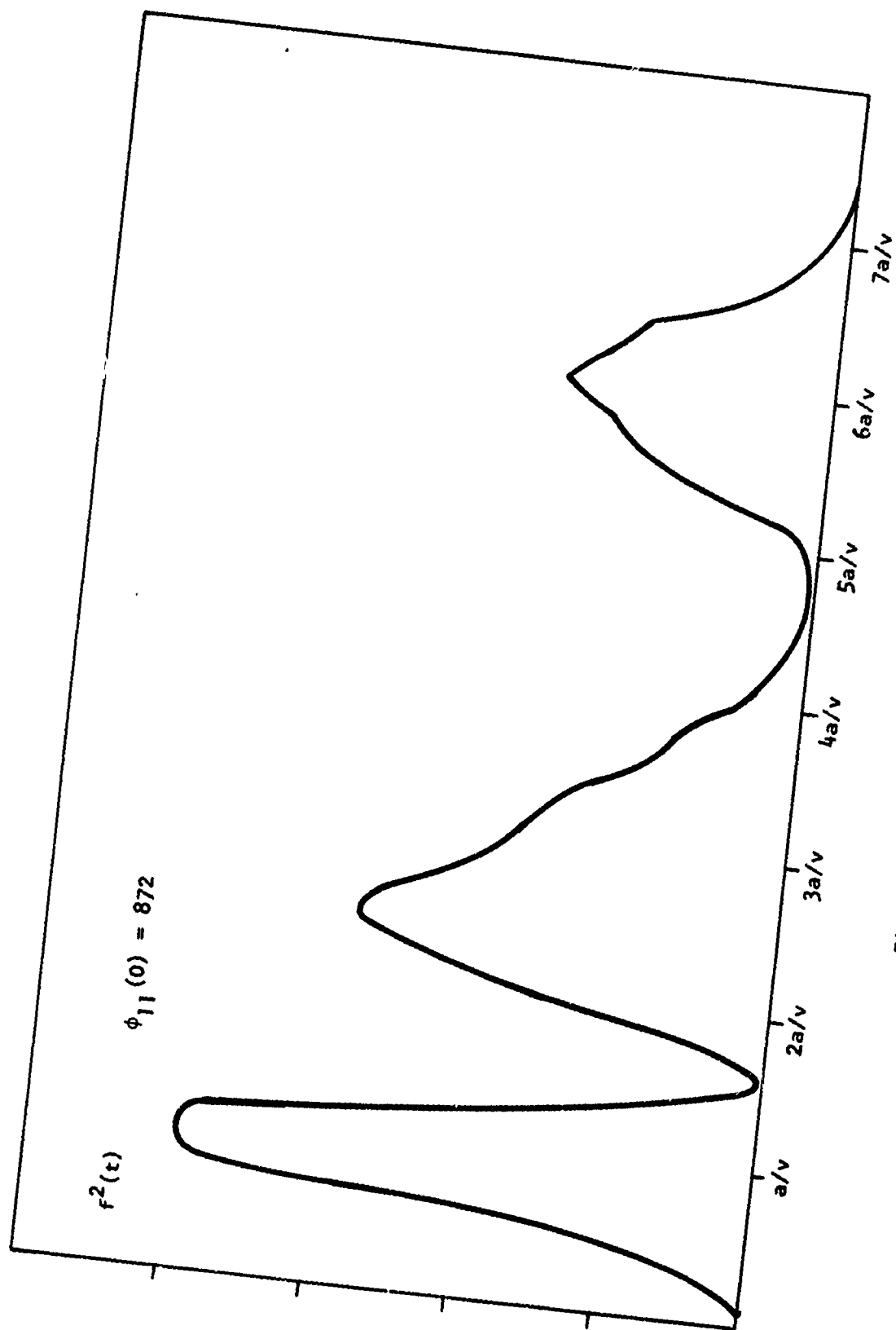
BDM-W-72-094

Figure 16. Measured Sphere's Response Squared

35
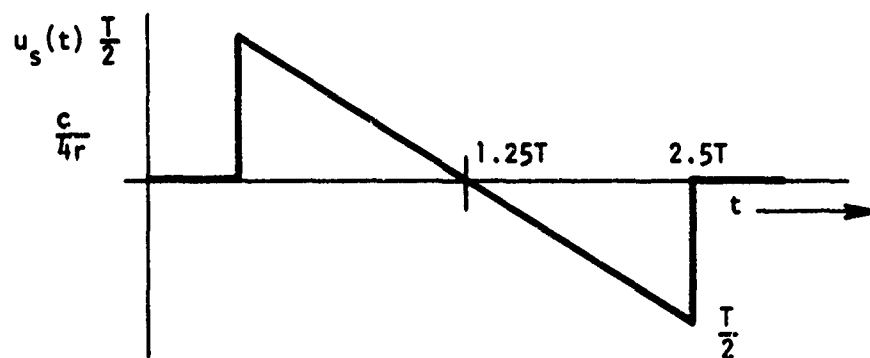
BDM-W-72-094

Figure 17. Normalized Step Response of a Sphere (Simplified Form)

36

This figure can be compared to Kennaugh and Moffatt's high accuracy curves of Figure 8a. The shape is approximately the same with the highest degree of accuracy occurring over the first positive interval. Notice that the cross-over time of 1.25T is the same in both. The deviations in the model essentially occur in the under-swing area. Although the shapes are similar, the model has a higher amplitude and is less broad than shown in Figure 8a. There also occurs a small positive alternation beyond 3T. Overall, the times that the peaks and crossovers occur do compare favorably making this simple model attractive.

b. **Ramp Response**

The ramp scattering response of a sphere may be obtained by integrating expression 17. The result is

$$\int_{0}^{t} u_s(t)\ dt = \frac{c}{4r}\left[\frac{T}{2}\ u(t)\ t + \frac{T}{2}\ u(t-2.5T)\ (t-2.5T) \right.$$
$$\left. - \frac{1}{5}\ u(t)\ t^2 + \frac{1}{5}\ u(t-2.5T)\ (t-2.5T)^2\right] \qquad (18)$$

Figure 18 shows the ramp scattered response.

Comparing this curve with that shown in Figure 8a produced by Kennaugh and Moffatt again the similarity is attractive, not only in shape but in crossover times. The portion where a small error occurs is in the undershoot.

It has been shown by these computations and comparisons with more detailed models and experimental data, that the simple model of Figure 13 is representative of impulse back scattering from a metallic sphere. This model will be used in the study for those cases where quick sketching results are of interest in order to obtain an insight into the problems under investigation.

37
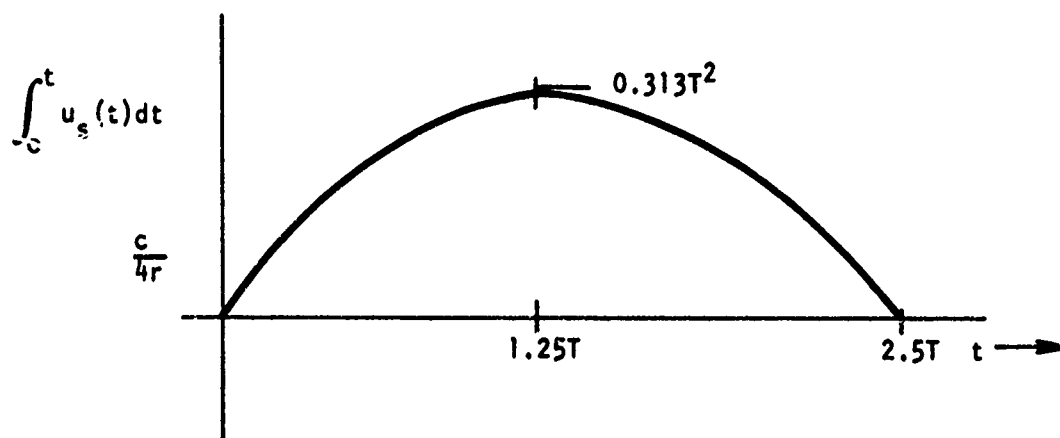
Figure 18. Normalized Ramp Response of a Sphere (Simplified Form)

BDM-W-72-094

38

10. Approximate Sphere Responses - Model B

Another form for the normalized sphere step response which becomes quite valuable in hand calculations is the one displayed in Figure 19, and may be described by expression 19 as

$$u_s(t) = \frac{c}{4r} \left(\frac{T}{2}\right) \left[u(t) \cos \frac{2\pi t}{5T} + u(t-2.5T) \cos \frac{2\pi}{5T} (t-2.5T)\right] \qquad (19)$$

Notice that the feature of this model is that the number of terms to be handled have diminished by a factor of two over those of Model-A. (See equation 17.) This model approximates that of Model-A and the Kennaugh and Moffatt model of Figure 8b.

The model's simple mathematical form makes calculation of cross-correlations, for example, a much more tractable matter, while preserving the Rayleigh moment conditions. The impulse excited sphere backscatter time waveshape which would give rise to a waveform of the type indicated in Figure 19 is shown in Figure 20. It is merely the functional derivative of Figure 19's waveform. Expression 20 describes this waveform. This investigation of the step response has, in effect, led us to yet another approximation to the impulse response of a perfectly conducting sphere.

$$\delta_s(t) = \frac{c}{4r} \left[\frac{T}{2} \delta(t) + \frac{T}{2} \delta(t-2.5T) - \frac{\pi}{5} u(t) \sin \frac{2\pi}{5T} t \right.$$
$$\left. - \frac{\pi}{5} u(t-2.5T) \sin \frac{2\pi}{5T} (t-2.5T)\right] \qquad (20)$$

The ramp response of this model is shown in Figure 21 and described by expression 21. As one can see, it is a single alternation of a sinusoid.

$$\int_0^t u(t) \, dt = \frac{c}{4r} \left(0.397T^2\right) \left[u(t) \sin \frac{2\pi t}{5T} \right.$$
$$\left. + u(t-2.5T) \sin \frac{2\pi}{5T} (t-2.5T)\right] \qquad (21)$$
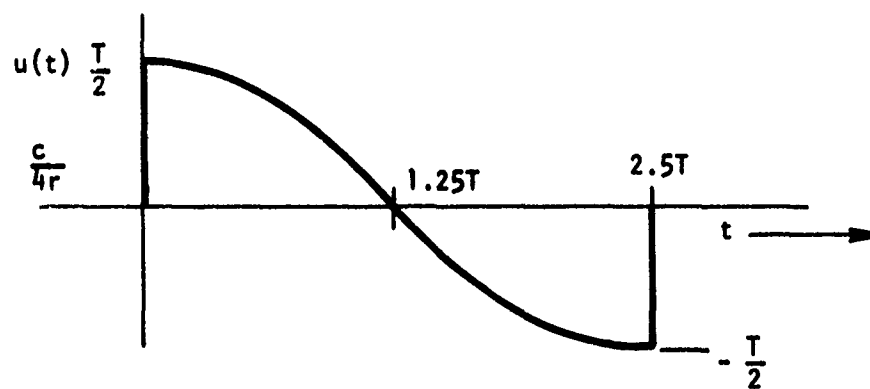
BDM–W–72–094

Figure 19.   The Cosine Approximation to the Step Response Model B

40
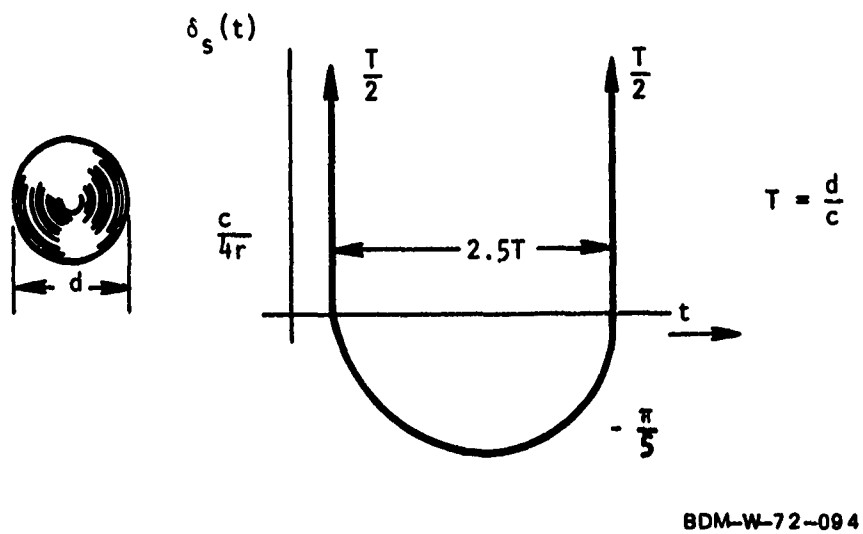
Figure 20. Sphere Impulse Response Approximation Selected for Tractability-Sine Approximation Model B

41

$$\int_0^t u(t)dt$$

$\dfrac{c}{4r}$

$-0.397T^2$

1.25T

2.5T

t
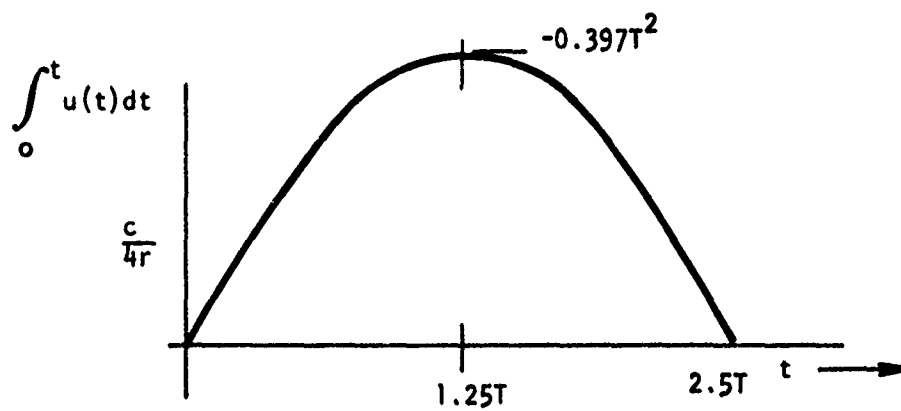
BDM-W-72-094

Figure 21.   Ramp Scattering Response of a Sphere - Model B

42

This response compares favorably to both Figures 8c and 18.

11. <u>Approximate Sphere Responses</u> - Model C

During the study, an investigation will be performed on the classical optimal filter. In order to perform the required factoring, the function to be operated upon must be of a polynomial nature. An approximate model will now be developed to meet this requirement which also follows the scattering laws.

From past discussions, it was pointed out that at low frequencies the Rayleigh field scattering varied as the square of the frequency of excitation. At the very high or optical frequencies, the field scattering is a constant for a spherical scatterer. Applying these conditions plus the fact that there can be no average or dc value, the following transfer function is postulated.

$$\Delta_s(j\omega) = \frac{c}{4r}\left(\frac{T}{2}\right)\frac{(j\omega)^2}{\left[j\omega + \frac{1}{1.25T}\right]^2} \tag{22}$$

The time domain expression for this response is

$$\delta_s(t) = \frac{c}{4r}\left(\frac{T}{2}\right)\left[\delta(t) - \frac{1}{1.25T}\epsilon^{-\frac{1}{1.25T}}\left(2 - \frac{t}{1.25T}\right)\right] \tag{23}$$

and it is plotted in Figure 22.

Notice that this function lacks the resonance or Mie region which accounts for the smearing and non-peaking of the second alternation as occurs in Figure 8a. However, the second alternation does contain the area that the second peak would have if the Mie region were included. The undershoot

43
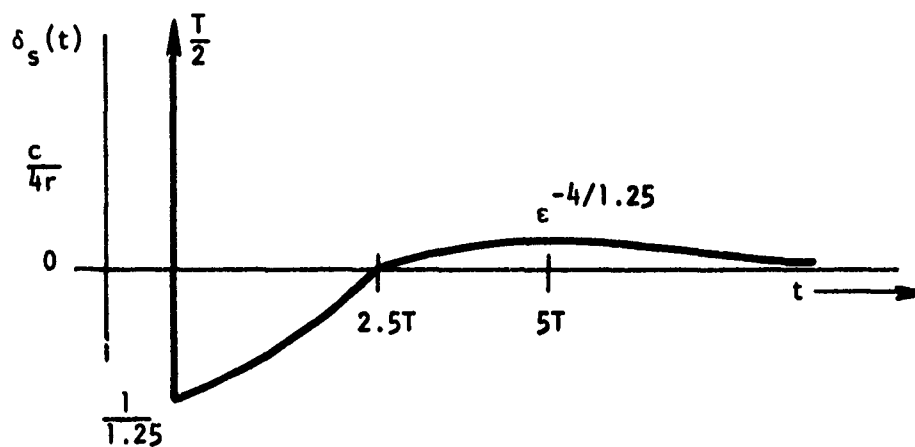
Figure 22. Approximate Polynomial Sphere Impulse
Response - Model C

BDM-W-72-094

area and impulse amplitudes can also be shown to be identical to all of the prior models. Certainly this model, as in all of the others, does describe the early time sphere scattering performance quite well.

Figure 23 shows the step response of the model as generated by expression 24.

$$u_s(t) = \frac{c}{4r}\left(\frac{T}{2}\right)\left[\epsilon^{-\frac{t}{1.25T}}\left(1 - \frac{t}{1.25T}\right)\right] \tag{24}$$

Notice that the response follows the early time well as in the other cases. The undershoot's amplitude is smeared but its area is identical to the positive portion.

Figure 24 shows the ramp response of the polynomial model as generated by expression 25.

$$\int_0^t u_s(t)\ dt = \frac{c}{4r}\left(\frac{T}{2}\right) t\ \epsilon^{-\frac{1}{1.25T}} \tag{25}$$

Comparing the crest amplitudes of the other ramp excited models, it is observed that the variation is not severe. The crest amplitude also occurs as for the other models at 1.25T.

It has been shown that the polynomial model does present the salient scattering responses from a metal sphere, especially in early time. Hence, it will later be used in the analysis.

To this point we have developed scattering models for the sphere only. Since we are also interested in other geometries in order to study the discrimination problem, we will also investigate a flat plate and a dipole rod. We shall begin with the flat plate.

45
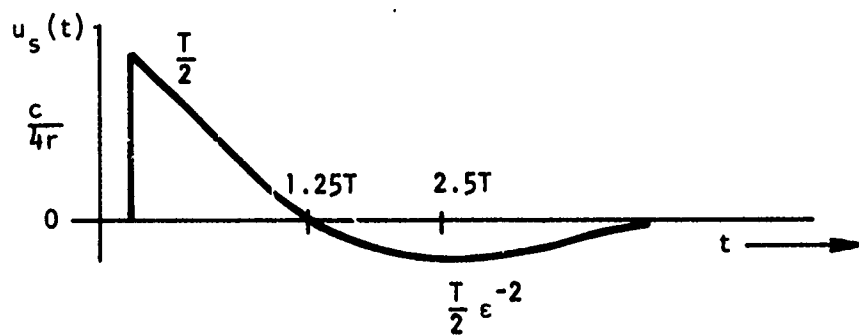
BDM-W-72-094

Figure 23. Approximate Polynomial Sphere
Step Response - Model C
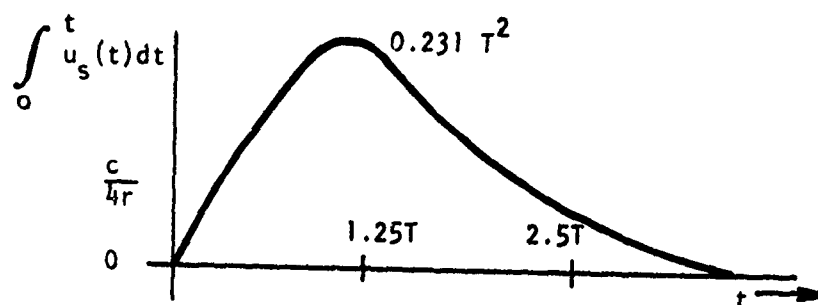
BDM-W-72-094

Figure 24. Approximate Polynomial Sphere
Ramp Response - Model C

12. Flat Plate Scattering Model

Figure 2c shows the waveform which physical optics considerations predict for a thin square plate when it is interrogated at an angle not perpendicular to the face of the plate. The area plot $A(z)$ indicated in the figure is easily predicted by merely inspecting the geometry. For the special case which will be considered in this section, the illumination and scatter of interest will be assumed to be perpendicular to the face of the plate. In this case, all of the energy will reach all points of the plate surface area at the same time. Thus, the area plot $A(z)$ will be as indicated in Figure 2c. Applying expression 4, one can then obtain the normalized solution shown in Figure 2c. For the case of a broadside excitation, the normalized impulse response can be found to be

$$\delta_p(t) = \frac{\ell^2}{\pi c^2} \cdot \frac{d}{dt} \, \delta(t) \tag{26}$$

The dimensions of the plate have been changed from d to ℓ in order to avoid any confusion later in the study when plate and sphere responses will be compared. Expression (26) lacks the multiplying factor that includes the effect of distance on the scattering. This is necessary so that a comparison can be made between the scattering amplitudes of different geometries. Notice that the time response is a doublet.

Scattering from a thin flat surface of any geometry that is uniformly excited can be determined from the following well known expression.

$$E_o(j\omega, \, r) = \frac{j\omega}{2\pi c r} \int_A E_i(j\omega, \, x, \, y) \, dA \tag{27}$$

48

The expression assumes that the observation point r from the surface is quite distant such that near field conditions are not of concern. This is generally not a problem unless the excitation has a very low frequency content and the observation point is close. Since it is assumed that the excitation is uniform, then the integration in (27) is only over the area, hence the equation may be written as

$$\frac{E_o(j\omega, r)}{E_i(j\omega)} = \frac{j\omega}{2\pi cr} \quad A \tag{28}$$

Substituting for the area A, ℓ^2 and transforming the function into the time domain gives

$$\delta_p(t) = \frac{\ell^2}{2\pi cr} \quad \frac{d}{dt} \delta(t) \tag{29}$$

Comparing expressions (29) and (26) it is seen that the results regarding the time waveshape are the same except that the function is now un-normalized and contains the distance factor r.

The solution presented applies at the very high frequencies where the excitation wavelength is much greater than ℓ. We require an approximate solution that applies over all frequencies. An inspection of expression 28 indicates that the zero average value condition is met since the function is zero at $\omega = 0$ but it does not satisfy the Rayleigh condition. Recall the Rayleigh condition requires that the scattering increase as ω^2 for excitation wavelengths large compared to the objects' dimensions. The following function is postulated to satisfy both the Rayleigh and the optical regions without emphasis on the Mie region. Experimental results obtained from an ongoing

49

RADC program (see Reference 7) where parabolic antennas have been excited by fields of impulse-like nature (pulse-widths measured in tenths of nanoseconds) have shown that the predominant scattering is derivative-like and the oscillations are quite small. This justifies the chosen model even over the Mie region.

$$\Delta_p(j\omega) = \frac{\ell^2}{2\pi cr} \frac{(j\omega)^2}{[j\omega + \alpha]} \tag{30}$$

where $\alpha = \frac{\pi c}{\ell}$

The factor α represents the frequency where the plate would experience its first resonance.

Performing an inverse transform on expression (30) gives the time domain scattered impulse response of a plate as

$$\delta_p(t) = \frac{\ell^2}{2\pi cr} \left[\frac{d\delta(t)}{dt} - \alpha \; \delta(t) + \alpha^2 \; \varepsilon^{-\alpha t} \right] \tag{31}$$

This response is a doublet and an impulse at $t = 0$ followed by a decaying exponential.

The step scattering response is obtained by integrating expression 31. Then

$$u_p(t) = \frac{\ell^2}{2\pi cr} \left[\delta(t) - \alpha\varepsilon^{-\alpha t} \right] \tag{32}$$

This completes the development of a plate's impulse and step scattering response. We shall consider next the scattering from a thin dipole-like rod.

13. Approximate Thin Rod Scattering Response

Figure 25 shows the scattering model, to be examined, where the incident electric field $E_t(j\omega)$ is polarized in the same axial direction as the rod. The rod has a length ℓ and a radius "a" and it is considered, as in the other past cases, to be in free space. The broadside sensed scattering field $E_o(j\omega, r)$ at a distance "r" is to be described.

50
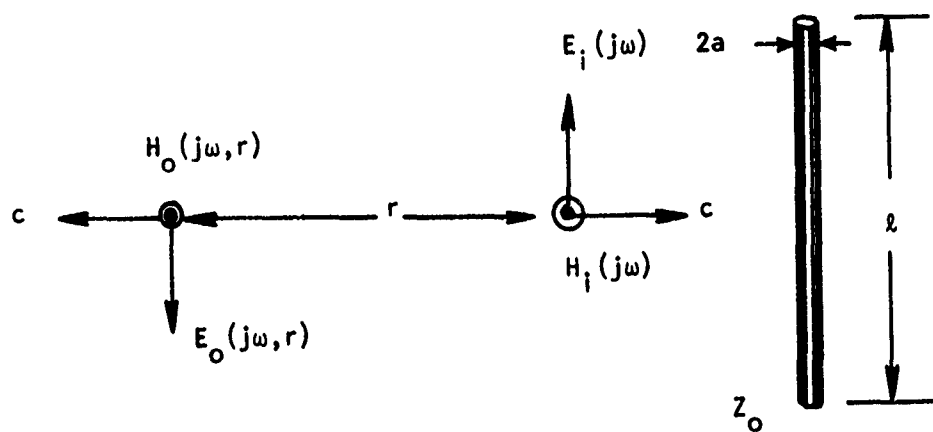
Figure 25.   Thin Rod Scattering Model

The transfer function scattering response for this model can be shown to be

$$\Delta_d(j\omega) = \frac{E_o(j\omega,r)}{E_i(j\omega)} = \frac{\eta\ell}{4\pi Z_o(\omega)r} \left[1 - \left(\frac{2c}{\omega\ell}\right) \frac{\tan\left(\frac{\omega\ell}{2c}\right)}{1 + j\left(1 - \frac{2}{T(\omega)}\right)\tan\left(\frac{\omega\ell}{2c}\right)} \right] \quad (33)$$

where $Z_o(\omega)$ is the rod's characteristic impedance, $T(\omega)$ is a transmission-like coefficient which accounts for the radiation from the rod's ends, and η, the free space wave impedance. The derivation of this expression will not be shown as it is extensive and beyond the scope of this effort. However, a verbal description will be given regarding its development after a brief discussion of its characteristics.

Notice that equation 33 satisfies the Rayleigh requirements. At $\omega = 0$ the function is zero (T, the transmission coefficient goes to 2 since the rod's ends appear as an open circuit), and for small ω values the expression increases as ω^2. The resonance or the Mie region is present as can be seen by the peaking of the function when the argument goes to $\pi/2$. There is also an optical region where the function approaches a constant value of

$$\Delta_d(j\omega) = \frac{\eta\ell}{4\pi Z_o r} \quad (34)$$

since the second term in the brackets approaches zero, this region presents a radar cross section, using expressions 10 and 34 of

$$\sigma = \frac{1}{4\pi}\left(\frac{\eta}{Z_o}\right)^2 \ell^2 . \quad (35)$$

The value of the characteristic impedance, for impulse-like excitations, has been demonstrated by Paul Van Etten of RADC and confirmed by BDM and IKOR

during the performance of an RADC contract and found to be approximately 220 ohms,

Satisfying the required scattering conditions has demonstrated the validity of the transfer function shown in expression 33.

The development of the expression was along classical lines where the rod's surface current was determined by the excitation of a uniform wave front and the requirement that the current go to zero at the rod's ends. Once this current was obtained, it was then possible to determine the magnetic vector potential on the axis of symmetry. The magnetic and electric fields followed from the curl and double curl, respectively, of the magnetic vector potential.

Figure 26 shows the rod's impulse response using expression 33, with the assumptions that the transmission coefficient and characteristic impedance are essentially real quantities. Had their complex values been introduced, the corners of each alternation would be rounded and the function would tend towards a damped sinusoid. Later in this study the sinusoidal approximation will be used for the purpose of calculating filter responses.

This completes the development of the electromagnetic approximate scattering models. We shall now turn to their application in seeking out the best filter which enhances the signal-to-clutter ratio and provides a high degree of target discrimination.
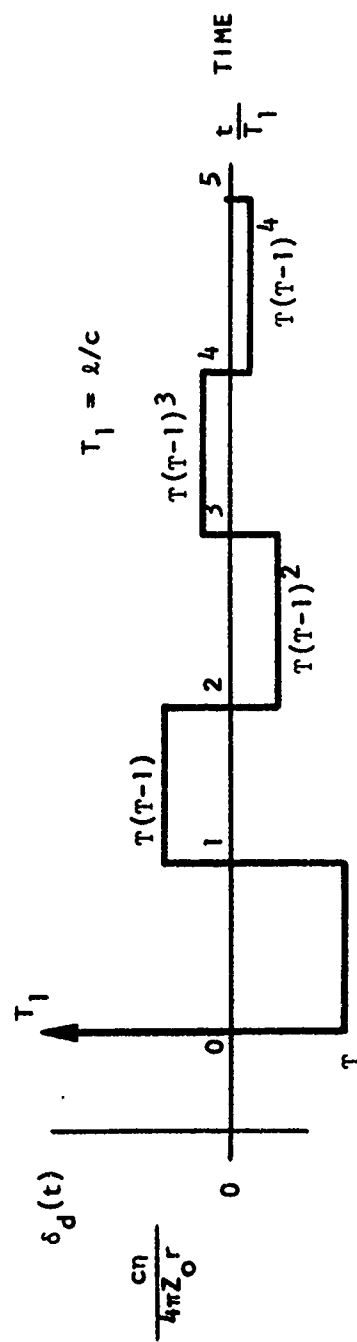
Figure 26. Thin Rod Impulse Scattering Response

BDM—W—72—09.4

CHAPTER III

THE CLUTTER PROBLEM

A. INTRODUCTORY STATEMENT - DEFINITIONS

In this section the subject will be clutter and clutter rejection techniques which are generally applicable to the Time Domain Radar System. One of the characteristics which is sometimes ascribed to clutter is that it is composed of a large number of scatterers, each having independent motions, which in turn are independent of the targets' motion. The clutter problem may be likened in some respects to the noise problem in communications work. In both cases a signal waveform exists in the presence of an additive component, the presence of which it is desired to minimize as much as possible. Our problem then is to devise an optimum transfer function which will output a signal which will exhibit the highest target-to-clutter signal component ratio.

The terms "optimum" and the input-output concept immediately suggest some type of filter strategy. The concepts of optimum filtering techniques and clutter rejection are by no means new to radar system design. What is new, however, is the application of this work to the time domain radar system philosophy.

Let us consider the special needs of the time domain radar system and the "knowns." When designing a system the first question to be answered is what is the desirable output. From the information to be presented later, it is seen that the most important items to be preserved are waveshape and magnitude information, and these should be kept as intact as possible in order that the discrimination be optimum.

55

A number of forms of clutter exist, dependent upon the environment and application to which the system is being made. Ground, weather, and sea clutter are only three of the types of interfering activities which oftimes hamper the identification of radar returns.

In a conventional radar system one of the "knowns" is the reflected waveform. The conventional monochromatic pulsed radar output signal will be reflected not only by the target, a desired response, but also by the clutter bodies, a highly undesired response. But here the reflected waveform's shape can be predicted because all reflected waveforms will be of the same frequency as that transmitted, except for phase and doppler frequency shifting due to distance velocity differences. The key factor in conventional radar design, then, is to use the doppler and phase shift information to calculate velocity, while sifting out that information which differs from that of the target. In designing optimum filters, the factors necessary to complete the design are a knowledge of the expected target and clutter waveforms, as will be seen later in the discussion. In a conventional radar system the backscatter waveform is certainly predictable because of its relation to the interrogating waveform, and in most cases the shape of the clutter waveform can be either measured or predicted. Thus, a filter which is optimal can be designed for each type of clutter, regardless of target. This type of filter will be called a target-fixed filter.

Let us now consider the characteristics of the time domain radar system which constrain the use of filtering schemes. As we have noted, one of the backscatter characteristics which marks the time domain radar system is that the reflected waveform is a function of target geometry. This means that

the optimum filter is not target fixed; i.e., for each target of interest and for each clutter waveform of interest, the optimal filter is required to change configuration to insure optimality. This immediately suggests a sequential scheme for inspecting an unknown waveform for adherence to an expected waveshape. The filter required here will be known as a target variable type of filter.

A characteristic of clutter which has been overlooked in the discussion above is that in many cases the individual clutter object size is much smaller than that of the target. This information can be used to develop a filter philosophy applicable to clutter of small relative dimensions.

Let us constrain the arguments in the following to stationary targets with the nature of the clutter as to stationarity here unspecified. The use of the range gate concept will be assumed possible in the following material, inasmuch as a given segment of range space can be singled out from the universe of all range space for processing and observation.

Techniques such as clutter mapping and blanking will not be considered since they merely act to avoid range cells in which clutterers are present.

The following investigation assumes that a range gate interval has been defined, and further that there is no $1/r^2$ amplitude dependence over this gate. The individual objects making up the clutter and target are assumed to not react or reverberate with one another and hence no time delay deviations are to be considered since the source wave will be unimpeded. An infinite bandwidth detector will be assumed unless otherwise specified.

57

B. DESIGN OF OPTIMUM FILTERS FOR CLUTTER REJECTION

1. Infinite Signal-to-Noise Ratio Filter

The optimum linear filter which causes the output signal-to-noise ratio to be infinite will be investigated in this section and it will be based upon the principle of orthogonality. A deterministic situation is assumed i.e., both the nature of the signal and the clutter waveforms can be specified.

Let $S(t)$ and $C(t)$ equal the signal and clutter over a specified interval from zero to t_o. Then, on the basis of orthogonality, for the condition, when no signal is present, we would like for the filter's output at t_o to be zero. Or

$$\int_0^{t_o} C(t)[S(t) - a\, C(t)]\, dt = 0 \qquad \text{at } t_o. \qquad (36)$$

The orthogonal functions are $C(t)$ and the postulated bracketed terms where "a" is a constant to be determined.

Expanding the function and solving for "a" gives

$$a = \frac{\displaystyle\int_0^{t_o} C(t)\, S(t)\, dt}{\displaystyle\int_0^{t_o} C^2(t)\, dt} \qquad (37)$$

Let us relate this information to general filter performance. The bracketed terms in expression 36 can be considered as the filter's impulse response or

$$h*(t) = [S(t) - \hat{a}\, C(t)]^* \qquad (38)$$

58

The star represents the reversal in time of this function since the filter's output is produced by a convolution process. Considering the convolution process "a" goes to $\hat{a}$ where

$$\hat{a} = \frac{\displaystyle\int_0^{t_o} S*(\tau) \ C \ (t-\tau) \ d\tau}{\displaystyle\int_0^{t_o} C*(\tau) \ C \ (t-\tau) \ d\tau} \tag{39}$$

Consider next the output that would occur from this filter if in the presence of the clutter there appeared a signal $S(t)$. Then convolving the signal plus clutter with the filter's impulse response of (38) gives

$$\int_0^{t_o} [S(\tau) + C(\tau)] \ h*(t-\tau) \ d\tau = \int_0^{t_o} S(\tau) \ S*(t-\tau) \ d\tau + (1-\hat{a}) \int_0^{t_o} S(\tau) \ C*(t-\tau) \ d\tau$$
$$-\hat{a} \int_0^{t_o} C(\tau) \ C*(t-\tau) \ d\tau \tag{40}$$

Substituting the value for $\hat{a}$ from expression (39) gives the filter's output as

$$\int_0^{t_o} S(\tau) \ S*(t-\tau) \ d\tau - \frac{\left[\displaystyle\int_0^{t_o} S(\tau) \ C*(t-\tau) \ d\tau\right]^2}{\displaystyle\int_0^{t_o} C(\tau) \ C*(t-\tau) \ d\tau} \tag{41}$$

The results of expression (41) are interesting. The first integral is the classical matched filter in white noise or the autocorrelation of the signal. The second integral is the cross-correlation of the signal and clutter squared

divided by the mean squared clutter value. The result shows that indeed an output signal will occur when the desired signal appears providing one samples at $t = t_o$. (Expression (41) will have a positive finite value.)

It has been shown that a filter can provide an infinite signal-to-clutter ratio for a signal burried in clutter providing the clutter is known exactly for all time, and that the occurrence of the signal and its form is also well known. We have just demonstrated the best of all possible filters however, its conditions are unrealistic. Generally the clutter's response for all time is not known nor the time of occurrence of the signal. These factors will be considered in the filters to follow.

2. Power Optimal Filter Criteria

Another criterion for optimality in filter design is that the ratio of the output signal to output rms value of clutter is to be maximized.

Let

$$\overline{C_o^2} = \frac{1}{t_o} \int_0^{t_o} C_o^2(t) \, dt \tag{42}$$

represent the clutter rms value.

where

$$C_o(t) = \int_0^{t_o} h(\tau) \, C(t-\tau) \, d\tau \tag{43}$$

Thus, the expression to be maximized is

$$\frac{S_o^2(t_o)}{\frac{1}{t_o} \int_0^{t_o} C_o^2(t) \, dt} \tag{44}$$

over the class L_h of all linear filters.

Here again the target's reflected waveform is represented by $S_o(t)$ and the clutter waveform is represented by $C_o(t)$.

An alternative expression for the clutter rms value is

$$\frac{1}{t_o} \int_0^{t_o} C_o^2(t) \, dt = \int_0^{t_o} \int_0^{t_o} h(\tau) \, h(\mu) \, R(\tau-\mu) \, d\tau d\mu \qquad (45)$$

where

$$R(\tau-\mu) = \frac{1}{t_o} \int_0^{t_o} C(t-\tau) \, C(t-\mu) \, dt \qquad (46)$$

Define $1/\lambda$ as the maximum signal-to-clutter ratio as defined in expression (45). Let $g(\tau)$ be any non-trivial impulse response for which

$$\int_0^{t_o} g(\tau) \, S(t_o-\tau) \, d\tau = 0. \qquad (47)$$

Then, normalizing the output of the optimal filter for $S(t_o)$ as an input

$$S(t_o) = 1 = \int_0^{t_o} h(\tau) \, S(t_o-\tau) \, d\tau, \qquad (48)$$

and further noting that

$$\int_0^{t_o} [h(\tau) + \varepsilon \, g(\tau)] \, S(t_o-\tau) \, d\tau = 1, \qquad (49)$$

We wish to have a maximum output signal-to-clutter ratio then

$$C_o^2(t_o) - \lambda \, S_o^2(t_o) \geq 0 \qquad (50)$$

61

Applying expression (45) and expanding gives

$$\epsilon^2 \int_0^{t_0} \int_0^{t_0} g(\tau) \ g(\mu) \ R(\tau-\mu) \ d\tau d\mu + 2\epsilon \int_0^{t_0} \int_0^{t_0} g(\tau) \ h(\mu) \ R(\tau-\mu) \ d\tau d\mu \geq 0 \quad (51)$$

To be satisfied for all values of ϵ the expression requires the following to be true.

$$\int_0^{t_0} \int_0^{t_0} g(\tau) \ h(\mu) \ R(\tau-\mu) \ d\tau d\mu = 0. \quad (52)$$

However, by construction, we know that

$$\int_0^{t_0} g(\tau) \ S(t_0-\tau) \ d\tau = 0. \quad (53)$$

Thus, the integral equation for the optimal filter becomes, in this case

$$\int_0^{t_0} h(\mu) \ R(\tau-\mu) \ d\mu = K \ S(t_0-\tau) \quad (54)$$

(K an arbitrary constant)

Now if $R(\tau-\mu) = \delta(\tau-\mu)$, then

$$\int_0^{t_0} h(\mu) \ \delta(\tau-\mu) = h(\tau) = K \ S(t_0-\tau) \quad (55)$$

and the result is the well known "matched" filter. Now let it be assumed that

62

$$R(t-\mu) = R(t) \qquad 0 \leq t \leq t_o \tag{56}$$

$$= 0 \qquad \text{otherwise}$$

and similarly
$$S(t-\tau) = S(t) \qquad 0 \leq t \leq t_o \tag{57}$$

$$= 0 \qquad \text{otherwise}$$

Then, taking the Fourier Transform of the filter integral equation, expression (54), the result is

$$H(j\omega) \ R(\omega) = K \ \epsilon^{-j\omega t_o} \ S(-j\omega) \tag{58}$$

or

$$H(j\omega) = \frac{K \ S(-j\omega)}{R(\omega)} \ \epsilon^{-j\omega t_o} \tag{59}$$

This result is quite well known and has been derived by many. See, for example, L. A. Zadeh and J. R. Ragazzini, Reference 8, where it is listed as an infinite memory filter. J. B. Thomas, Reference 9, lists this as a solution for a matched filter by prewhitening techniques.

This result will be used later in the determination of the optimal signal-to-clutter ratios that can be achieved for the various conditions to be investigated for the geometries of interest.

In this and the prior filter the assumption was made that the situation of interest is completely deterministic; i.e., both signal and clutter waveforms are known. Perhaps in the case of atmospheric noise, when the noise can be assumed a priori to be white noise, the clutter distribution and waveform can be assumed to be known. But in cases other than those where the clutter waveform is either known or can be determined, optimal filter theory

63

has a rather limited meaning simply because not enough a priori information is usually available to enable a design of the optimal linear filter configuration.

Classical optimal filter theory traditionally has been built in an atmosphere of synthesis and circuit theory, which serves to constrain solutions to relatively simple ones, however, digital solutions can be used to extend the optimal filter to more complex waveforms and transfer functions.

3. The Lee Correlation Technique

The Lee correlation technique is a periodic sampling technique which allows the removal of a non-periodic component from the presence of a periodic component. (See Reference 10.) This technique applies only to the situation where the signal or target is stationary, i.e., allows the waveforms sampled at different times to retain the same waveshape, and in addition, the clutter or noise waveform must be specified as unstationary with a zero average value. One of the requisites for this solution is that the target waveform be periodic. The latter situation can be forced by storing all backscatter returns taken periodically and forming a pseudo-periodic function which can then be processed as a continuous periodic function. This method is presented by way of demonstration to show that if the clutter is moving the signal-to-noise ratio can be identified by a simple relationship.

Consider the total incoming waveform as an additive mixture of

$$S(t) + C(t) \tag{60}$$

where again $S(t)$ represents the signal waveform and $C(t)$ represents the clutter waveform. Let us apply the definition of autocorrelation and form the expression

64

$$\phi_{11}(\tau) = \lim_{\substack{t_o \to \infty}} \frac{1}{2t_o} \int_{0}^{t_o} [S(t) + N(t)] [S(t+\tau) + N(t+\tau)] \, dt \qquad (61)$$

$$= \phi_{SS}(\tau) + \phi_{NN}(\tau) + \phi_{SN}(\tau) + \phi_{NS}(\tau) \qquad (62)$$

The first two terms of the expansion are the autocorrelations of the signal and of the noise, respectively. The function ϕ_{NN} is non-periodic and tends to zero as τ goes to infinity since a property of autocorrelation is that the autocorrelation of a random wave without a hidden periodic component tends to the square of the mean value as $\tau \to \infty$. Because of incoherence between signal and clutter waveforms, the third and fourth terms of expression (62) also vanish. As a result of these factors, the general shape of the auto-correlation function of expression (62) would appear as in Figure 27 for a periodic waveform of sinusoidal form.

The fact that the noise or clutter component of the autocorrelation tapers off to small values essentially zero and that the signal component persists on a periodic function suggests that perhaps only the periodic output function will be outputted for large values of τ.

Lee also presents a scheme utilizing cross-correlation of the periodic signal waveforms with impulses having a period equal to the period of the signal waveform. In deriving the mathematical expressions for this operation, particular emphasis will be placed here upon the use of the periodic unit impulse function $\delta(t)$. Let us look first at the fourier representation of a periodic function $f(t)$, as indicated in expression (63)

$\phi_{11}(\tau)$
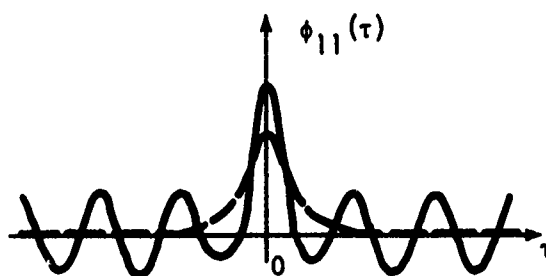
BDN-W-72-094

Figure 27. Autocorrelation Function of Sine Wave Plus Random Noise.
Dotted Curve is Component Due to Random Noise (Reference 10)

$$f(t) = \sum_{n=-\infty}^{n=+\infty} \varepsilon^{jn\omega_1 t} \; 1/t_0 \int_{-t_0/2}^{+t_0/2} f(\tau) \; \varepsilon^{-jn\omega_1 \tau} \; d\tau \qquad (63)$$

An exchange of the order of the integration and summation operations allows writing the expression in the form

$$f(t) = \int_{-t_0/2}^{+t_0/2} f(\tau) \; d\tau \sum_{n+-\infty}^{n=+\infty} 1/t_0 \; \varepsilon^{jn\omega_1 (t-\tau)} \qquad (64)$$

The fourier series for the periodic unit impulse function can be written in the form

$$\delta(t) = \sum_{n=-\infty}^{n=+\infty} 1/t_0 \; \varepsilon^{jn\omega_1 t} \qquad (65)$$

Thus, expression (64) can be written in the alternate form

$$f(t) = \int_{-t_0/2}^{+t_0/2} f(\tau) \; \delta(t-\tau) \; d\tau, \qquad (66)$$

which, except for a factor of $1/t_0$ is a convolution integral which expresses the periodic function as a convolution of a periodic unit-impulse function of the same frequency with itself. Because $\delta(t)$ is a symmetric function, the integral expression (66) is equivalent to the cross-correlation expressed in (67).

$$1/t_0 \; f(t) = 1/t_0 \int_{-t_0/2}^{+t_0/2} f(\tau) \; \delta(\tau-t) \; dt \qquad (67)$$

Since $f(t)$ and $\delta(t)$ are both periodic and have the same period, (67) may be written over an infinite interval rather than over one period

$$\frac{1}{t_o} f(t) = \lim_{t_o \to \infty} \frac{1}{2t_o} \int_{-t_o}^{+t_o} f(\tau)\ \delta(\tau-t)\ d\tau \tag{68}$$

Now write the cross-correlation of the signal plus clutter waveform $S(t) + C(t)$ with the unit impulse periodic function

$$\phi_{11}(-\tau) = \lim_{t_o \to \infty} \frac{1}{2t_o} \int_{-t_o}^{+t_o} [S(t) + C(t)]\ \delta(t-\tau)\ dt$$
$$= \lim_{t_o \to \infty} \frac{1}{2t_o} \int_{-t_o}^{+t_o} S(t)\ \delta(t-\tau)\ dt + \lim_{t_o \to \infty} \frac{1}{2t_o} \int_{-t_o}^{+t_o} C(t)\ \delta(t-\tau)\ dt \tag{69}$$

The first term is by (67) $1/t_o\ S(t)$.

On the other hand, the second term in (69) may be interpreted as the average of an infinite series of values of $C(t)$ which are taken at intervals of t_o. The randomness of $C(t)$ and its zero average value insure that the second term of (69) is zero. Thus, the cross-correlation of the periodic unit impulse waveform with a waveform whose components are a periodic plus a random one results in the periodic pulse as output.

This operation can be carried out physically rather simply by periodically sampling the composite waveform at a large number of points each separated by a time t_o equal to the period of the periodic component. (In the pseudo-periodic case the sampling period would simply be the data sampling rate or range cell repetition rate.) Then determine the output waveform by averaging the data taken with a phase shift of τ. This method is illustrated in Figure 28.

68

$$f(\tau) = \sum_{n=1}^{N} \frac{f(\tau + nT)}{n+1}$$
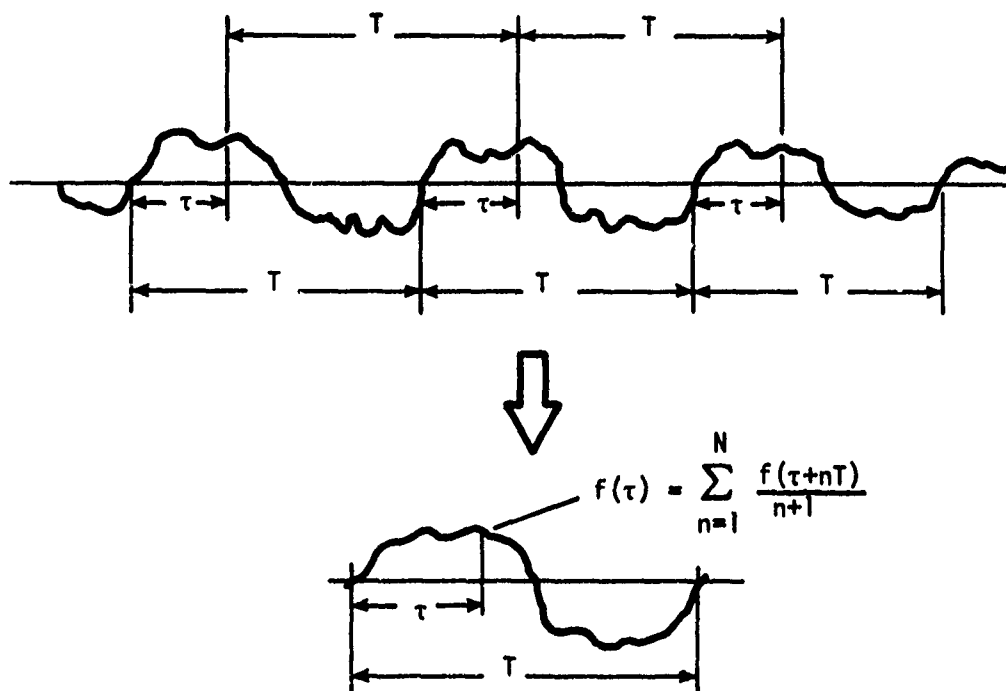
BDM-W-72-094

Figure 28. Illustration of Sampling a Periodic Signal Plus Noise

Having determined the functional value for a delay of τ, the procedure is repeated on subsequent sections of the pseudo-periodic function with an adjustment in τ to reflect other values of the return.

The signal-to-clutter ratio is easily determined if the original assumptions of the problem are met. Computing the variance of the values $f(nt_o+\tau)$, it is evident that since the periodic component contributes equal values for arguments of $t = nt_o + \tau$, its contribution to the variance is zero. Therefore, the variance of the output is equal to that of the random or clutter contributed component

$$\sigma_f^2 = \frac{1}{n}\, \sigma_c^2 \tag{70}$$

Alternatively, the rms value of the output noise is given by $\sigma_c/(n^{1/2})$, where n is the number of sample points. σ_c is the autocorrelation of the clutter for a zero argument.

Since in this method, the ideal output is the periodic component S, let S^2 be the square of the periodic component. Then the output signal-to-clutter ratio is

$$\frac{S^2}{c^2} = \frac{S^2 n}{\sigma_c^2} \tag{71}$$

This result is interesting because it shows that for clutter moving relative to the target signal of interest the signal-to-clutter ratio is proportional to the sample size n. Here again, but for the moving clutter condition, we have demonstrated that an almost infinite signal-to-noise ratio may be theoretically achieved (for an infinite number of samples). This approach is more attractive than the others, as it assumes no detailed information of the clutter. As mentioned earlier, this one was presented for information only, as the problem at hand is the signal detection for a fixed randomly spaced clutter environment.

70

4. Signal-to-Clutter Output Relationship for a White Noise Matched Filter

Under this section we will develop the signal-to-clutter ratio relationship for a filter whose impulse response is the time image of the desired signal to be detected. No consideration will be made in the filter for a general clutter source; hence the filter is essentially the well known white noise matched filter. The process is then, in effect, the autocorrelation for the signal and cross-correlation for the clutter.

In order for the autocorrelation process to occur when a signal $S(j\omega)$ is present, the filter's frequency and time response must have the form of

$$H(j\omega) = S(-j\omega) \, \epsilon^{-j\omega t_o}$$

and (72)

$$h(t) = S(t_o - t)$$

where t_o is a delay that allows $h(t)$ to be zero at $t = 0$.

When a signal appears at the input to the filter, the filter's output response will be

$$S_o(j\omega) = S(j\omega) \, H(j\omega) = |S(\omega)|^2 \, \epsilon^{-j\omega t_o} \tag{73}$$

The transfer into the time domain of this function can be shown to be the combination of the signal with its time displaced image or

$$S_o(t) = \int_0^t S(t_o - \tau) \, S(t - \tau) \, d\tau \tag{74}$$

To prove that this is identical to an autocorrelation process let

$$x = t - \tau \tag{75}$$

and expression (74) becomes

$$S_o(t) = \int_0^t S(x) \, S[(t_o - t) + x] \, dx \tag{76}$$

71

The maximum value of an autocorrelation function occurs when the argument is zero or, in the case of expression (76), $t = t_o$. It will have a value of

$$S_o(t=t_o) = \int_o^{t_o} s^2(x)\ dx \tag{77}$$

which is the mean square of the power of $S(t)$.

When the clutter $C(j\omega)$ arrives, the filter's output is then

$$C_o(j\omega) = H(j\omega)\ C(j\omega) = S(-j\omega)\ C(j\omega)\ \epsilon^{-j\omega t_o} \tag{78}$$

The time response for this result is the same as for (76) except interchanging $C(x)$ for $S(x)$; hence it gives

$$C_o(t) = \int_o^{t_o} C(x)\ S[(t_o-t) + x]\ dx \tag{79}$$

which is the cross-correlation between the signal and clutter.

For the general clutter case where the clutter may be random, we must work with the clutter's power density spectrum $\Phi_o(\omega)$

$$\Phi_o(\omega) = \Phi_i(\omega)\ |S(j\omega)|^2 \tag{80}$$

The signal-to-clutter power ratio (see expression (44)) may then be expressed using expression (77) and the implied transform of (80).

$$\frac{s^2(Max)}{C_o(t)^2} = \frac{\left[\int_o^{t_o} S(x^2)\ dx\right]^2}{\frac{1}{2\pi}\int_{-\infty}^{\infty} |S(j\omega)|^2\ \Phi_i(\omega)\ d\omega} \tag{81}$$

This ratio and the ratio formed by expressions (77) and (79) will be used in the later computations.

72

Notice if the input clutter is a series of impulses of amplitude C and a density of K clutterers per second, $\Phi_i(\omega)$ becomes a constant in expression (81), therefore, leaving the form of expression (73). But this expression was shown to be identical to (77). The resultant signal-to-clutter ratio is then

$$\frac{S_o^2(Max)}{C_o(t)^2} = \frac{1}{KC^2} \int_0^{t_o} S^2(x) \, dx \tag{82}$$

which is the solution for the matched white noise filter.

5. Signal-To-Clutter Output Relationship for the Optimal Filter Criteria

The optimal filter based upon maximizing the signal-to-clutter power was derived under Section B.2 of this chapter and shown to be (notice that $|C(j\omega)|^2$ has replaced $R(\omega)$),

$$H(j\omega) = \frac{S(-j\omega) \, \epsilon^{-j\omega t_o}}{|C(j\omega)|^2} \tag{83}$$

See expression (59). We shall now develop the signal-to-clutter output expression in order to facilitate later calculations.

When the signal $S(j\omega)$ appears, the output from the filter will be

$$S_o(j\omega) = S(j\omega) \, H(j\omega) = \left| \frac{S(j\omega)}{C(j\omega)} \right|^2 \epsilon^{-j\omega t_o} \tag{84}$$

which is the signal-to-clutter ratio of the power densities. Let us define the function

$$F(j\omega) = \frac{S(j\omega)}{C(j\omega)} \tag{85}$$

Expression (84) can then be written as

$$S_o(j\omega) = F(j\omega) \, F(-j\omega) \, \epsilon^{-j\omega t_o} \tag{86}$$

73

which has a time domain solution of

$$S_o(t) = \int_o^t f(x) \, f[(t_o-t) + x] \, dx \tag{87}$$

similar to the form of (76). The maximum value of (87) occurs at the time $t = t_o$ or

$$S_o(t=t_o) = \int_o^{t_o} f^2(x) \, dx \tag{88}$$

Consider next the clutter performance through the filter. For a clutter input $C(j\omega)$, the filter's output is

$$C_o(j\omega) = C(j\omega) \, H(j\omega) = \frac{S(-j\omega)}{C(-j\omega)} \, \varepsilon^{-j\omega t_o} = F(-j\omega) \, \varepsilon^{-j\omega t_o} \tag{89}$$

However, when signal-to-clutter ratios are formed, the assumption is that the average clutter power is sought. This may be achieved by taking the magnitude squared of expression (89). Then

$$|C_o(j\omega)|^2 = |F(j\omega)|^2 \tag{90}$$

It can be shown that this function transformed into the time domain has a value of

$$\frac{1}{2\pi} \int_{-\infty}^{\infty} |F(\omega)|^2 \, \varepsilon^{j\omega t} \, d\omega = \int_o^{t_o} f^2(t) \, dt = \overline{C_o^{\,2}(t)} \tag{91}$$

Then the signal-to-clutter ratio is shown by expressions (88) and (91)

$$\frac{S_o^{\,2}(\text{Max})}{\overline{C_o^{\,2}(t)}} = \frac{\left[\int_o^{t_o} f^2(x) \, dx\right]^2}{\int_o^{t_o} f^2(t) \, dt} \tag{92}$$

But the numerator and denominator integrals are the same; hence,

74

$$\frac{S_o^2(\text{Max})}{\overline{C_o^2(t)}} = \int_o^{t_o} f^2(t) \, dt \qquad (93)$$

The signal-to-clutter ratio for the optimal filter is then the mean of the square of $f(t)$ (which is the ratio of the signal-to-clutter). This result will be applied in the determination of the best filter for signal-to-clutter rejection in randomly spaced fixed clutter.

Notice if the clutter density is allowed to take on the value of KC^2, the output from the filter will be identical to the white noise filter of expression (82).

At this point the tools for performing the analyses to come have essentially been developed. We shall now concentrate upon applying them to the scattering geometries of interest.

C. CORRELATION TECHNIQUES AS APPLIED TO CLUTTER REJECTION

Under this section we shall investigate the signal-to-clutter enhancement that may be achieved using a white noise matched filter both for an idealized impulse and rectangular excitation. The principal target and clutter scatterers will be spheres of various sizes, and the model used in the analysis will be the approximate one of Figure 12.

The investigation will begin by considering one target and one clutterer in order to determine the peak ratio of the signals. Later this will be followed by investigating the effect on the signal-to-clutter ratio as a function of many clutterers.

1. White Noise Matched Filter Performance for Detecting a Large Target Sphere in the Presence of a Clutter Sphere

a. Case I - Idealized Impulsive Interrogator

Figure 29 indicates a configuration for an active filter which utilizes a generator that forms a waveform like that of the scattered impulse response

75
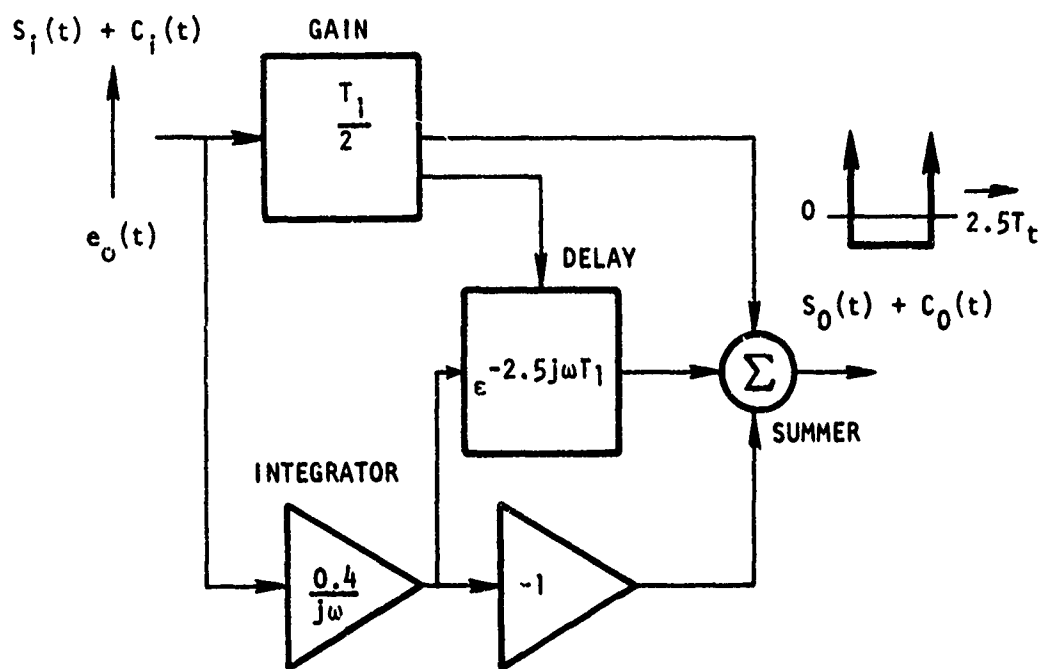
Figure 29. Sphere Approximate Impulse Generator

$e_o(t)$ of a given sphere (see Figure 12).

Recall that essentially a matched-filter may be considered as a transfer function which performs an autocorrelation. This configuration is an optimal matched filter when the noise or clutter is white or gaussian, but for the moment let us look at its response characteristics as a detection tool. When the input $S_i(t)$ and transfer impulse responses are identical, the output is a maximum. On the other hand, when the input is clutter, which may be characterized by one or more small spheres in this example, the waveform will be unlike that of the target sphere and thus the correlator output will be less than the maximum value of the matched case. An amplitude threshold detector at the output completes the sphere discriminator and thus detects the presence of the large target sphere by comparing the cross-correlator maximum output with the known autocorrelation value.

The impulse response of a "matched filter" correlator of this type should be the time reverse of the desired signal, but for the case where the impulse response of the scatterer is symmetrical, then the processes of correlation and convolution are functionally equal and the result will be the same. This principle will be used in calculating the filter's output time response.

The filter for detecting the target sphere depicted in Figure 29 contains an integrator, a delay network, and a gain term. The gain $T_{1/2}$ and delay $2.5T_1$ are adjusted for the response corresponding to the sphere size one is seeking.

Let us look at the output of this filter for the two cases, matched and unmatched spherical backscatter input.

Since the impulse response has been shown to be symmetrical, then the process can be represented by convolution. Then convolving expression (15), in the manner shown in expression (76), for the impulse response of a sphere

77

of parameter T_1 with itself gives the white noise matched filter output response of

$$\delta(t)_{\text{Matched}} = \frac{T_1^2}{4} \left[\delta(t) + 2\,\delta(t-2.5T_1) + \delta(t-5T_1) \right]$$
$$-0.4[u(t) - u(t-5T_1)]$$
$$+\frac{1}{6.25} \left[u(t)\,t - 2u(t-2.5T_1)\,(t-2.5T_1) \right.$$
$$\left. +u(t-5T_1)\,(t-5T_1) \right] \tag{94}$$

Recall that T_1 represents the ratio of the sphere's diameter to velocity of free space propagation.

Figure 30 shows the output waveform of the matched correlator for this matched input case (expression 94).

For comparison, Figure 31 shows the waveform which would be produced with an idealized sphere backscatter input waveform, but here the sphere scattering the radiation is smaller than that for which the filter is matched. This small sphere might represent a single clutter object, of size T_2 for example.

This result was obtained by convolving expression (15) for two different values of T.

In the unmatched case, the four impulses increase in size as the product of the sphere sizes $(T_1 T_2 = \frac{d_1}{v}\,\frac{d_2}{v})$. The solid negative portion of the waveform's duration is proportional to the diameter of the smaller sphere T_2; however, the amplitude of the undershoot remains constant for all $T_1 \gg T_2$. Size discrimination information is in the waveform and this information can be achieved by measuring the interval between the impulses, which is $2.5T_2$ or $2.5\frac{d_2}{v}$, a function of the unknown sphere's diameter. As the size of the target sphere goes to zero, the amplitude and duration of the filter output waveform goes to zero.
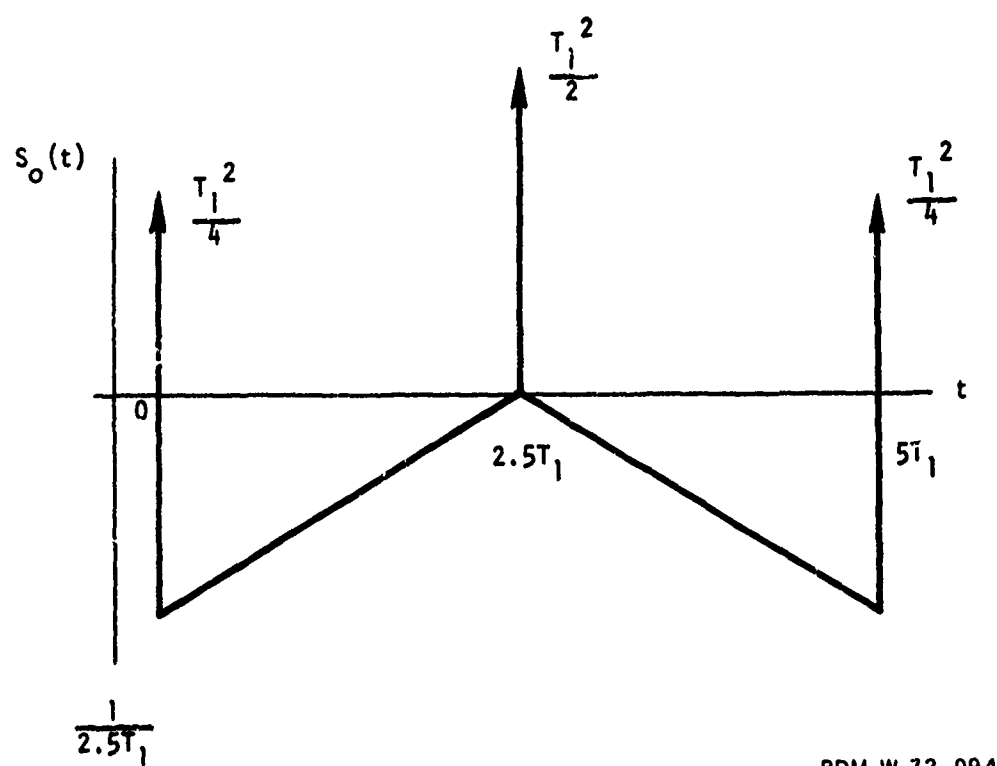
Figure 30. "Matched Filter" Correlator Output Waveform with Input
(Sphere Idealized Response)

BDM-W-72-094

79
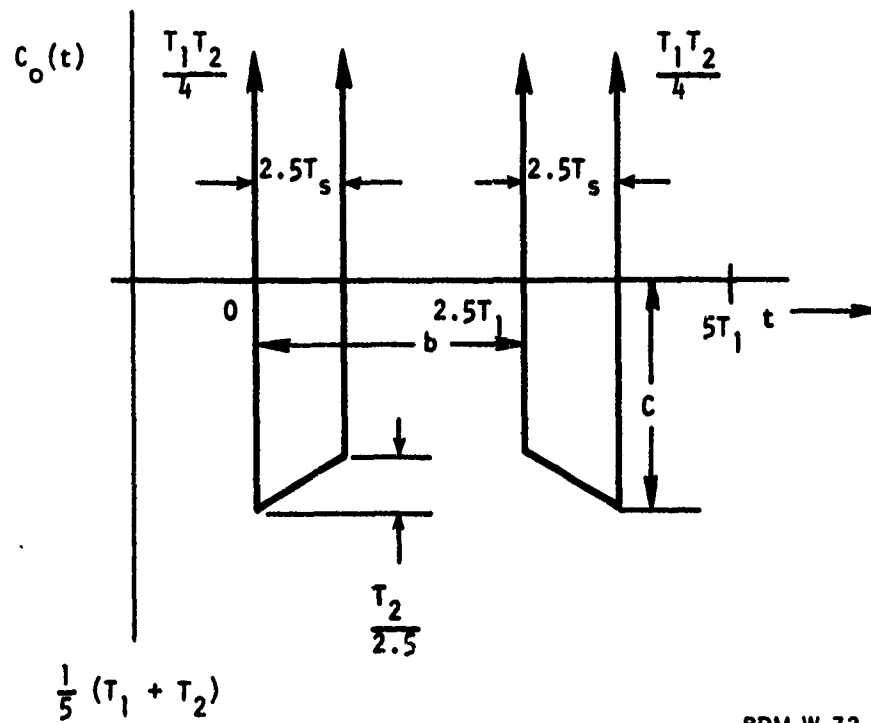
Figure 31. "Matched Filter" Correlation Output Waveform with Unmatched Input

BDM-W-72-094

Figure 32 traces the growth of the parameters of Figure 31 as a function of the sphere ratios as the filter's waveform evolves into the matched waveform of Figure 30. Plot (a) indicates that as T_2 approaches T_1 the spacing (represented by the letter "b" on Figure 31) approaches a value of $2.5T_1$. Plot (b) shows the variation of impulse height values, and (c) indicates the variation of the undershoot magnitude. Notice in Figure 32b that when the sphere sizes are identical the amplitude abruptly doubles. This is the amplitude of the matched case for the center pulse.

In the case where the target sphere is greater in size than that for which the filter is matched, the output amplitude again increases in direct proportion to that sphere's diameter, but the variables T_1 and T_2 in Figure 31 are interchanged.

Let us now calculate the enhancement that is possible from input to output in the signal-to-clutter ratio. Since only one clutter sphere is present (more will be handled later), the ratio is essentially that of voltage rather than power. It will also be shown in the section to follow that the amplitude of the impulse, if it is given a finite width however small, is always larger than the other portions of the scattered or filter-produced waveform. The ratio will therefore be taken between the amplitudes of the impulses.

From Figure 12, the ratio of the filter inputs for a target sphere of size T_1 to a clutter sphere is

$$\frac{S_i(\text{Max})}{C_i(\text{Max})} = \frac{T_1}{T_2} \quad \text{(Filter Input)} \tag{95}$$

However, the maximum output from the filter is shown in Figure 30 for the signal and Figure 31 for the clutter to be

81
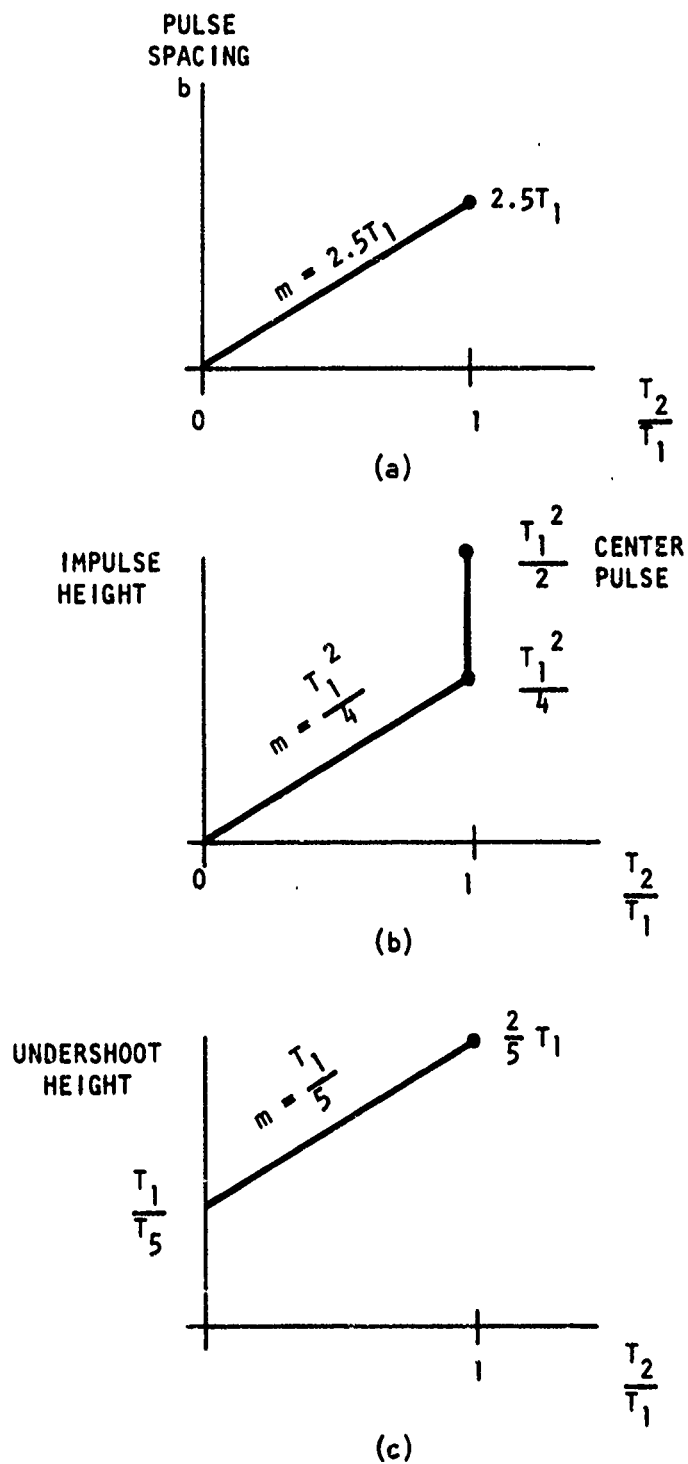
Figure 32. Variation of Critical Parameters of Matched Sphere Filter as a Function of Target to Clutter Diameter

$$\frac{S_o(\text{Max})}{C_o(\text{Max})} = \frac{T_1{}^2/2}{T_1{}^2/4} = 2\frac{T_1}{T_2} \qquad (96)$$

The enhancement that can be achieved by this filter from the input to the output is the ratio of (96) and (95) or a factor of two in voltage or four in power. Notice also that the ratio is independent of the sphere sizes, making this filter undesirable as a clutter rejection filter where the excitation is impulse-like. The ratio may be expressed in dB as

$$dB = 20 \log_{10} 2 = 6 \text{ dB} \qquad (97)$$

We shall next look at the same filter where the excitation is pulse-like rather than an impulse to see if there is any advantage gained.

b. **Case II - Finite Pulse Width Interrogator Waveform**

Consider an interrogating pulse to the spherical scatterers of the form shown in Figure 33. The scattered response from a spherical target can be obtained by time displacing a sphere's step response (Figure 17) and subtracting the waveforms. Figure 34 shows the resultant waveform.

The output response for the filter's signal matched case may be obtained by convolving or cross-correlating (same process since the functions are symmetrical) the matched filter's output with the rectangular pulse's autocorrelation function. Figure 33a shows the autocorrelation of the pulse and expression (94) gives the matched filter's output. Figure 35 shows a sketch of the response for a narrow pulse width τ. Figures 36 through 39 plot the filter's output as the interrogating pulse width τ is increased. Notice that its output is of the autocorrelating form as expected. Figure 40 is a plot of the maximum values of the output as τ is increased and it shows a peaking of the output for $\tau = 1.75\,T_1$. The crest amplitude time varies according to the pulse width as is shown in Figure 35 and the series.

(a) INTERROGATING PULSE

(b) PULSE'S AUTOCORRELATION
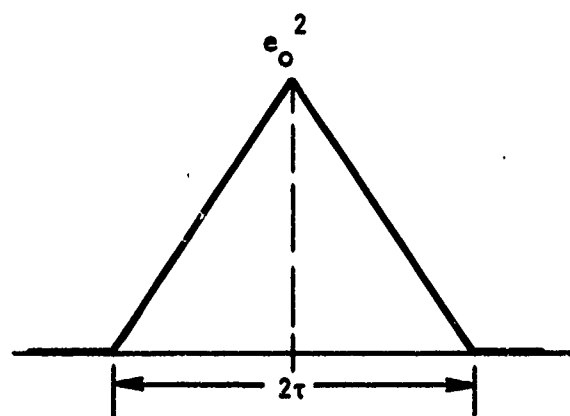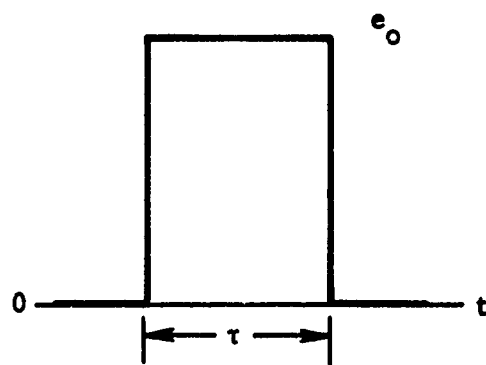
BDM-W-72-094

Figure 33. Finite Pulse Width Interrogation Waveforms

84
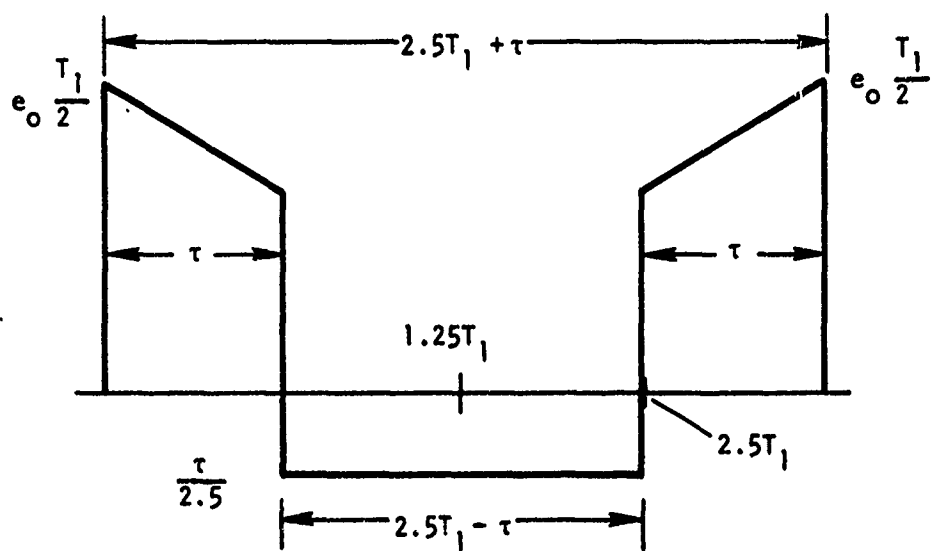
Figure 34. Approximate Sphere Pulse Scattering Response
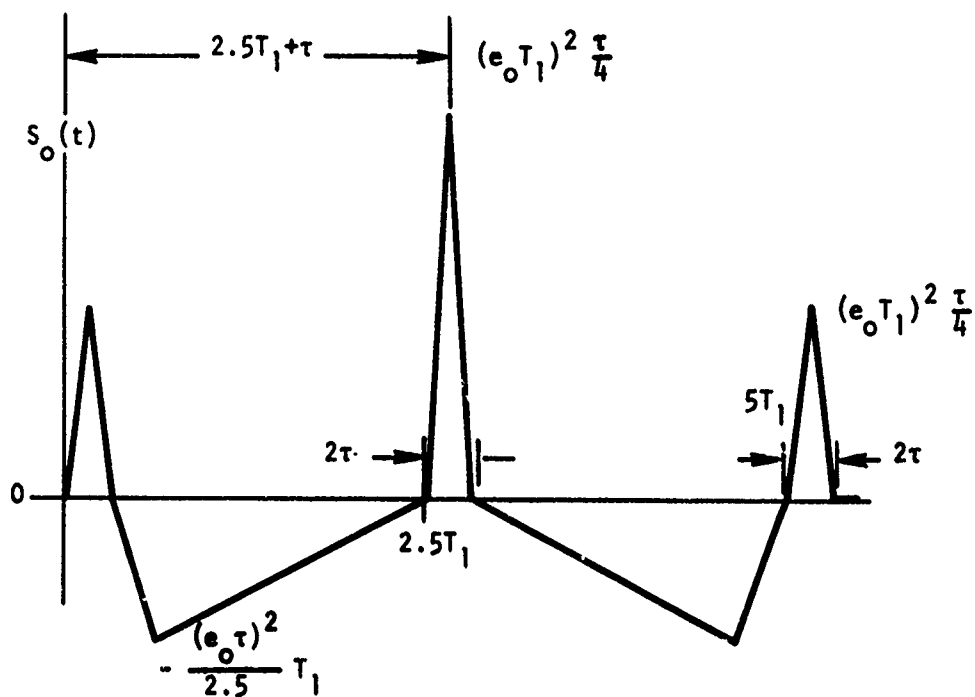
Figure 35. Matched Filter Output Waveform for a Narrow Pulse Interrogator
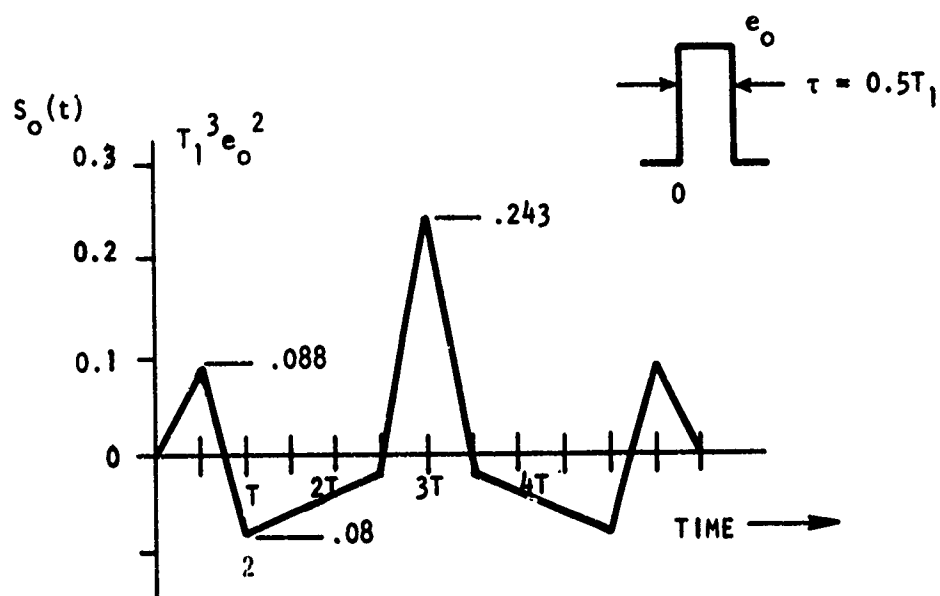
Figure 36. Matched Filter Output, Pulse Width Input $\tau = 0.5T_1$
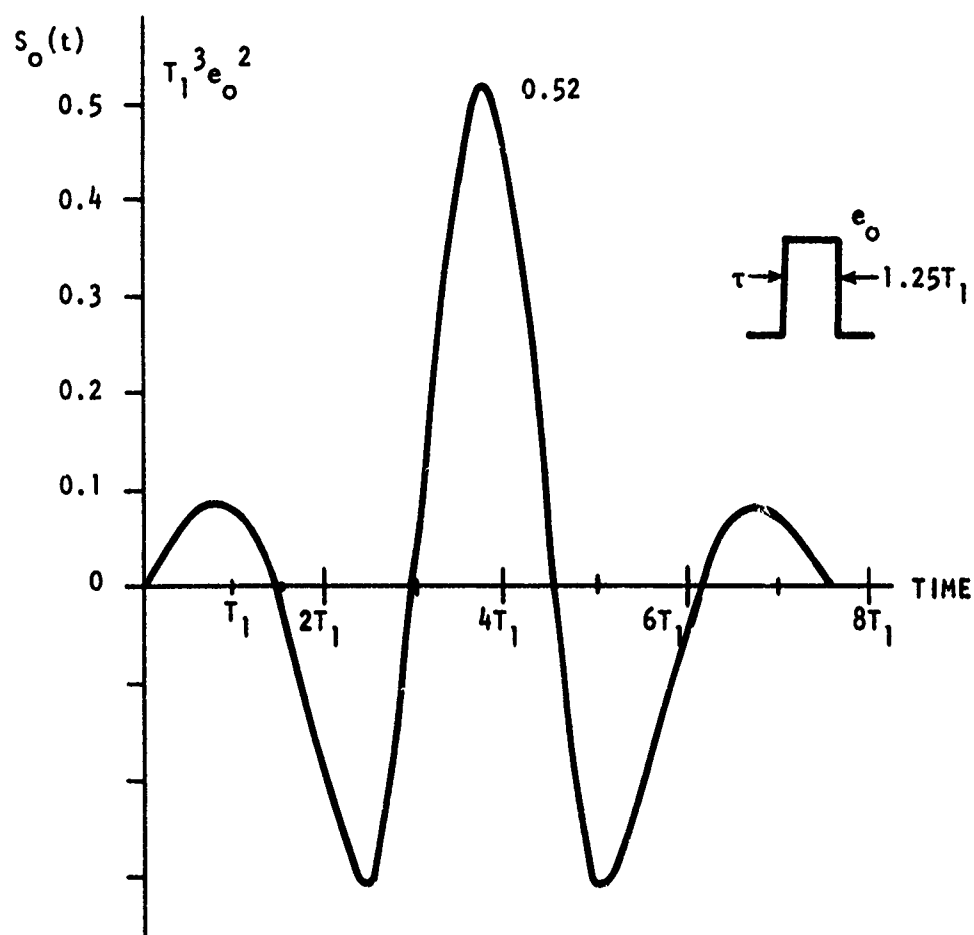
Figure 37. Matched Filter Output, Pulse Width Input $\tau = 1.25T_1$
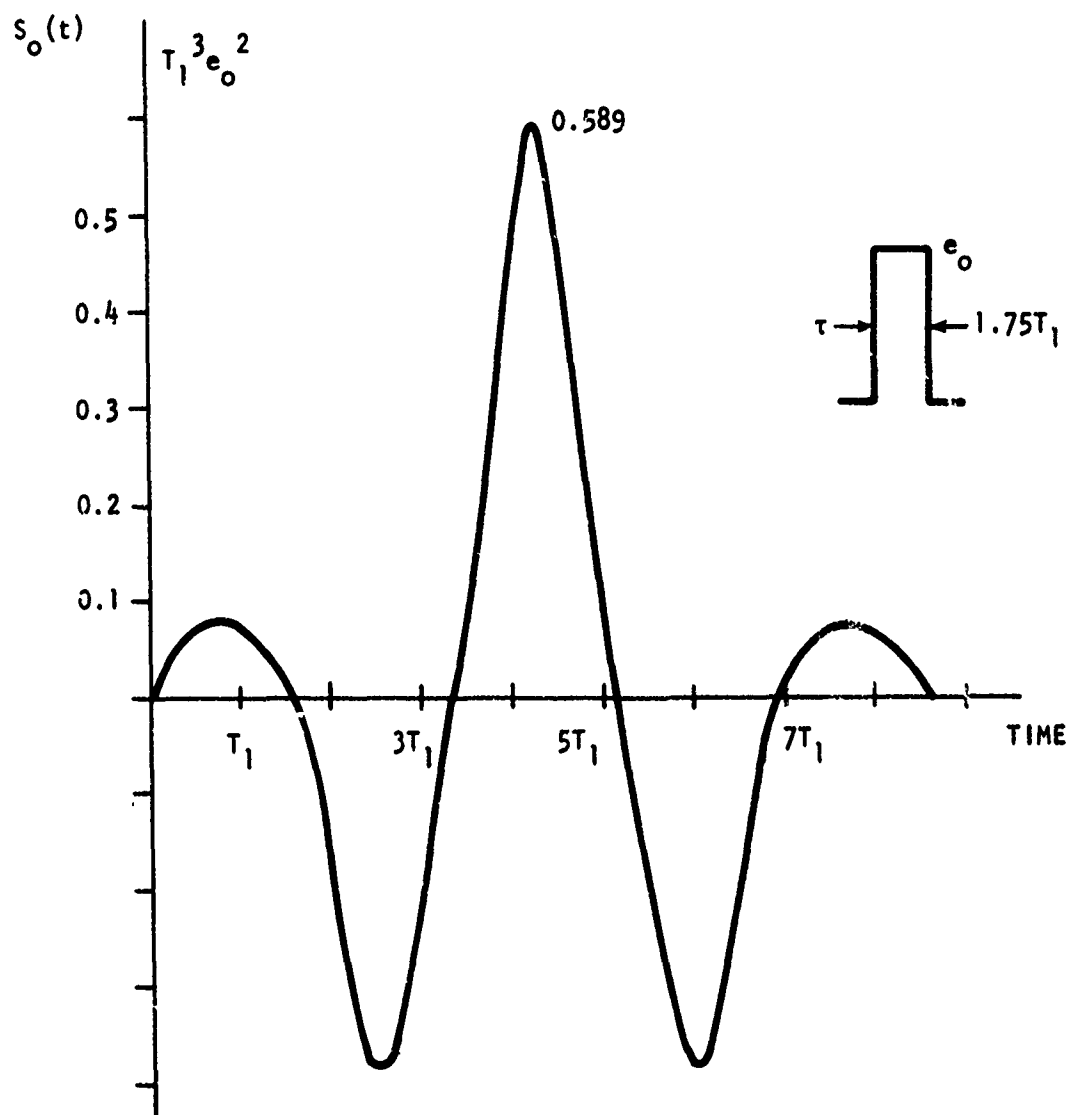
Figure 38. Matched Filter Output, Pulse Width Input $\tau = 1.75T_1$
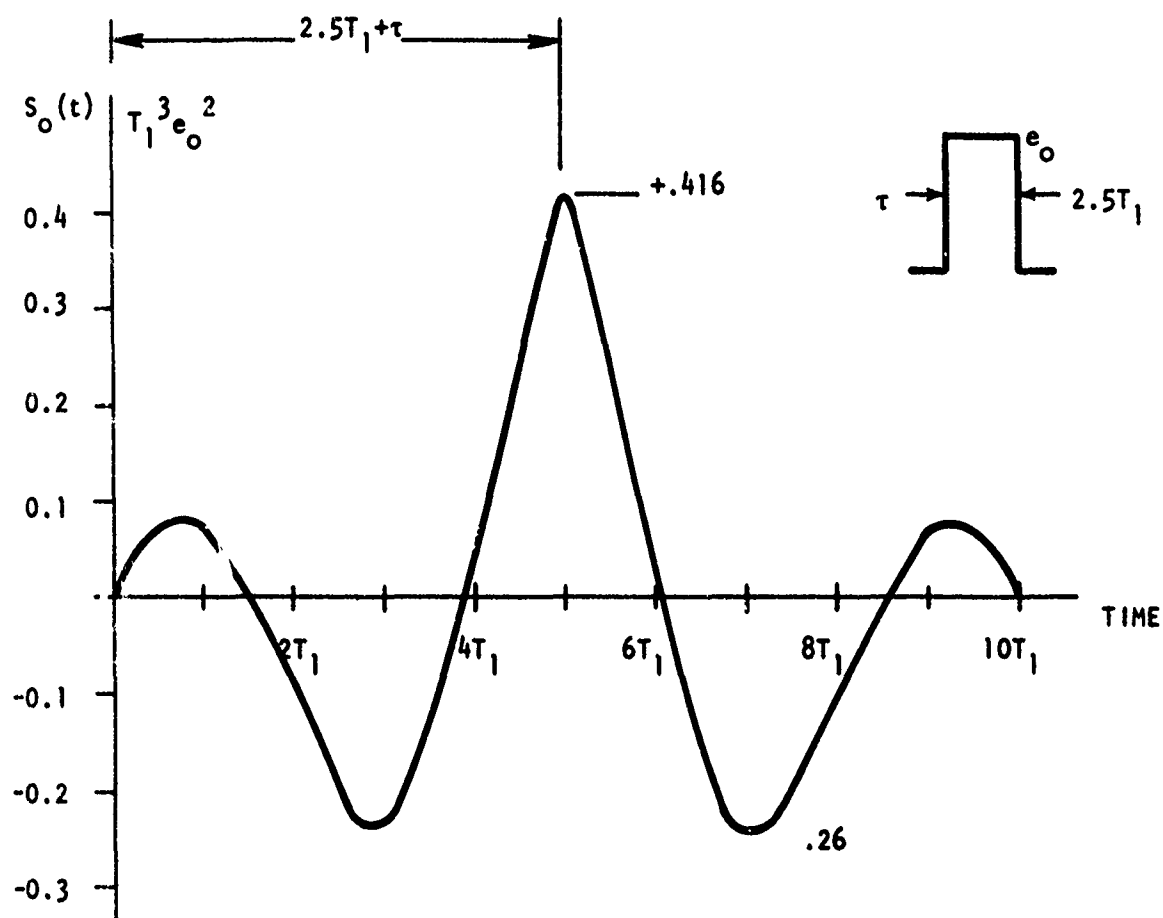
BDM-W-72-094

Figure 39.   Matched Filter Output Pulse Width Input $\tau = 2.5T_1$
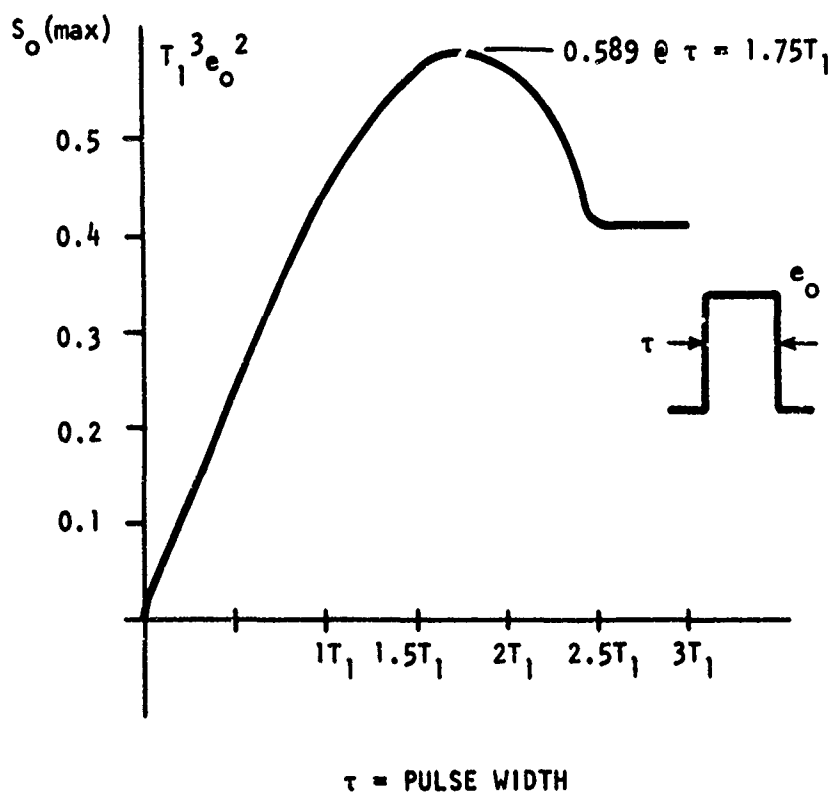
BDM-W-72-094

Figure 40.   Matched Filter Maximum Output as a Function of
Interrogator Pulse Width

BDM-W-72-094

91

We are now in a position to calculate the possible clutter rejection effect of using a pulse interrogater. The input signal-to-clutter amplitude, as can be seen by Figure 34, can be obtained by applying the proper designation for T. Then

$$\frac{S_i(Max)}{C_i(Max)} = \frac{T_1}{T_2} \qquad \text{(Filter Input)} \qquad (98)$$

because the crest amplitudes in the figure are not affected by τ up to 2.5T. The result obtained is the same as for the impulse excitation case.

The maximum filter output was shown in Figure 40 to be

$$S_o(Max) = 0.589\ T_1^3\ e_o^2 \qquad \text{at} \quad \tau = 1.75T_1 \qquad (99)$$

Now, in the case of a small sphere as clutter, one can show that if T_2 is less than τ, which will be the case for small clutter, the filter's output will be the convolution of a ramp and the expression used to construct Figure 31. The ramp is the early time portion of Figure 33b since all of the action will take place (for a small sphere scatterer) prior to reaching the time τ. The maximum value of the filter's output for this case is

$$C_o(Max) = 0.306T_2^2\ T_1\ e_o^2 \qquad \text{at} \quad t = 1.25T_2 \qquad (100)$$

The ratio of the two is then

$$\frac{S_o(Max)}{C_o(Max)} = 1.88\left(\frac{T_1}{T_2}\right)^2 \qquad \text{for} \quad T_1 >> T_2 \qquad (101)$$

which is an encouraging value over that of the impulse interrogator [see expression (102)], because the filter's output increases with the sphere's ratio squared.

The filter enhancement in signal-to-clutter ratio over its input value is obtained by the ratio of expressions (102) and (98) as

$$\frac{S_o(Max)/C_o(Max)}{S_i(Max)/C_i(Max)} = 1.88\left(\frac{T_1}{T_2}\right) \quad \text{for} \quad T_1 >> T_2 \qquad (102)$$

The relationship shows that the enhancement increases linearly as the ratio of sphere and clutter diameters for voltage and as the square for power.

The question may be asked regarding the cause of this enhancement. The answer will lead to a filter class investigation to be performed later. The cause is due principally to the attenuation of the clutter signal as can be seen by comparing expressions (99) and (100). The reason is that since the clutter is smaller than the target and the pulse duration τ, its response is essentially over during the excitation interval τ, as caused by the pulse's autocorrelation function of Figure 33b. This being the case, the driving function to be applied to the filter's impulse clutter response (Figure 31), in order to obtain the filter's clutter pulse output, is a ramp function. This is the key, since a ramp is generated by an impulse exciting a double integrator. Therefore, in effect, the clutter's high frequency content is attenuated by the $1/\omega^2$ character which is indicative of a low-pass filter. Later in this study we shall investigate the low-pass filter as a clutter rejection filter.

The result that has been obtained is quite interesting, since no consideration was made to match the filter to the clutter's performance, as in the case of the optimal filter. Speaking of the optimal filter, it will be shown that its output signal-to-noise ratio is independent of the type of interrogater waveshape used, because a ratio is taken between the signal and

93

clutter in forming the matched filter, therefore dropping out the driving function.

Another interesting aspect of this filter is that when the clutter size is small compared to the signal size for which the filter is matched, it will produce an output, for a rectangular pulse, that approaches the impulse response of the filter. Actually three impulse responses will occur, each displaced by the pulse's duration, where the one at $2.5T_1$ will be twice that of the others and of opposite polarity. The amplitudes of these pulses could further be reduced if the exciting pulse did not have such a sharp rise time. Reducing the rise time amounts to adding more low pass filtering.

The dB enhancement for this filter may be described as

$$dB = 10 \log \left[1.88 \frac{T_1}{T_2} \right] \quad T_1 >> T_2 \tag{103}$$

for the single target and clutter case. We shall consider the multi-clutter case next.

2. Multiple Clutter Input to the White Noise Matched Filter

Under this section we shall investigate the signal-to-clutter ratio out of the white noise matched filter for twin conditions which are the periodically and randomly spaced clutter. The reason for investigating the periodic clutter is to determine the spacing conditions for a line of given size clutter in order to obtain the maximum possible clutter level and to determine the level. This latter determination will provide a lower bound for the signal-to-clutter ratio from a white noise matched filter.

a. Waveform - Spacing Dependence of Targets and Clutter

Often clutter is composed of many small target objects which are each interrogated individually. Because of their placement, however, the wave

94

which is returned to the radar site for detection may be composed of a composite of these individual waveforms. There are a number of constraints on the physical orientation and placement, number and range cell size which should be explored to ascertain the limitations of a detection and discrimination system.

First, define a geometry which is spherical and has the idealized waveshape indicated in Figure 41. This combination will be used to implement the investigation.

Recall that the duration of the pulse is directly related to the diameter of the sphere.

Let us consider first the placement situation indicated in Figure 42 Here the target objects are perpendicular to the direction of travel of the wavefront.

The distance D between the radar antenna and the front surface of the target objects is assumed to be much larger than the largest distance ℓ defined by the target area as seen at the receiving antenna. This constraint implies that $\alpha \rightarrow o$ and that the time differential in wave travel caused by the lengthened path P is much smaller than the time 2.5T. The range cell is defined as encompassing only the volume about the target spheres.

Because of the small value of α, the points a and b will receive the transmitted energy at the same time as seen in the 2.5T regime. Similarly, the backscatter wave components from points a and b will both be returned at the same time. Because there is no time shift in receive times, both spheres will also be subject to traveling waves which act at the same time. Thus, each sphere will scatter exactly the same waveform to be received at the receiving antenna. Of course, wave components in the same direction in space
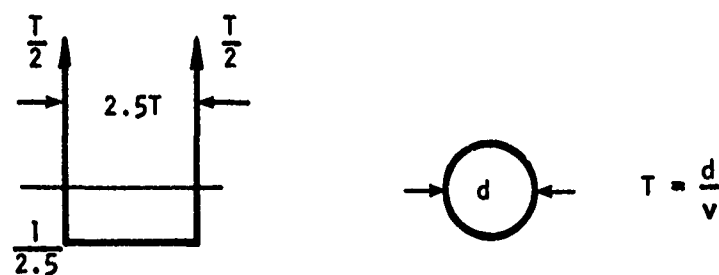
Figure 41. Geometry and Waveform of Interest in the Examples of This Section

FRONT SURFACE OF
TARGET ELEMENTS

ILLUMINATING &
DETECTION ANTENNA

WAVEFRONT

P

α

a

b

DIRECTION OF
WAVE TRAVEL

D

ℓ

RANGE
CELL
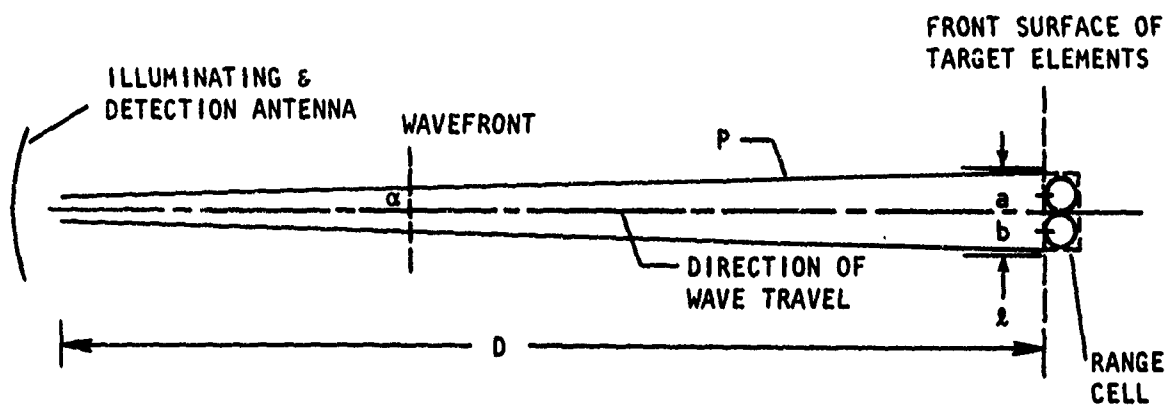
BDM-W-72-094

Figure 42.   Two Target Objects Interrogated and Scattering Broadside to the
Radar Antenna

add, as do all vector fields. Therefore, the waveform as seen at the receiving antenna will be a composite of all individual backscatter waveforms, as indicated in Figure 43.

Generalizing the situation, the waveform resulting fron n targets in the range cell will exhibit an impulse height of $\frac{nT}{2}$ and an undershoot amplitude of $\frac{n}{2.5}$. When the value of $\propto$ becomes larger with respect to the conditions set forth earlier in the discussion, the impulses, rather than adding, will be time shifted from one another in a fashion indicated in Figure 44.

In the case of targets or planes of targets which are offset from one another in depth from the radar antenna, again the backscatter from each individual object may be thought to occur independent of the others, but the resultant received waveform is a composite of all of the individual waveforms. The difference in depth will be reflected in a time shift in individual scattered waveforms resulting from a difference in the wave travel time which is equal to twice the value $\frac{\ell}{v}$, where v is the wave velocity and ℓ is the offset distance.

This situation is depicted in Figure 45a, where the range cell is defined here to encompass the volume surrounding the two spheres of interest. The resultant waveform is indicated in Figure 45b.

It is of some interest to investigate the offset depth which will produce a time delay in the second waveform which is equal to the duration of the first. This offset distance will be such that leading and trailing impulses of successive waveforms will add, thus causing the magnitude of the composite waveform to be twice the magnitude of a single target positive impulse magnitude for the two body situation.
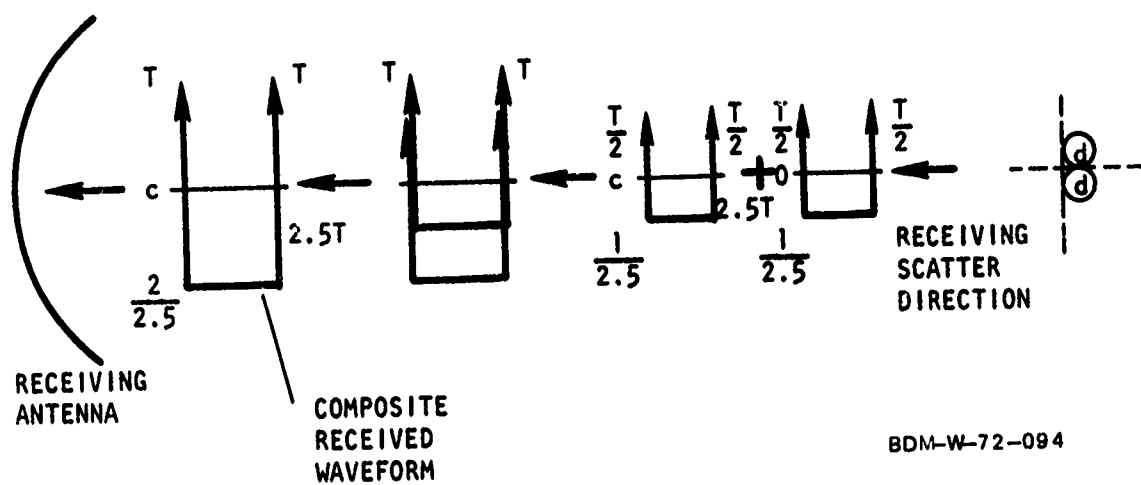
Figure 43. Waveform Resulting From Two Targets Broadsided to the Transmit/Receive Antenna
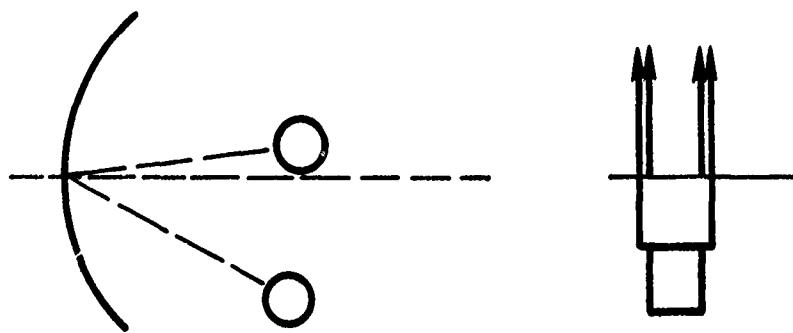
(a) TARGETS PLACED IN CLOSE
    PROXIMITY TO ANTENNA

(b) RESULTANT WAVEFORM

BDM-W-72-094

Figure 44. Waveshape Resulting From Broadside Planar Target Excitation of
            Close Proximity Objects
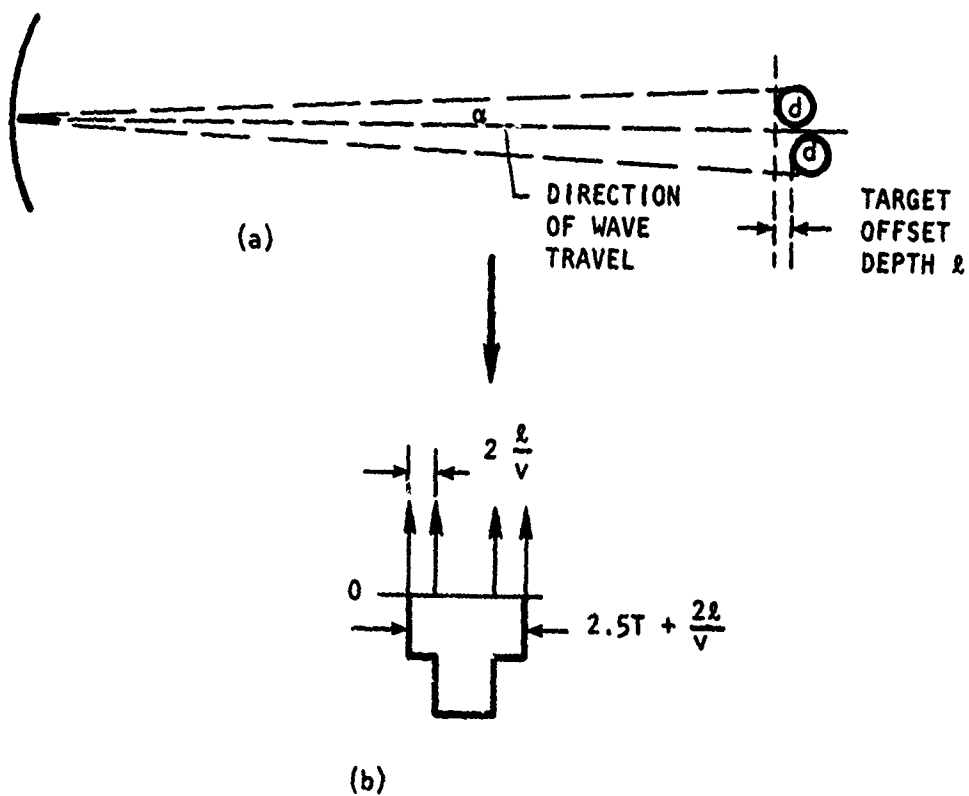
Figure 45. Two Target Spheres Offset In Depth From One Another In a
Scattering Situation

Figure 46 illustrates the composite waveform resulting from this target situation. The distance for which impulse addition due to offset occurs is computed as 1.25d between centers. Setting the impulse offset value $\frac{2\ell}{v}$ equal to the duration of an individual waveform, $2.5T = 2.5\frac{d}{v}$, the critical value of ℓ is indeed equal to 1.25d.

Having considered the effect of multiple targets in the same range cell having multiplicities in both depth and field in the antenna pattern, it is possible to predict a composite backscattered waveform, given the individual backscatter waveforms and the distance and pattern of the target objects.

As an example, consider the configuration indicated in Figure 47. The two-by-two configuration of four equal sized spheres is arranged in four layers, each a different distance from the transmit/receive antenna, and labeled with the letters c, d, e, and f, with a second layer lying upon it. Utilizing the rules developed in the preceding discussion, the waveform can be seen to evolve as a composite, indicated in Figure 47c, which has the components indicated in Figure 47b.

The worst case condition for multiple scatterers, from the prior results of two bodies, occurs when the scatterers are periodically separated by the distance $1.25d_2$; for this condition the steady state composite will be a series of positive impulses of amplitude T_2 (twice that of a single clutterer) with a constant negative amplitude of $\frac{1}{2.5}$. This result will be applied later to the calculation of periodic signal-to-clutter ratio determinations.

One of the results of this discussion has been that it is possible to predict the composite backscatter waveform from a multiplicity of objects providing their spacing is known.

(a)   (b)
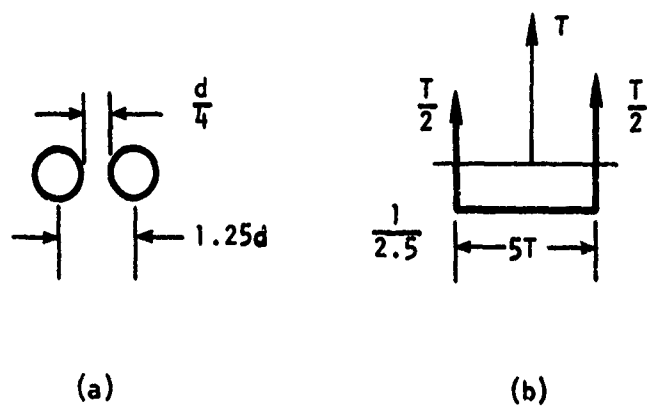
BDM-W-72-094

Figure 46. Critical Target Spacing and Waveform for Positive Impulse Addition

(a) MODEL

(b) INDIVIDUAL
CONTRIBUTIONS
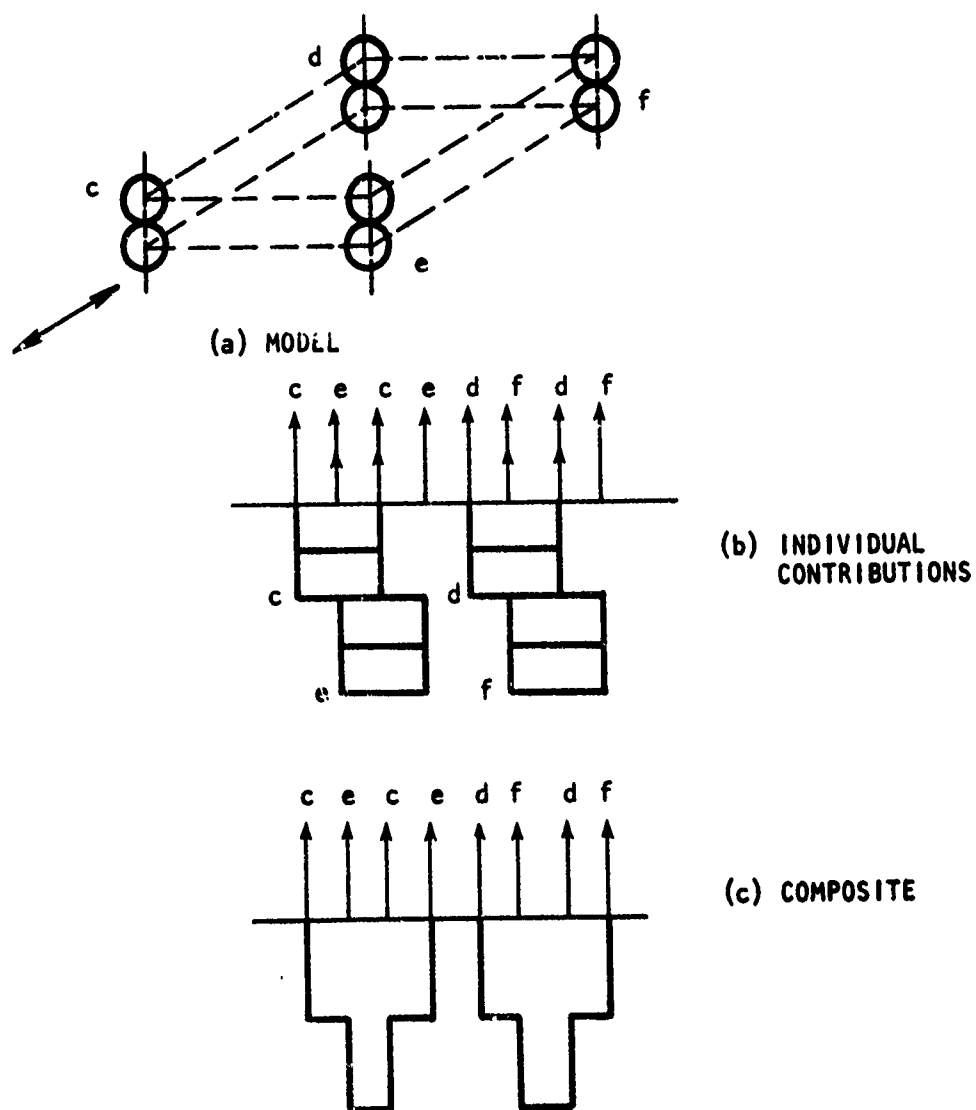
(c) COMPOSITE

BDM-W-72-094

Figure 47. Example of a Multiple Target Geometry and its Composite Waveform

A further result is a study of the limit upon the effect of range gating which the waveform duration and spacing have upon one another. Specifically, range gating (in depth), to be completely effective in separating waveforms, cannot be any more selective than the limit determined by equating the back-scatter pulse duration to twice the wave travel time differential between the two object layers.

For example, when spheres are located one behind another within a given solid angle cell, gating by blanking would be ineffective for separating waveforms for sphere spacings in the region $1.0 < \ell \leq 1.25d$ between centers, simply because waveforms overlap in a manner similar to that indicated in Figure 44b.

More detailed considerations of the constraints upon minimum target spacing and range cell and gate size with respect to the expected target waveform will be made in a later section after the requirements and techniques of target waveform discrimination have been treated in detail.

3. Maximum Matched Filter Output Resulting From Multiple Clutter Spheres

Continuing the discussion regarding waveforms associated with multiple target and clutter objects, this section specifically treats the white noise matched filter of Section C. That is, a filter matched to a waveform from a large sphere which has as its input the composite waveform from many smaller spheres.

The spacing between positive impulses from the output of a target-matched filter excited by a single clutterer was shown to be as indicated in Figure 48 (see Figure 31).

From the figure, it can be seen that when the clutter spheres are within the same solid angle cell one behind another, the impulses of the backscatter

105
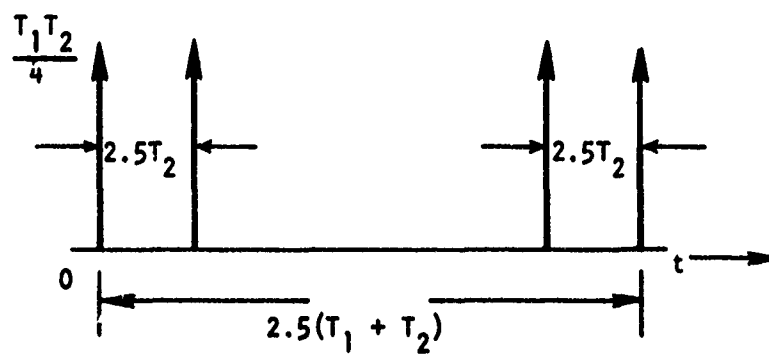
Figure 48. Impulse Spacing for Non-Matched Case-Matched Filter

BDM-W-72-094

waveform can be made to add if the spacing is made such that the waveform from the second sphere is delayed for a time equal to $2.5T_2$. The offset distance between centers can be computed for this case by letting $\frac{2\ell}{v} = 2.5T_2$. Then the offset distance ℓ is calculated as $1.25\, d_2$, as was indicated in the previous section. For the condition $\frac{T_1}{2} = T_2$ (or the clutter diameter is half that of the target) the maximum positive value will add to a maximum value of four times that of one positive impulse, as indicated in Figure 49, as an output from the filter. (This case causes the impulses of Figure 48 to be equally spaced.) Notice that the negative portion of Figure 49 becomes a constant negative level. This occurs by adding the underswing of Figure 31 for each clutterer.

Note that the positive maximum amplitude occurs at the end of the filter's output for a single sphere, which represents a time delay of $t' = 2.5(T_1 + T_2)$ and has an amplitude equal to four times that produced by a single clutterer.

In the case where $T_2 = \frac{T_1}{4}$, it is shown that for a spacing $\ell = 2.5T_2$ the same time delay is required before the positive maximum is reached. This case is documented in Figure 50. The contribution of an infinite number of spheres, each spaced $\ell = 1.25\, d_2$ between centers from the next, with $T_2 = \frac{T_1}{4}$ will also be equal to four times the positive impulse magnitude of a single sphere of the same size. A minimum of six spheres in line are required to provide this output, which again occurs at a time equal to the pulse width of a single sphere.

In the case where the spacing is not equal to the periodic $\ell = 1.25d_2$, the maximum amplitude of the output waveform will be less.

In general then, the minimum number N of T_2 sized spheres in line, spaced $\ell = 1.25d_2$ between centers, required to provide a maximum cross-correlation
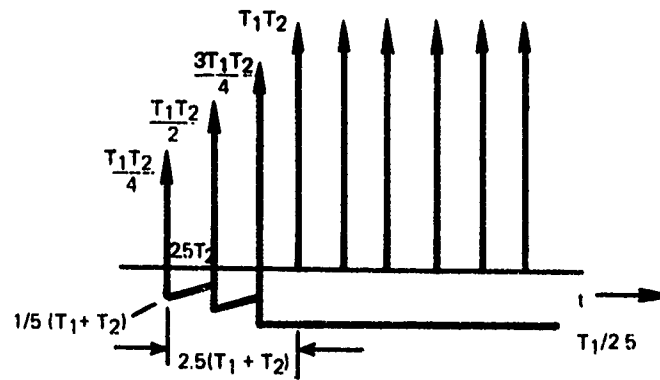
BDM-W-72-094

Figure 49. Matched Filter Output for $\ell = 1.25\ d_2$ Sphere Spacing, $T_2 = T_1/2$
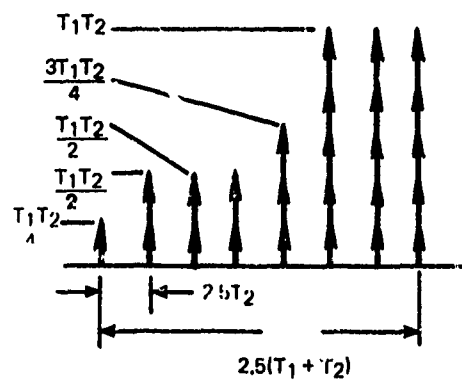
BDM-W-72-094

Figure 50. Matched Filter Output for $\ell = 1.25\ d$, Sphere Spacing $T_2 = T_{1/4}$

filter output of $T_1 T_2$ amplitude is given by

$$N = 2 + \frac{T_1}{T_2} \tag{104}$$

and this maximum will first occur at the time

$$t' = 2.5[T_1 + T_2] \tag{105}$$

After this time there will occur constant amplitude periodic impulses of $T_1 T_2$ spaced $2.5T_2$ in time, plus a constant level negative amplitude of $T_1/2.5$.

The significance of the preceding discussion is that the output from a matched filter, with a periodic sphere clutter input, will be limited to a positive maximum of no more than four times that of a single clutter body, and that the negative maximum for this same configuration can be less than twice that of a single clutter body when the clutter bodies are smaller than the sphere to which the filter is matched.

We are now in a position to determine the enhancement that the white noise filter will provide for impulse-like periodically spaced or excited clutter. The peak input clutter amplitude condition was shown for clutter periodically spaced at intervals of $2.5T_2$ to be T_2. For a target sphere amplitude in this clutter of $\frac{T_1}{2}$, the peak filter input signal-to-clutter ratio is then

$$\frac{S_i(Max)}{C_i(Max)} = \frac{1}{2} \frac{T_1}{T_2} \tag{106}$$

Notice that this periodic condition has only reduced the peak amplitude signal-to-clutter ratio by a factor of two over that of the non-periodic case. (See Expression 95.)

Let us now represent the clutter in the classic form as an average power value over a given interval. (See expression [44].) Since the clutter is

periodic, the average value irrespective over the interval taken (provided it incompasses complete cycles) is the same as that of a single cycle. The average value for the clutter is then

$$\overline{c_i^2} = \frac{1}{2.5T_2} \int_0^{2.5T_2} \delta_s^2(t) \, dt \tag{107}$$

where $\delta_s(t)$ is the impulse response of one clutter sphere as given by (15). In order to perform this calculation and avoid complications, let us assume that the interrogating pulse to the clutter is finite having a very narrow width τ and an amplitude e_i. Then

$$\overline{c_i^2} = e_i^2 \, \tau \left[\frac{T_2}{2.5} + \frac{\tau}{6.25} \right] \tag{108}$$

where the first term in the bracket is the impulse contribution and the second the undershoot. If we allow τ to approach zero or $T_2 \gg \tau$, then only the impulse contribution remains.

The classic signal-to-clutter ratio in power is then (apply 108 with the square of the signal's crest amplitude for a narrow pulse interrogation).

$$\frac{S_i^2(\text{Max})}{\overline{c_i^2}} = \frac{2.5}{4} \frac{T_1^2}{T_2 \tau} \tag{109}$$

If one is willing to accept the definition of the signal-to-clutter ratio as specified above, then the value would approach infinity as τ goes to zero.

Consider next the filter's output signal-to-clutter ratio for the periodic clutter model where the clutterers are spaced $2.5T_2$ apart. It was shown that the filter's output, for clutter, will have the same shape as the input except that the impulse amplitudes will be $T_1 T_2$. Since we are now working with a

pulse of finite width but very small, this modifies the clutter response from that shown in Figure 49 to that of Figure 51. This response can be obtained by convolving the pulse shown in Figure 33b with the impulse train of Figure 49. Performing the integration over a cycle of the figure as directed by expression (107) gives the filter's average clutter power of

$$\overline{C_o^2} = e_i^4 \, T_1^2 \, \tau^3 \left[\frac{T_2}{3.75} + \frac{\tau}{6.25} \right] \qquad (110)$$

The maximum signal-to-clutter ratio then follows from the crest signal amplitude of Figure 9 squared and $\overline{C_o^2}$ or

$$\frac{S_o^2(\text{Max})}{\overline{C_o^2}} = 0.235 \, \frac{T_1^2}{T_2 \tau} \qquad (111)$$

The filter enhancement then follows from the ratio of the filter's output to input signal-to-clutter ratio (expression [108] and [110]) or

$$\frac{S_o^2(\text{Max})/\overline{C_o^2}}{S_i^2(\text{Max})/\overline{C_i^2}} = 0.375 \qquad (112)$$

The result shows that the signal-to-clutter ratio is actually reduced by using the matched white noise filter, where the clutter is periodically spaced in a single line, and where the interrogation is impulse-like. The reduction is essentially a factor of two and one half or -8 dB.

If this same ratio is performed only on the basis of amplitude rather then average power, the filter's output signal-to-clutter ratio from Figures 35 and 51 is

$$\frac{S_o(\text{Max})}{C_o(\text{Max})} = \frac{1}{4} \frac{T_1}{T_2} \qquad (113)$$
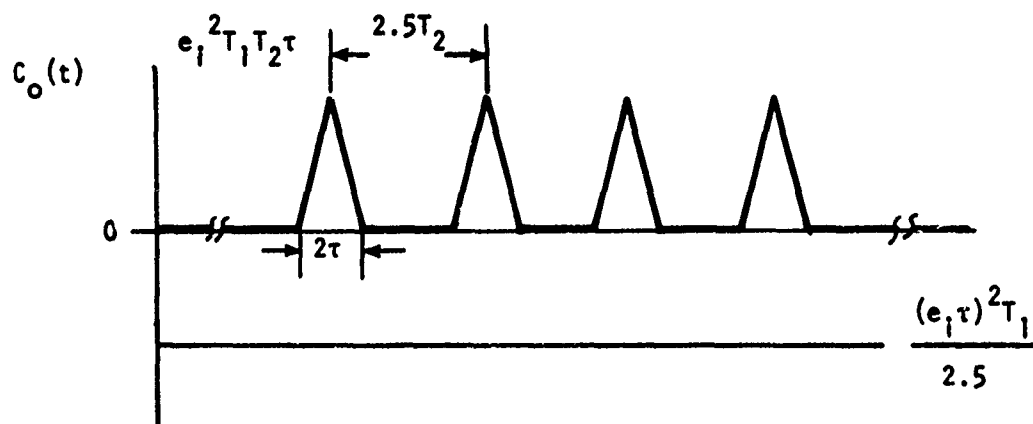
Figure 51. Steady State Matched Filter Clutter Output

BDM-W-72-094

113

and the input signal-to-clutter ratio is given by (107) or the ratios are,

$$\frac{S_o(Max)/C_o(Max)}{S_i(Max)/C_i(Max)} = 0.5 \tag{114}$$

This represents a six-dB degradation.

We have just shown that the white noise matched filter does not provide clutter rejection for a periodic return from clutter for impulse integration.

We shall next consider, as in this case, periodically spaced clutter, however the excitation will be pulse-like rather than an impulse. It is of interest to determine if by varying the pulse's width whether the clutter may be reduced or made to disappear.

a. Clutter Rejection for Periodically Spaced Spherical Clutter That Is Pulse Excited

Earlier it was shown that impulse excited spherical clutter periodically spaced 1.25d/c apart produced a periodic clutter response consisting of impulses and a constant negative level. This behavior applied as an input to the white noise matched filter produced a similar steady state output as shown in Figure 49. The last section, Section 2, showed that the presence of the white noise matched filter only served to reduce the signal-to-clutter ratio between the input and output. Here we will now consider the same conditions except that the matched filter is removed and replaced by a filter that causes out of phase total cancellation. This can also be accomplished with a rectangular pulse interrogation.

Consider a filter that has a $1/\omega$ frequency response (an integrator) and pass the periodic signal through it. The output will then be periodic and have a time waveshape as shown in Figures 17 or 19 depending upon the approximation selected. Now if the integrator is followed by a delay network, a polarity reversing amplifier, and a summer as shown in Figure 52, the clutter may be
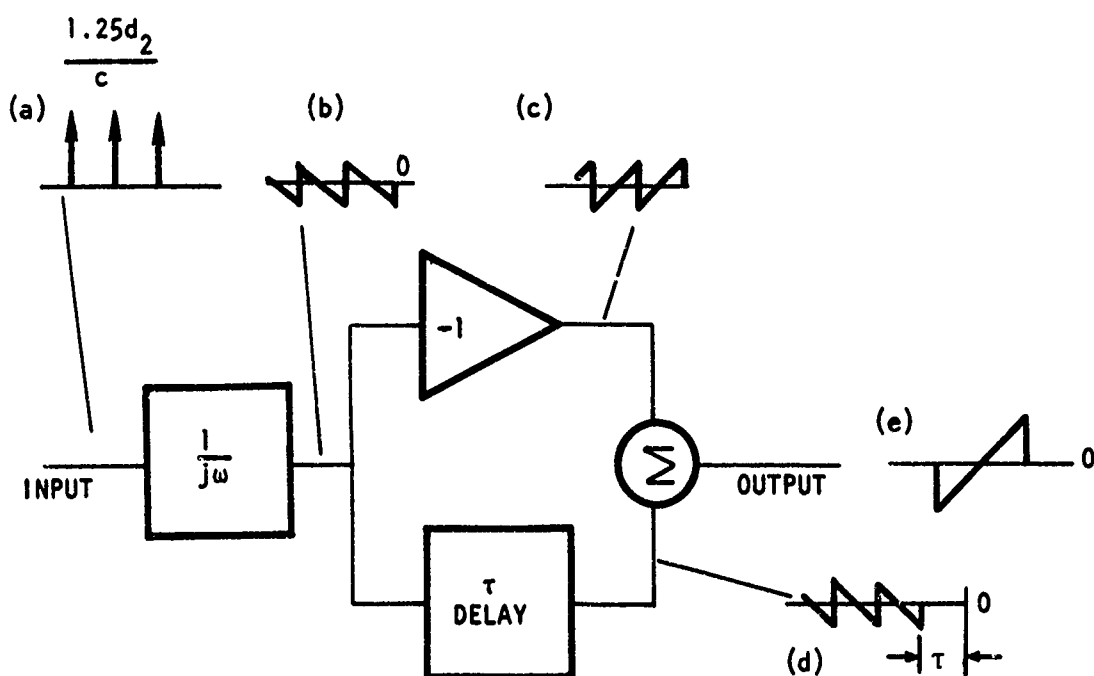
Figure 52. Filter For Periodically Spaced Clutter Rejection

made to go to zero. This is accomplished by adding the clutter out of phase with itself, the delay being multiples of $\tau = n(1.25d_2/c)$. This arrangement would then provide an infinite target to clutter ratio as there will be no clutter. Of course the next question is what happens to the signal through this filter. If the target is much larger than the clutter and the delay is for $n = 1$, the output will be the target's scattered response not its integral. This occurs because the output will be derivative-like, however, the input was integrated, hence, cancelling it and returning the input function.

This discussion applies equally well to the condition where the interrogating pulse is rectangular and has a duration equal to $\tau = n (1.25d/c)$. The same result will occur as produced for the impulse interrogator and the filter of Figure 52. When $n = 1$ in the delay time, then for a large target relative to the clutter, the pulse will appear as an impulse; hence it will scatter the targets' response not its integral.

It has been demonstrated that for periodic clutter that either a filter of the form of Figure 52 where the interrogating pulse is an impulse or the interrogating pulse is rectangular and of a proper duration, then an infinite signal-to-clutter ratio can be achieved.

There remains one more test for the white noise matched filter and that is for the condition where the clutter spheres are randomly spaced. This will be the subject of the next section.

b. Clutter Rejection for Randomly Spaced Clutter

Lee has shown (Reference 10) that a train of randomly spaced pulses each having the same time waveshape $f(t)$ and being Poisson distributed, will have an average power of

$$P_{ave} = k \int_{o}^{t_o \to \infty} f^2(t) \, dt \qquad (115)$$

116

where $k = n/t_o$ the average number of pulses expected over the interval t_o. The above expression applies both for the same sign and alternately positive and negative pulse cases that we will consider. The reason is that for the positive pulse case generally one must consider the dc component in the calculation. Since the scattering does not contain a dc component it need not be considered.

We may now return to the previous investigations of the matched filter and consider the random aspect. For the impulse excitation case of C.1.a it was shown that no enhancement in clutter rejection will occur between the input and output using the matched filter for a single input. One can argue rather easily that the randomness of the signal will not alter the condition. Let us continue next to the finite pulse condition of C.1.b.

Figures 33 and 34 show the expected responses for a pulse-type excitation of a target sphere. The crest input signal value squared is then

$$S_i^2(\text{Max}) = \left(\frac{e_o T_1}{2}\right)^2 \qquad (116)$$

The clutter response for the case where the individual clutter size is smaller than the target can be shown to consist of two phases of the form of Figure 17 but displaced in time by τ the exciting pulse width. These shapes occur because the pulse essentially integrates the clutter's scattering response. (The second pulse will be the negative of the first due to the discontinuance of the pulse.) Notice that for each excitation pulse two scattering pulses occur. This, of course, will increase the average power.

Performing the operation described by expression (115) on the above function provides an average input power of

$$\overline{C_o^2} = \frac{1}{6.4} k T_2^3 e_o^2 \qquad (117)$$

117

The input signal-to-clutter power ratio is then from expression (116) and (117),

$$\frac{S_i^2(\text{Max})}{\overline{C_o^2}} = \frac{3.2}{kT_2}\left(\frac{T_1}{T_2}\right)^2 \tag{118}$$

This result indicates that the ratio is squared for the power consideration case which it should be since the voltage is only the ratio. (See expression [98].)

Now for the output signal-to-clutter determination, expression (99) provides the crest value squared of the signal from the filter. The average clutter determination requires considerable more effort and an outline for obtaining it follows. Since the filter's impulse response is symmetrical (it is like Figure 34) and the clutter waveshape is also symmetrical than the filter's output may be expressed as the product of the two functions in the frequency domain or (see expression [22]).

$$C_o(j\omega) = \left(\frac{T_1 T_2}{2}\right)^2 \frac{(j\omega)^4[1-\varepsilon^{-j\omega\tau}]^2}{(s+\alpha_1)^2(s+\alpha_2)^2} \tag{119}$$

Since we are interested in the average power, operating on $C_o(j\omega)$ as indicated in expression (120)

$$P_{\text{ave}} = \overline{C_o^2} = \frac{k}{2\pi}\int_{-\infty}^{\infty} |C_o(j\omega)|^2 \, d\omega \tag{120}$$

gives

$$\overline{C_o^2} = 0.122 \, k \, T_1^2 T_2^5 e_o^2, \text{ for } T_2 << T_1 \tag{121}$$

The signal-to-clutter ratio may then be formed for the output as

$$\frac{S_o^2(Max)}{\overline{C_o^2}} = \frac{(0.589\,T_1^3)^2\,e_o^2}{0.122\,k\,T_1^2 T_2^5 e_o^2} = \frac{2.95}{k\,T_1}\left(\frac{T_1}{T_2}\right)^5 \tag{122}$$

The overall filter enhancement is then the output to input signal-to-clutter ratio or expression (122) over (118). Hence,

$$\frac{S_o^2(Max)/\overline{C_o^2}}{S_i^2(Max)/\overline{C_i^2}} = 0.92\left(\frac{T_1}{T_2}\right)^2 \tag{123}$$

We observe for the power ratio case of a random clutter model that the enhancement goes as the ratio of the sphere sizes squared.

We have demonstrated under Section C that the signal-to-clutter ratio is larger for a pulse rather than an impulse excitation (by an additional power in the ratio) when applied to a white noise matched filter. This suggests that preceding the matched filter by a low-pass filter enhances the clutter rejection. We shall pursue in the section to follow various low pass and matched filter combinations.

D. LOW PASS AND INTEGRATION SCHEMES FOR CLUTTER MINIMIZATION

1. <u>System Philosophy</u>

Having studied some simple geometries and their associated impulse excited backscatter waveforms in an earlier section of this document, it is possible now to make some general conclusions regarding the relationships between size and waveform parameters which will help in the formulation of yet another detection scheme.

The first generalization is that the amplitude of the waveform from a single scatterer is a function of its size. The second is that the composite

wave amplitude of n objects in the same cell is limited to a finite value.
Finally, the duration of the backscatter pulse in time is a function of its
size, the larger objects having larger durations than the smaller objects of
the same class.

These wave characteristics suggest a number of detection techniques,
some of which have been considered in previous sections.

Here the primary interest, however, is in the frequency content of the
target and clutter waveforms as a possible means of sifting the two com-
ponents from one another. Qualitatively, one would expect small objects
having short duration waveforms to be composed primarily of high frequency
components and, on the other hand, large objects having long duration wave-
forms to be constituted primarily of lower frequency components in the fre-
quency spectrum.

These characteristics make filtering by selecting passbands of target
interest a possible means of rejecting the clutter waveform component while
retaining the components which are desirable and emanate from the target of
interest.

One characteristic which this process possesses, and one which is
desirable, is that it acts as a smoothing process. For example, waveforms
which possess sharp spikes like those of the idealized impulses of the
approximations utilized here, are more difficult to successfully process
utilizing some of the proposed discrimination schemes, as will be noted in
a later section. However, a smoothing process such as the integral process
makes it possible to more successfully process these types of waveforms. One
reason for this facility is that smoothing makes the waveforms more readily
adaptable to digital processing in the time domain.

120

2. Integration Followed by Low-Pass Filtering

This two stage process represented by integration and low-pass filtering was chosen primarily because smoothing of the impulses in the sphere impulse response, as well as of other known responses is desirable since it provides a much smoother waveform which is more tenable both in terms of processing but also in terms of mathematical tractability.

A signal processing scheme utilizing this filter scheme is envisioned in Figure 53.

The a priori knowledge of the target of interest enables the selection of an appropriate sized range cell and range gate interval which is inspected for appearance of a waveform. The waveform $S_i(t) + C_i(t)$ enters the clutter detector package which, in this case smooths and filters all high frequency components from the waveform. From this package the desired output is a clutter free waveform which enters the discriminator or identification package for processing. The resultant output is a logic statement which identifies the geometry.

Let us examine the detector package in greater detail to ascertain its effectiveness in clutter discrimination. Here the individual clutter body will be modeled as a small sphere of diameter d_1 and the target will be modeled as a large sphere of diameter d_2. Because of its tractability, the approximation to the impulse response indicated in Figure 20 will be used in this section.

Now if expression (20) were integrated and then convolved with the time domain expression for the low-pass filter configuration, it can be shown that the overall filter's output performance may be described as

121
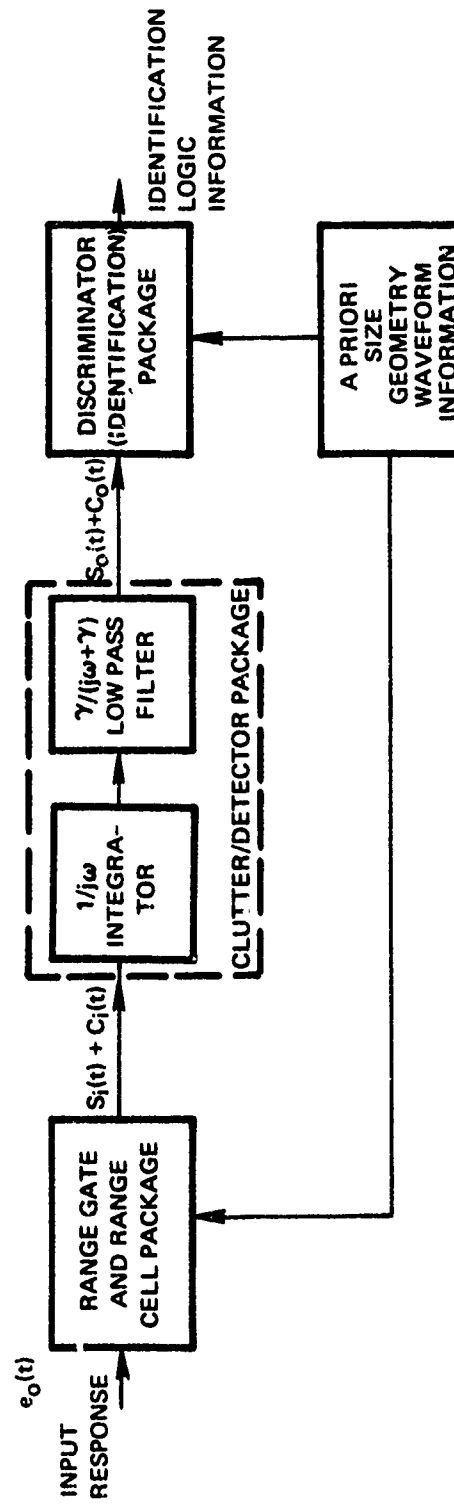
Figure 53. A Signal Processing Scheme Utilizing Low-Pass Filtering & Integration for Detection in the Presence of Small Sized Clutter Bodies

BDM-W-72-094

122

$$S_o(t) = \frac{T/2}{\sqrt{1+(\beta/\gamma)^2}} \left\{ \left[\cos\left(\beta t - \tan^{-1} \beta/\gamma\right) - \frac{1}{\sqrt{1+(\beta/\gamma)^2}} e^{-\gamma t} \right] u(t) \right.$$

$$\left. + \left[\cos\left(\beta(t-2.5T) - \tan^{-1}\beta/\gamma\right) - \frac{1}{\sqrt{1+(\beta/\gamma)^2}} e^{-\gamma(t-2.5T)} \right] u(t-2.5T) \right\} \tag{124}$$

As before T is the ratio d/c, γ is the filter's cutoff frequency and $\beta = 2\pi/5T$. This expression applies equally as well to the case when the clutter is present by allowing T to take on the clutter dimension.

Figure 54 shows $S_o(t)$ plotted for a range of β/γ ratios. The waveforms resulting from low β/γ ratios are passed relatively unaltered. On the other hand, waveforms which have associated with them high β/γ values are shown to be highly attenuated and altered in shape. We wish to take advantage of this effect in order to reject the clutter. Note that the individual clutter in general is smaller than the target hence the large β/γ ratio will prevail.

It is of interest to determine the relationship that establishes the maximum value of $S_o(t)$ as a function of β/γ. This can be obtained by classical techniques and it will be found to be

$$S_o^-(\text{Max}) = \frac{\pi}{5\beta} \bullet \frac{1}{[1+(\beta/\gamma)^2]} [1+\varepsilon^{-\gamma\pi/\beta}] \tag{125}$$

for β large and γ small. This crest value is negative and it occurs at the time $t = \pi/\beta$. See Figure 54 for a plot of the negative maximum of $S_o(t)$ as a function of β/γ, (point C).

There also occurs a positive maximum that shifts to the right as a function of β/γ. In the limit as β/γ goes to infinity, the crest value will center about the time $t = \pi/2\beta$ shown as point B in the figure. For the limit, for large values of β/γ the amplitude approaches a value

$$S_o^+(\text{Max}) = \frac{\pi}{5\beta} \left(\frac{\gamma}{\beta}\right) \tag{126}$$
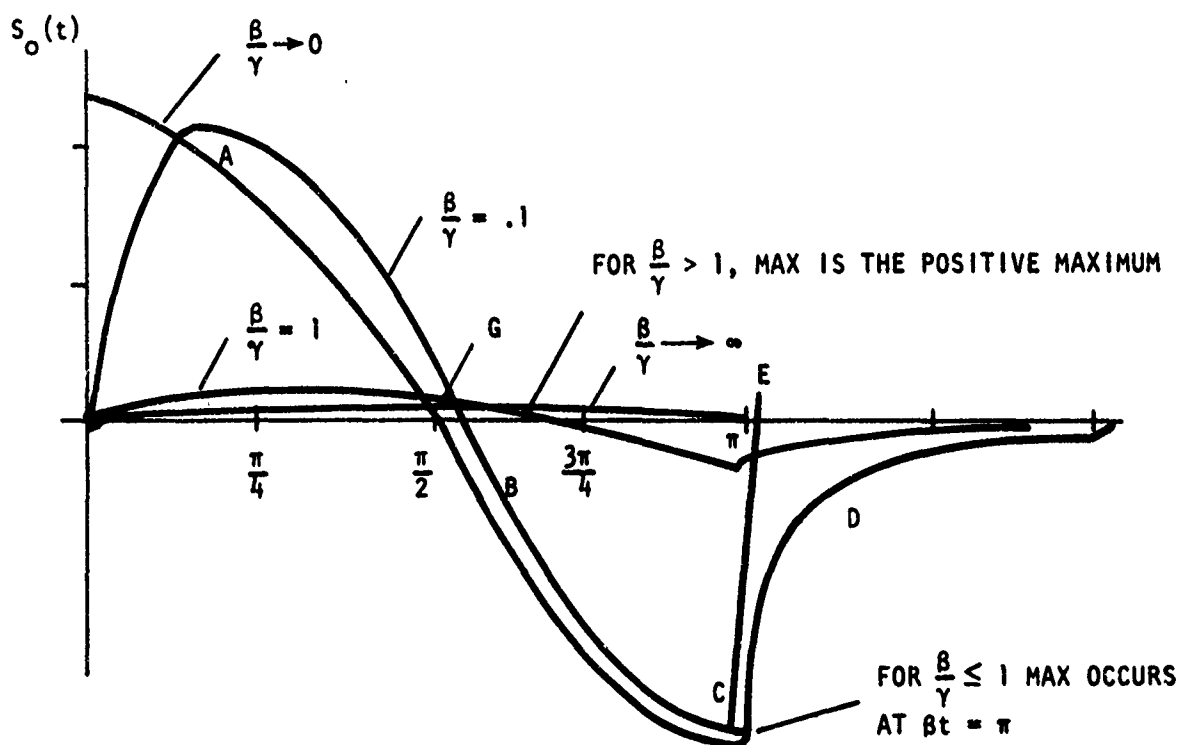
Figure 54. Integrator - Low Pass Filter Output as a Function of $\frac{\beta}{\gamma}$

Figure 55 shows a plot of this positive crest amplitude for a range of values.

Before proceeding to the signal-to-clutter calculation, let us dwell for a moment on Figure 54. Notice for the case where $\beta/\gamma = 0.1$ the waveshape is essentially the integral of the scattered sphere response (see Figure 19) with a slight distortion. Now for $\beta/\gamma \gg 1$, not only does the amplitude diminish but the shape changes. This suggests that one select a value of $\beta_1/\gamma = 0.1$ for the signal to be detected and hopefully the clutter's β_2/γ is very large which in general will be the case for small clutter.

Let us now calculate the signal-to-clutter ratio for the filter arrangement of Figure 53 for the conditions as stated in the prior paragraph ($\beta_1/\gamma = 0.1$ and $\beta_2/\gamma \gg 1$). The amplitude ratio of 155 and 156 is then (where $S_o^+(\text{Max})$ represents the clutter crest amplitude).

$$\frac{S_o^-(\text{Max})}{C_o(\text{Max})} = \frac{\beta_1}{\gamma}\left(\frac{\beta_2}{\beta_1}\right)^2 \frac{[1+\varepsilon^{-\pi\gamma/\beta_1}]}{[1+(\beta_1/\gamma)^2]} \tag{127}$$

or in the limit

$$\frac{S_o^-(\text{Max})}{C_o(\text{Max})} = \frac{(\beta_2/\gamma)^2}{(\beta_1/\gamma)} = \left(\frac{\beta_1}{\gamma}\right)\left(\frac{T_1}{T_2}\right)^2 \tag{128}$$

The above expression is the ratio of the crest values. Notice that it has the same form as for the pulse excitation case studied under C.1.b (see expression [101]). Figure 56 is a plot of expression (128).

For the power signal-to-clutter ratio the results of voltage signal-to-clutter expressions are squared.
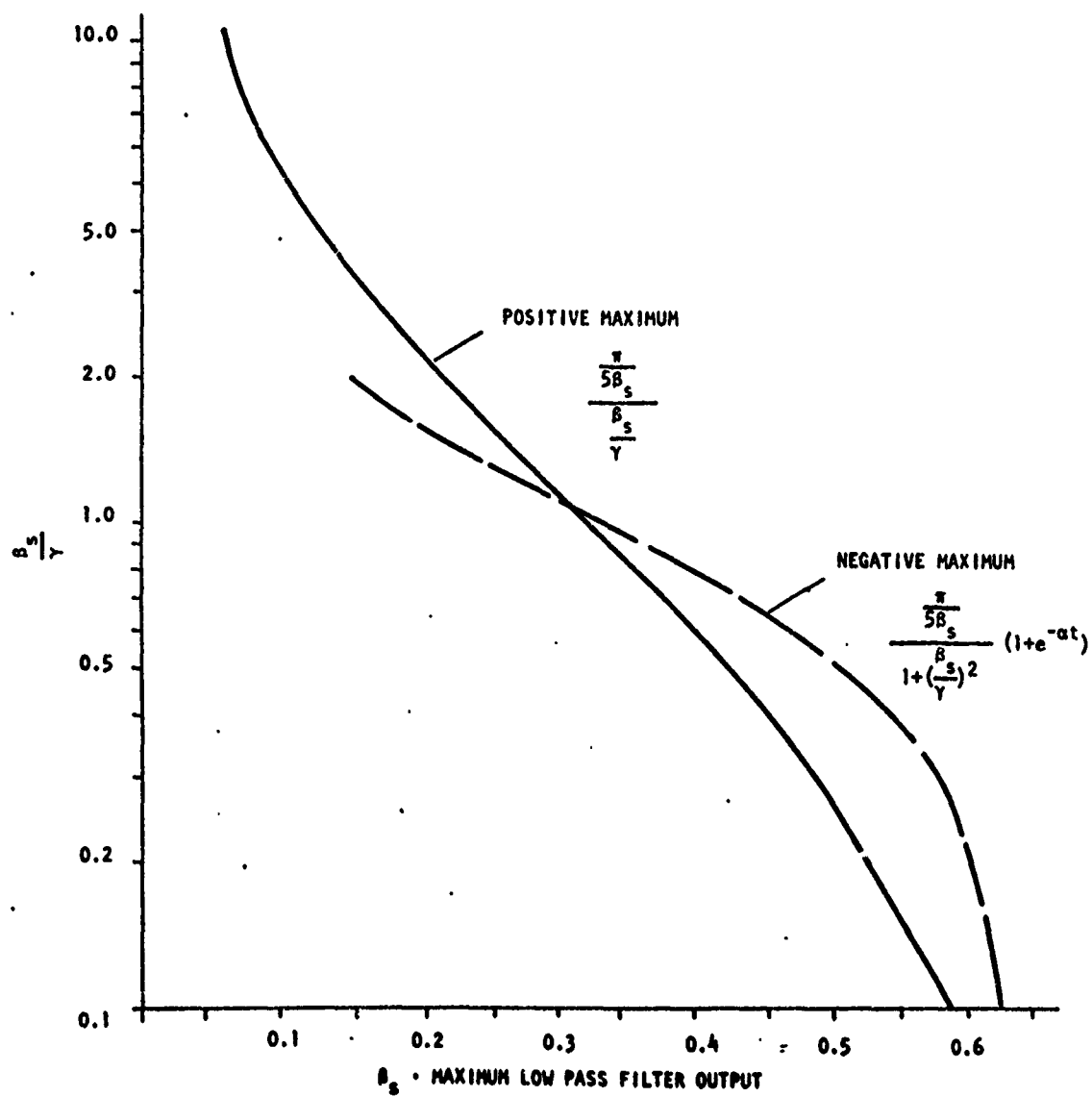
Figure 55. Maximum Low Pass Filter Output as a Function of the $\frac{\beta_s}{\gamma}$ Ratio
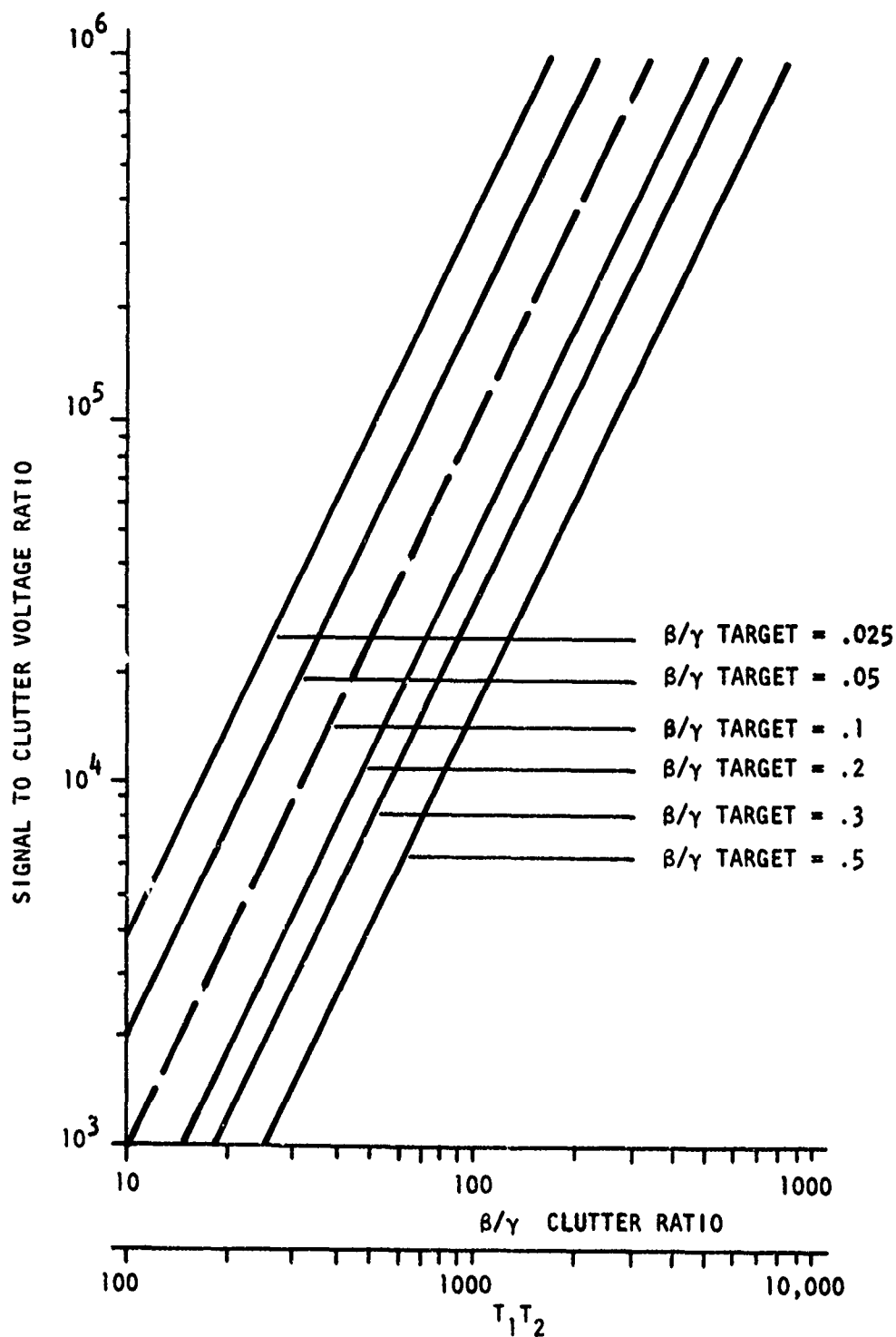
Figure 56. Signal-to-Clutter Voltage Ratio vs. Target-to-Clutter Size Ratio

127

Let us now determine the enhancement between the output and input signal-to-clutter ratios. The input signal-to-clutter ratios for impulsed spheres was shown earlier to be

$$\frac{S_i(Max)}{C_i(Max)} = \frac{T_1}{T_2} \tag{129}$$

therefore

$$\frac{S_o(Max)/C_o(Max)}{S_i(Max)/C_i(Max)} = \left(\frac{\beta_1}{\gamma}\right)\left(\frac{T_1}{T_2}\right) \tag{130}$$

In terms of power the enhancement is

$$\left[\frac{S_o(Max)/C_o(Max)}{S_i(Max)/C_i(Max)}\right]^2 = \left(\frac{\beta_1}{\gamma}\right)^2\left(\frac{T_1}{T_2}\right)^2 \tag{131}$$

If we wished to preserve the waveshape for the case $\beta_1/\gamma = 0.1$ in Figure 54 for the signal of interest, then the result of expression (131) is reduced by a factor of one hundred. That is to say then for a zero dB enhancement, the ratio of the target-to-clutter must be 10. However, if the preservation is not of interest, making γ small increases the enhancement. This will be the subject of the next section.

3. The Multi-Pole Low-Pass Filter

Having achieved a favorable signal-to-clutter ratio utilizing a single pole filter and an integrator, the investigation continues by applying additional sections.

A two-pole filter and integrator detector package is shown in Figure 57. The conditions are the same as for the prior section with the exception of the additional filter. The output from this arrangement may be obtained by

128

$e_O(t) = 1$ — **INTEGRATOR PACKAGE** $1/j\omega$ — **LOW PASS FILTER** $\gamma_a/(j\omega+\gamma_a)$ **(POLE 1)** — **LOW PASS FILTER** $\gamma_a/(j\omega+\gamma_a)$ **(POLE 2)** — $S_O(t) + C_O(t)$

$S_i(t) + C_i(t)$
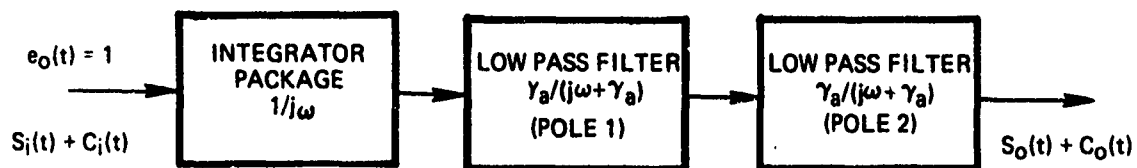
BDM–W–72–094

Figure 57.   Two-Pole Low-Pass Filter With Integrator Detector Package

convolving the impulse response of the additional filter with the results
of the prior section (expression [124]). The result for the case where
$\gamma_a = \gamma_b = \gamma$ is

$$S_o(t) = \frac{T/2}{1+(\beta/\gamma)^2}\left\{\sin(\beta t+\psi) + \left[\frac{(\beta/\gamma)^2 -1}{(\beta/\gamma)^2 +1} - \gamma t\right]\epsilon^{-\gamma t}+u(t-2.5T)\left[\sin(\beta[t-2.5T]+\psi)\right.\right.$$
$$\left.\left.+\left\{\frac{(\beta/\gamma)^2 -1}{(\beta/\gamma)^2 +1} - \gamma(t-2.5T)\right\}\epsilon^{-\gamma(t-2.5T)}\right]\right\} \tag{132}$$

where

$$\psi = \pi/2 - 2 \tan^{-1} \beta/\gamma \tag{133}$$

We shall now investigate the limiting conditions where the desired sphere
backscattered signal is minimally distorted, (hence $\gamma/\beta_1 \ll 1$ or that the band-
width is much larger than the significant frequency of the signal β_1) and
where the clutter sphere's size is so small as to place its significant fre-
quency β_2 much beyond the bandwidth γ or $\beta_2/\gamma \gg 1$. For the first condition
expression (132) gives

$$S_{o1}(Max) = T_1\big/2 \tag{134}$$

For the second, the output becomes

$$S_{o2}(Max) = C_o(Max) = \left(\frac{\gamma}{\beta_2}\right)^2 T_2 \tag{135}$$

hence, the signal-to-clutter ratio (Voltage) is

$$\frac{S_{o1}(Max)}{C_o(Max)} = \frac{1}{2}\left(\frac{\beta_2}{\gamma}\right)^2 \frac{T_1}{T_2} = \frac{1}{2}\left(\frac{\beta_1}{\gamma}\right)^2 \left(\frac{T_1}{T_2}\right)^3 \tag{136}$$

This is quite an encouraging solution since the signal-to-clutter ratio
increases as the cube of the dimension ratios. However, notice that the

multiplier β_1/γ must be made small if one wishes to preserve the desired signal and it varies as the square. This causes the multiplying factor to be small in expression (136).

Addition of one pole to the original configuration is shown to raise the order of the signal-to-clutter maximum amplitude ratio by one. (See expression [128].) In addition, the multipole low-pass filter sections leave the integral of the target waveform unaltered for values of $\beta/\gamma < 0.1$ but the waveform of the clutter signal becomes distorted from its original shape and its amplitude is highly attenuated. Thus, the target integral waveform is available in essentially its original form at the discriminator input for comparative processing, which will be considered in detail later in this report.

Consider next the performance of a bandpass filter and an integrator.

4. Integrator With a Bandpass Filter

Having investigated the frequency domain expression for the sphere's impulse response, it was noted that much of the power in the waveform is centered about the frequency $\omega = \beta_1$. (This can be deduced from the frequency response of expression [20].) A filter configuration which takes advantage of this characteristic is the Bandpass Filter characterized in the Figure 58.

The outputs resulting from feeding this filter with both sphere and plate related backscatter waveforms will be developed here to determine specifically the discrimination possible for similar sized objects. This will be followed by the sphere-on-sphere case.

Driving the system with a sphere's return results in an expression of the form

$$S_{o1}(j\omega) = \frac{T_1\big/2\ j\omega[j\omega+\gamma][1+\varepsilon^{-j\omega(2.5T_1)}]}{[j\omega^2+\beta_1^{\ 2}][(j\omega+\gamma)^2+\beta_o^{\ 2}]} \tag{137}$$

131

INTEGRATOR   BAND PASS FILTER

$$\frac{1}{j\omega}$$

$$\frac{j\omega+\gamma}{(j\omega+\gamma)^2 + \beta_o{}^2}$$

$\frac{T}{2}$

2.5T

$S_i(t)$

$S_o(t)$
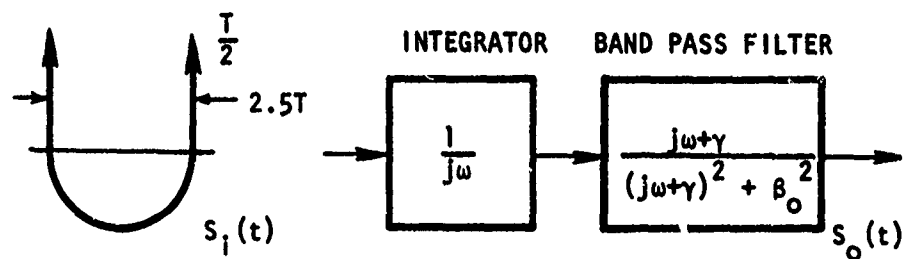
BDM–W–72–094

Figure 58. Integrator With Band Pass Filter

where T_1 and β_1 are the sphere's parameters and as identified in the past, γ determines the filter's bandwidth and β_o is the frequency that filter is centered on.

The transform of this expression to the time domain for the case $\beta_1 = \beta_o$ gives

$$S_o(t) = \frac{T_1}{2\gamma[\gamma^2+4\beta_1^2]} \left\{ (\gamma^2+2\beta_1^2)\ (1-\varepsilon^{-\gamma t})\ \cos\beta_1 t + \gamma\beta_1(1+\varepsilon^{-\gamma t})\ \sin\beta_1 t \right\}$$

$$* \left\{ u(t)-u(t-2.5T_1) \right\} \tag{138}$$

The star represents convolution and makes the result appear less complicated. The total expression should be interpreted as the time function, as specified on the first line, plus superimposed $\cdots$ $\cap$ it the same function but displaced $2.5T_1$.

Next applying the plate's impulse response, in place of the sphere, through the filter arrangement gives

$$S_{o2}(j\omega) = 2\frac{T_2^2}{\pi} \frac{(j\omega)\,(j\omega+\gamma)}{(j\omega+\alpha_2)[(j\omega+\gamma)^2 + \beta_o^2]} \tag{139}$$

where

$$T_2 = \frac{\ell}{c} \text{ and } \alpha_2 = \frac{\pi}{T_2} \tag{140}$$

The plate's expression was obtained from the early development where the result is shown in expression (30). The transform of this expression into the time domain is

$$S_{o2}(t) = \frac{2^{T_2^2}}{\pi[(\gamma-\alpha_2)^2 + \beta_o^2]} \left\{ \alpha_2(\gamma-\alpha_2)\ \varepsilon^{-\alpha_2 t} + \varepsilon^{-\gamma t}\left[[\gamma(\alpha_2-\gamma) - \beta_o^2] \right]\cos\beta_o t \right.$$

$$\left. + \beta_o\alpha_2\ \sin\beta_o t \right\} \tag{141}$$

133

Computer calculations were made varying the sphere-to-plate area ratios plus the bandwidth γ on expressions (138) and (141). Figure 59 is a plot of the maximum amplitudes of the sphere-to-plate ratios using these expressions. The areas of the bodies are their projected cross-sectional ones.

From this plot it can be seen that discrimination is enhanced for cases where the bandwidth is reduced. Also it is seen that the signal-to-clutter (voltage) ratio is reduced to 1.0 when the sphere-to-plate area ratio becomes approximately 1.

Now as the ratio γ/β_1 is made small and α_2 is much larger than β_1 then the signal-to-clutter ratio becomes

$$\frac{S_o(\text{Max})}{C_o(\text{Max})} = \frac{\pi T_1}{8\gamma T_2^2}\left[1 - \varepsilon^{-\pi\gamma/\beta_1}\right] \doteq 1.25\left(\frac{\pi}{4}\right)\left(\frac{d}{\ell}\right)^2 \tag{142}$$

The above conditions refer to a narrow bandwidth and a large dimension ratio between the sphere and the plate. Notice when the ratio γ/β_1 is very small then the signal-to-clutter (voltage ratio) varies as the ratio of the dimensions squared. It is interesting that the final result is independent of the precise value of the bandwidth.

Consider next the same arrangement as in Figure 58 except we shall now determine the signal-to-clutter ratio where the clutter consists of small spheres. For this case the clutter β_2 is much much larger than the β_o of the filter. Then performing the inverse transform on expression (137) where the subscripts are changed to 2 to represent the clutter, and taking the limit of the resulting function $\beta_2/\beta_o \gg 1$ gives the crest amplitude of

$$S_{o2}(\text{Max}) = \frac{T_2}{4\gamma} = C_o(\text{Max}) \tag{143}$$

134
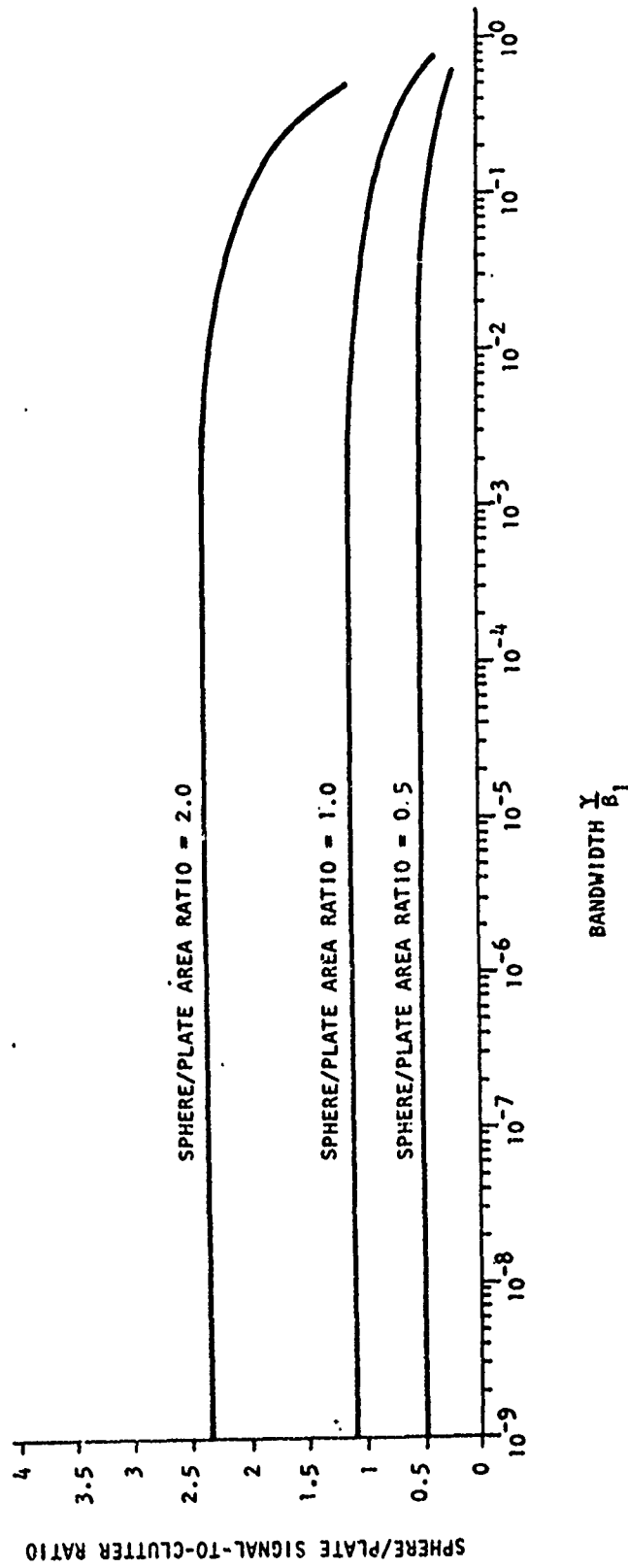
Figure 59. Sphere/Plate Signal-To-Clutter Ratio for a Band Pass Filter and an Integrator as a Function of Bandwidth and Size

135

The maximum signal amplitude of the desired larger sphere is

$$S_{o1}(Max) \approx \frac{T_1}{4\gamma} = [1-\epsilon^{-\pi\gamma/\beta}1]$$ (144)

hence, the signal-to-clutter ratio is

$$\frac{S_{o1}(Max)}{C_o(Max)} = \frac{T_1}{T_2} [1-\epsilon^{-\pi\gamma/\beta}1] \doteq \pi\left(\frac{\gamma}{\beta_2}\right)\left(\frac{T_1}{T_2}\right)^2$$ (145)

for the case where γ/β_1 is small.

Comparing the filter's output for the plate and spherical clutter cases, equations (142) and (145), we see that the bandpass filter is more effective against plate clutter than it is against spherical clutter for the same target impulse excitation.

We shall now turn to the addition of a matched filter to the low-pass filters in order to observe the enhancement in clutter rejection.

E. COMBINATIONS OF LOW PASS AND MATCHED FILTERS

Our prior results have shown that an integration or a low-pass filter scheme tends to enhance the overall clutter rejection. We shall now precede a white noise matched filter with various low pass filters to determine the scheme that provides the best rejection.

We shall begin by investigating the signal-to-clutter ratio that may be obtained from an integrator and a matched filter. In particular the case where the target sphere and the plate clutter have the same cross-sectional areas and the limit as the clutter becomes quite small.

1. Integrator and Matched Filter Combination

a. Spherical Target-Plate Clutter

Consider passing the returns from a sphere and a plate through a filter matched to the target (sphere) response. The filter scheme is indicated in

136

Figure 60 where the matched filter has the integrated response of the spherical target to be detected. Figure 19 shows its impulse waveshape.

The frequency response function for passing a plate through the filter is as follows (where the 1 subscript applies to the sphere and 2 applies to the plate).

$$C_o(j\omega) = \frac{T_1 T_2^2}{\pi} \frac{(j\omega)^2 (1+\varepsilon^{-j\omega 2.5T_1})}{\left[(j\omega)^2 + \beta_1^2\right](j\omega + \alpha_2)} \tag{143}$$

Its output time response can be shown to be

$$C_o(t) = \frac{T_1 T_2^2 (\beta_1/\alpha_2)^2}{\pi[1+(\alpha_2/\beta_1)^2]} \left\{ \left(\frac{\alpha_2}{\beta_1}\right)^2 \varepsilon^{-\alpha_2 t} - \cos \beta_1 t + \left(\frac{\alpha_2}{\beta_1}\right) \sin \beta_1 t \right\}$$

$$* \left\{ u(t) + u(t-2.5T_1) \right\} \tag{144}$$

The maximum output occurs at a time of

$$t_{max} = \frac{\pi}{\beta_1} \tag{145}$$

with a value of

$$C_o(\text{Max}) = \frac{T_1 T_2^2}{\pi} \left[\frac{1+\varepsilon^{-\pi\alpha_2/\beta_1}}{1+(\beta_1/\alpha_2)^2} \right] \tag{146}$$

Now for the case of the signal passing through the filter, its frequency response is the square of the expression shown for the matched filter in Figure 60. The time response is

$$S_o(t) = \frac{T_1^2}{8\beta_1} (\sin \beta_1 t + \beta_1 t \cos \beta_1 t)$$

$$* \left\{ \delta(t) - 2\delta(t-2.5T_1) + \varepsilon(t-5T_1) \right\} \tag{147}$$

and its maxima occurs also at the time of expression (145) but with an amplitude of

137

$$\text{INTEGRATOR} \qquad \text{MATCHED FILTER}$$

$$S_i(t) + C_i(t) \longrightarrow \boxed{\dfrac{1}{j\omega}} \longrightarrow \boxed{\dfrac{T_1 j\omega\left(1 + \varepsilon^{-j\omega 2.5T_1}\right)}{2\left[(j\omega)^2 + \beta_1^{\ 2}\right]}} \longrightarrow S_0(t) + C_0(t)$$

FILTER COMBINATION
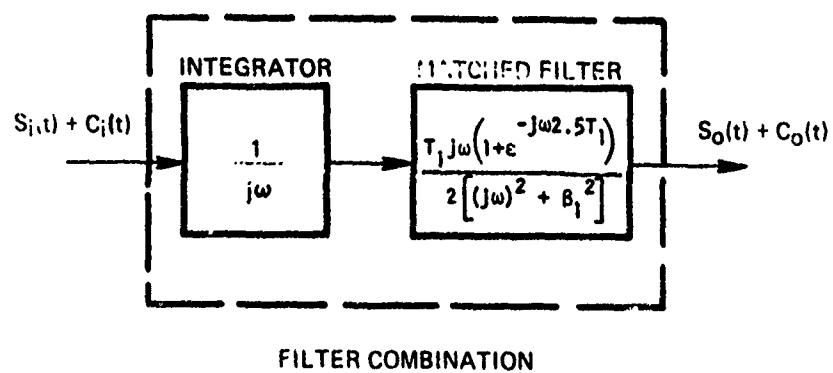
BDM-W-72-094

Figure 60.   Integrator-Matched Filter Combination

138

$$S_o(\text{Max}) = \frac{\pi T_1^2}{8\beta_1} \qquad\qquad (148)$$

The signal-to-clutter ratio may then be formed between the sphere target and the plate clutter as

$$\frac{S_o(\text{Max})}{C_o(\text{Max})} = \frac{2.5\pi}{8} \left(\frac{T_1}{T_2}\right)^2 \frac{[1+(\beta_1/\alpha_2)^2]}{[1+\epsilon^{-\pi\alpha_2/\beta_1}]} \qquad (149)$$

We see in the expression that the signal-to-clutter voltage ratio varies as the square of the ratio of their sizes. However, as the ratio increases beyond three times then it varies as

$$\frac{S_o(\text{Max})}{C_o(\text{Max})} = \frac{(2.5)^3}{8} \pi \left(\frac{T_1}{T_2}\right)^2 \qquad\qquad (150)$$

This investigation indicates that the integrator-matched filter combination may be a good filter arrangement for rejecting plate clutter since the signal-to-clutter ratio varies as the second power of voltage and the fourth power for power.

Let us see how well this filter performs for a spherical clutter passing through it.

b. Spherical Target - Spherical Clutter

The expression describing the filter's output for spherical clutter may be obtained by the product of the matched filter function of Figure 60 with itself except making the second function have the subscripts 2. The inverse transform of this expression can be shown to be

139

$$S_{02}(t) = C_o(t) = \frac{T_1 T_2}{4(\beta_2^2 - \beta_1^2)} [\beta_1 \sin \beta_1 t - \beta_2 \sin \beta_2 t]$$

$$* \left\{ \delta(t) + \delta(t-2.5T_2) + \delta(t-2.5T_1) \right. \tag{151}$$

$$\left. + \delta(t + 2.5(t_1 + T_2)) \right\}$$

The crest value for this function where the target is larger than the clutter is

$$C_o(\text{Max}) = \frac{T_1 T_2}{4\beta_2} \frac{1}{[1-(\beta_1/\beta_2)^2]} \tag{152}$$

The signal-to-clutter ratio then for spheres is the ratio of equations (148) and (152) or,

$$\frac{S_o(\text{Max})}{C_o(\text{Max})} = \frac{\pi}{2} \left(\frac{T_1}{T_2}\right)^2 \left[1 - \left(\frac{T_2}{T_1}\right)^2\right] \text{ for } T_1 > T_2 \tag{153}$$

a very interesting result. Comparing expression (153) for the spheres to the sphere-plate result of (150) suggests that this filter is better for plate than sphere clutter. This effect will be noticed again further along in this discussion and it will be shown that the least similar that the clutter is to the matched filter, the better will be its performance.

We shall continue our investigation by next considering a two-pole or double integrator filter preceding a matched filter.

2. **Double Integrator and Matched Filter Combination**

This investigation will prove quite interesting as it will be shown that for small clutter sizes relative to the target of interest, this arrangement is an optimum case since the integrators serve to essentially "whiten" the clutter signal, and the arrangement becomes the classical matched filter for white noise. Figure 61 shows the combination.

DOUBLE INTEGRATOR

MATCHED FILTER

$S_i(t) + C_i(t)$

$\dfrac{1}{(j\omega)^2}$

$C_1(t)$
$S_1(t)$

$\dfrac{T_{1/2}[1 \cdot \epsilon^{-j\omega 2.5 T_1}]}{(j\omega)^2 + \beta_1^2}$

$S_o(t) + C_o(t)$

FILTER COMBINATION
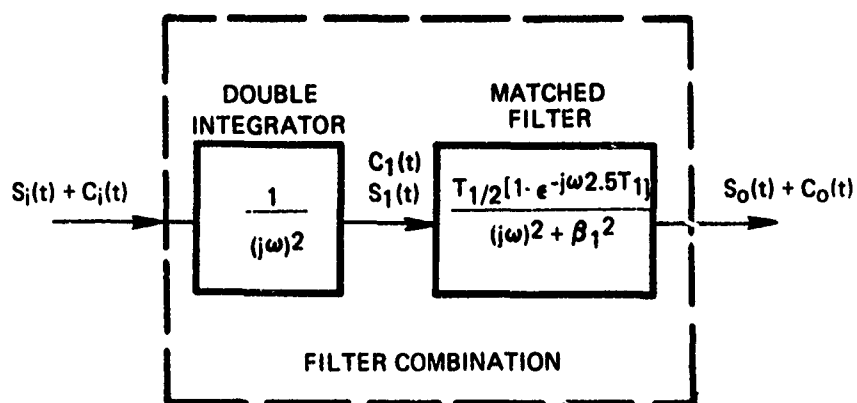
BDM-W-72-094

Figure 61. Double Integrator-Matched Filter Combination

141

The investigation to follow will include clutter that consists of spheres, plates, and rods with the target of interest being a large sphere.

a. Spherical Target with Spherical Clutter

When the desired spherical target $S_i(t)$ appears at the input to the filter it will have the waveform as shown previously in Figure 20. After it has passed through the double integrator, the signal will change to that of Figure 21. This shape of course is what the impulse response of the matched filter $S_1(t)$ of Figure 61 is patterned after.

Let us now determine the maximum signal amplitude $S_o(Max)$ for the case when the desired target signal $S_i(t)$ appears. We know that the maximum output will occur for an auto-correlation process when one signal is identically atop of the other; hence

$$S_o(Max) = \int_0^{2.5T_1} S_1^2(t)\ dt = 0.2T_1^5 \tag{154}$$

Expression (21) may be used for $S_1(t)$.

Consider next the effect of applying a small spherical clutter input to this filter. The double integrator output $C_1(t)$ will appear for this case as shown in Figure 62a. For $T_2 \ll T_1$, the clutter sphere much smaller than the target sphere, the duration of the clutter sphere becomes much less than that of the target $S_1(t)$, hence, its effect on the matched filter is similar to exciting it with an impulse of the area of $C_1(t)$ as shown in Figure 62b. This is quite important as we have shown that the integrator tends to pre-whiten the clutter sphere's response.

The impulse amplitude is found by performing the integration shown in expression (154) except for $S_1(t)$ rather than $S_1^2(t)$. The resultant area is shown in the figure and the clutter impulse time representation becomes

$-0.4T_2^2$

$2.5T_2$

$\frac{2}{\pi} T_2^3$

(a) $C_1(t)$

(b) $C_1(t)$ IMPULSE REPRESENTATION
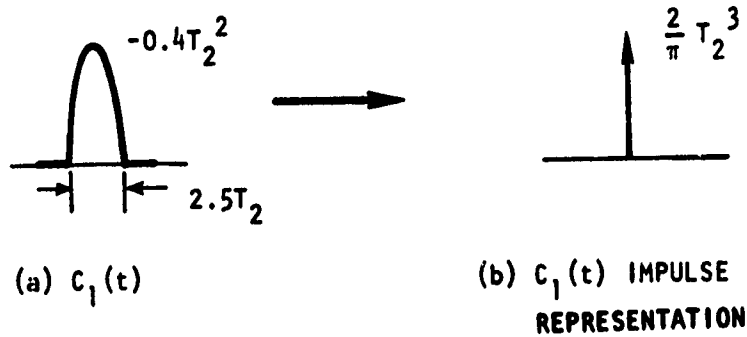
BDM-W-72-094

Figure 62. $C_1(t)$ Clutter Representation for Small Spheres

143

$$\delta_c(t) = \frac{2}{\pi} T_2^3 \delta(t) \tag{155}$$

The output $C_0(t)$ that this impulse function produces is $S_1(t)$ multiplied by the coefficient of (155) or

$$C_0(t) = \frac{0.8}{\pi} T_2^3 T_1^2 \sin \beta_1 t \qquad 0 < \beta_1 t < \pi \tag{156}$$

The output voltage signal-to-clutter ratio may then be formed as the ratio of expressions (154) and (156) as

$$\frac{S_0(\text{Max})}{C_0(\text{Max})} = \frac{\pi}{4}\left(\frac{T_1}{T_2}\right)^3 \tag{157}$$

This solution is very encouraging as it represents the largest signal-to-clutter ratio obtained for targets and clutter of the same form (sphere-on-sphere).

For the signal-to-clutter power ratio calculation where there will be "k" random clutterers per range gate sampling time, the average clutter power is obtained by multiplying (154) by "k" or

$$\overline{C_0^2} = 1.25 \left(\frac{0.8}{\pi}\right)^2 T_2^6 T_1^5 k \tag{158}$$

The power signal-to-clutter output ratio is then

$$\frac{S_0^2(\text{Max})}{\overline{C_0^2}} = \frac{\pi^2}{2.5} \frac{1}{kT_1}\left(\frac{T_1}{T_2}\right)^6 \tag{159}$$

Notice that the result is dimensionally correct and that the ratio diminishes proportionally to the number of clutterers in the gate. The ratio also increases as the sixth power of the sphere ratios. Also if the range gate time is $2.5T_1$, which allows the entire spherical target to be processed, and

k is the average number of clutter for that time $(n/2.5T_1)$, then n may replace $k T_1$ and the absolute ratio value is then obtainable.

The clutter rejection enhancement that occurs between the filter's output and input is a function of the interrogating waveshape. The use of the impulse response of targets creates problems since the impulse's energy is infinite. A way around this problem is to assume that the interrogating pulse is an exponential of the form

$$\delta_i(t) = \gamma \varepsilon^{-\gamma t} \quad \text{as } \gamma \text{ approaches } \infty. \tag{160}$$

This expression is impulse-like and has a finite energy.

Performing an average power calculation similar to (154) for "k" random spaced clutter spheres per sampling interval and assuming that $2.5T_2 \gamma \gg 1$, gives for the input side

$$\overline{c_i^2} = \frac{k\gamma}{2}\left(\frac{T_2}{2}\right)^2 \tag{161}$$

The assumption makes the interrogating pulse also appear impulse-like for the small clutter sphere. Notice the problem that one would encounter if the actual impulse were used. In that case as $\gamma \to \infty$, $\overline{C_o^2}$ also would become infinite.

The input signal-to-clutter power ratio is then

$$\frac{S_i^2(\text{Max})}{\overline{c_i^2}} = \frac{2\gamma}{k}\left(\frac{T_1}{T_2}\right)^2 \tag{162}$$

The maximum signal $S_i(\text{Max})$ is the impulse amplitude $T_1/2$ multiplied by exponential γ.

145

The output to input enhancement will then be by the ratio of expressions (159) and (162) or

$$\frac{S_o^2(Max)}{C_c^2} \bigg/ \frac{S_i^2(Max)}{C_i^2} = \frac{\pi/5}{\gamma T_1}\left(\frac{T_1}{T_2}\right)^4 \tag{163}$$

The latter expression shows that the enhancement varies as the ratio of the dimensions to the fourth power. The γ in the denominator suggests that this ratio is very much dependent upon the shape of the interrogating pulse.

If one wished to determine the same enhancement using voltage amplitudes, the approach is as follows. The input signal-to-clutter ratio is just the ratio $\frac{T_1}{T_2}$. Expression (157) gives the output ratio; hence

$$\frac{S_o(Max)/C_o(Max)}{S_i(Max)/C_i(Max)} = \frac{\pi}{4}\left(\frac{T_1}{T_2}\right)^2 \tag{164}$$

Notice that the same ratio occurs if we square this value (to relate to power) and compare it with (163). This result is quite encouraging.

We shall next investigate passing plate clutter through the arrangement of Figure 61.

b. **Spherical Target with Plate Clutter**

Passing a single plate clutter of dimension T_2 through the double integrator of Figure 61 gives the following response

$$C_i(t) = \frac{2}{\pi} T_2^2 \varepsilon^{-\alpha_2 t} \tag{165}$$

where the parameters are as identified under expression (137). Here we see if α_2 is very large (inversely proportional to the clutter size), this function will be impulse-like for a large target size. This is the same

146

argument that was used under "a" of the prior section and it amounts to a pre-whitening process of the clutter. Then the clutter may be represented as an impulse or

$$\delta_c(t) = \frac{2}{\pi} \frac{T_2^2}{\alpha_2} \tag{166}$$

Exciting the matched filter with this impulse gives the matched filter's impulse response which is

$$C_o(t) = \frac{0.8}{\pi^2} T_1^2 T_2^3 \sin \beta_1 t \qquad 0 < \beta_1 t < \pi \tag{167}$$

The amplitude signal-to-clutter ratio may then be formed between expressions (154) and (167) as

$$\frac{S_o(\text{Max})}{C_o(\text{Max})} = \frac{\pi^2}{4} \left(\frac{T_1}{T_2}\right)^3 = \frac{\pi^2}{4} \left(\frac{d}{\ell}\right)^3 \tag{168}$$

Notice that the ratio is raised to the same power as for the sphere-on-sphere case (see expression [155]), however, it produces π times more enhancement. This appears reasonable since in past calculations we have noted that the enhancement is better between geometries that are different.

Performing the power calculation as described in the prior section gives

$$\frac{S_o^2(\text{Max})}{\overline{C_o^2}} = \frac{\pi^4}{2.5T_1 k} \left(\frac{T_1}{T_2}\right)^6 \tag{169}$$

which is π^2 or approximately ten times greater than for the sphere-on-sphere case. See expression (157).

Obtaining the output-to-input amplitude or power clutter rejection for this case is meaningless since one must deal with impulses and doublets for which energies are undefined. We must look at this filter's performance in

147

terms of its relative enhancement in output signal-to-clutter ratio as compared to the other filters considering that their outputs occur as a result of impulse interrogation.

c. Spherical Target With Rod Clutter

We shall now consider the problem of passing a rod or dipole type clutter through the filter arrangement of Figure 61. The transfer function describing the rod's scattering was given as expression (33), however, in order to make it manageable for this analysis it will be approximated by the following relationship

$$\Delta_r(j\omega) = \frac{K \, T_r \, (j\omega)^2}{(j\omega + \alpha_o)^2 + \beta_r^2} \tag{170}$$

where

$$K = \frac{\eta}{\pi Z_o}, \quad T_r = \frac{\ell}{c} \text{ and } \beta_r = \frac{\pi}{T_r} \tag{171}$$

This approximation will provide a time waveshape similar to that shown in Figure 26 except that the edges are not as sharp. The degree to which the function is damped is determined by α_o.

Passing expression (170) through the double integrator of the filter, and transforming the result into the time domain gives

$$c_1(t) = \frac{KT_r}{\beta_r} \epsilon^{-\alpha_o t} \sin \beta_r t \tag{172}$$

For the same argument that was applied to the sphere and plate clutter where it is assumed that the clutter size is very small compared to the target sphere, the impulse-like representation of the rod is then

$$\delta_r(t) = \frac{KT_r}{\alpha_o^2 + \beta_r^2} \delta(t) \tag{173}$$

148

This input will cause, as for the other cases, a filter impulse response of the form

$$C_o(t) = \frac{0.4T_1{}^2 T_r K}{\alpha_o{}^2 + \beta_r{}^2} \sin \beta_1 t \qquad o < \beta_1 t < \pi \tag{174}$$

The amplitude signal-to-clutter ratio between the sphere and the rod is then the ratio of (154) and (174) or

$$\frac{S_o(Max)}{C_o(Max)} = \frac{\pi^3}{2}\left(\frac{Z_o}{\eta}\right)\left(\frac{T_1}{T_r}\right)^3\left[1 + \left(\frac{\alpha_o}{\beta_r}\right)^2\right] \tag{175}$$

For the thin rod case, it is conceivable that the ratio of characteristic to wave impedance can be approximately one half, and that the damping term is smaller than the resonant frequency. Under these conditions, the multiplier is $\pi^3/4$. This represents a signal-to-clutter enhancement of π times greater (for the filter) for the rod case over the plate for the same length, and π^2 for the rod over the spherical clutter.

The output signal-to-clutter power ratio can be shown to be for the sphereical target and the rod clutter, for the prior mentioned conditions and a random input, is then

$$\frac{S_o{}^2(Max)}{\overline{C_o{}^2}} \approx \frac{\pi^6}{2.5T_1 k}\left(\frac{T_1}{T_r}\right)^6 \tag{176}$$

The enhancement that the filter offers in amplitude signal-to-clutter ratio may be calculated since the rod's crest is an impulse of KT_r which the input of the filter will see. The input signal-to-clutter ratio is then

$$\frac{S_i(Max)}{C_i(Max)} = \frac{T_1}{2KT_r} \tag{177}$$

149

The output signal-to-clutter ratio is obtained from (175) hence,

$$\frac{S_o(\text{Max})/C_o(\text{Max})}{S_i(\text{Max})/C_i(\text{Max})} = \pi^2 \left(\frac{T_1}{T_r}\right)^2 \tag{178}$$

Notice that this filter has an output-to-input enhancement of 4π times as great as the sphere-on-sphere.

These series of calculations have indicated that the filter arrangement of 61 appears to be the best all around filter investigated thus far. We shall next consider the optimal filter case.

F. OPTIMAL FILTER PERFORMANCE

We have examined various forms of filter networks and conditions with and without correlation schemes such as the matched filter. The next logical step is to investigate the so-called optimal filter and determine if it can perform as well or better than any of the prior ones for the conditions of interest.

The approach is to essentially apply the principles discussed under Chapter III, Section B.5 to the target sphere immersed in small clutter consisting of spheres, plates and rods.

1. Spherical Target with Spherical Clutter

The approach here will be, as before, to determine the signal and clutter output from a filter, but in this case the filter has a frequency response given by expression (83). As a result of this response, there is generated a function $F(j\omega)$ (see expression [85]) which is the ratio of the target-to-clutter frequency response. This function is then operated upon in order to determine the power signal-to-clutter ratio in a random clutter environment (see Figure 63 for the filter configuration).

150
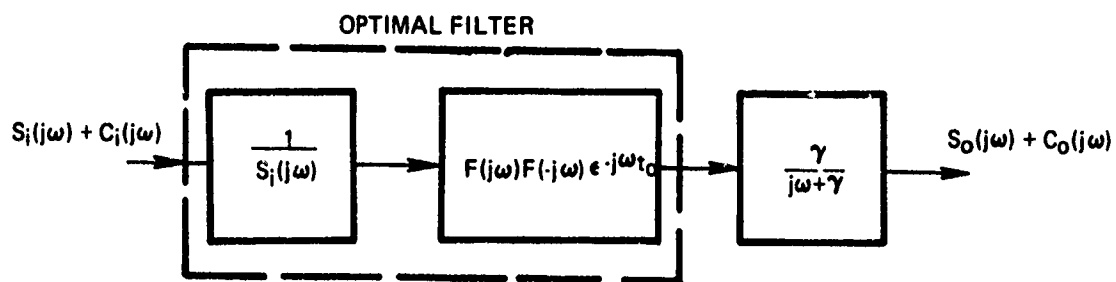
Figure 63.   Optimal Filter Arrangement

151

Because of the nature of $F(j\omega)$ it becomes necessary in the cases of similar geometries to limit its bandwidth by introducing a low-pass filter of the form shown in Figure 57 or

$$C_1(j\omega) = \frac{\gamma}{j\omega+\gamma} \tag{179}$$

This will be made clear soon. Also in order to assess the filter's output-to-input enhancement, the input signal must be something other than an impulse because of the energy argument expressed earlier. A good substitute for the interrogating impulse is the function given by expression (160) which turns out to be the time response of (179). It will be shown shortly that the filter's output is independent of the interrogating pulse since it gets factored out in $F(j\omega)$.

We begin by forming $F(j\omega)$ by using model-C for the sphere's scattering transfer function (see equation [22]) therefore

$$F(j\omega) = \frac{S_1(j\omega)}{C_1(j\omega)} = \frac{1}{\sqrt{\kappa}}\left(\frac{T_1}{T_2}\right)\left[\frac{j\omega+\alpha_2}{j\omega+\alpha_1}\right]^2 \tag{180}$$

Notice that "k" the random occurrence parameter is also included. Observe also that the interrogating function would be factored out whatever it is. Hence this function deals essentially with the ratio of the objects' transfer functions.

An inspection of expression (180) indicates that there are as many zeros as there are poles; hence, the frequency response is not zero at infinity which will give rise to impulses in the time domain. This is the reason for the bandlimiting filter.

The transform into the time domain of $F(j\omega)$ to $f(t)$ with the bandlimiting filter gives

152

$$\gamma \epsilon^{-\gamma t} * f(t) = \frac{T_1}{\sqrt{k}\,T_2}\left[\gamma \epsilon^{-\gamma t} + 2(\alpha_2 - \alpha_1)\epsilon^{-\alpha_1 t} + t(\alpha_2 - \alpha_1)^2 \epsilon^{-\alpha_1 t}\right] \qquad (181)$$

The sphere parameter α_1 is defined as

$$\alpha_1 = \frac{1}{1.25 T_1} \qquad (182)$$

and α_2 is the same except a change of the subscript.

Now when the signal $S_i(j\omega)$ appears, we see from Figure 63 that the output is the combination of $f(t)$ with its image limited by the bandpass filter. This is essentially correlation, as has been discussed earlier, and its maximum output occurs at $t=t_o$ when one function is exactly on top of the other. The value is obtained from equation (93). This also turns out to be the filter's signal to clutter power ratio; hence

$$\frac{S_o^2(t=t_o)}{\overline{C_o^2}} = \int_0^{t_o \to \infty} f^2(t)\ dt \qquad (183)$$

Performing this operation, but taking the product of $f(t)$ and expression (181) for $f^2(t)$ under the integrand, provides a series of terms where the largest is the impulse-like one or

$$\frac{S_o^2(t=t_o)}{\overline{C_o^2}} = \frac{2\gamma}{k}\left(\frac{T_1}{T_2}\right)^2 \qquad (184)$$

We see here that if γ is allowed to go to infinity, the output is also infinite. The result indicates that the upper limit is determined by the bandwidth of the filter. Otherwise, the ratio increases as the ratio of the dimensions squared. This solution may be deceptive. Let us investigate the input signal to clutter ratio and then determine the overall enhancement.

The crest amplitude of the target sphere's response as caused by the impulse-like excitation of expression (158) is

$$S_i(max) = \frac{\gamma T_1}{2} \tag{185}$$

The average clutter sphere's power for the random condition is by the following integral

$$\overline{c_i^2} = k \int_0^\infty c_i^2(t) \, dt = \frac{k\gamma T_2^2}{8} \tag{186}$$

where $c_i(t)$ describes the small sphere's impulse response (expression 23) as caused by the impulse-like excitation. The principal term of the integration of (186) is shown as it is so much greater than the others. It is due entirely to the impulse-like excitation. The input signal to clutter ratio is then

$$\frac{S_i^2(Max)}{\overline{c_i^2}} = \frac{2\gamma}{k} \left(\frac{T_1}{T_2} \right)^2 \tag{187}$$

However, a scan back to (184) shows the same answer; hence, for an impulse-like excitation there is no clutter rejection enhancement with the optimal filter. In reality, there can be and that depends entirely on the form of the input signal to clutter ratio. Recall that the filter's output signal to clutter ratio is independent of its input shape. Now if we had made the input impulse's time constant γ_a and the filter's bandwidth γ_b, the enhancement becomes

$$\frac{S_o^2(Max)/\overline{c_o^2}}{S_i^2(Max)/\overline{c_i^2}} = \frac{\gamma_b}{\gamma_a} \tag{188}$$

or the ratio of the interrogating signal to filter bandwidth.

In terms of the output to input signal to clutter voltage ratio, this can be shown to be

154

$$\frac{S_o(\text{Max})}{C_o(\text{Max})} \bigg/ \frac{S_i(\text{Max})}{C_i(\text{Max})} = \frac{1}{\sqrt{k}} \qquad (189)$$

for the impulse case.

We have observed from this investigation that the configuration of Figure 63 does not provide the desired enhancement in clutter rejection for the impulse excitation case.

Consider next passing a rod through the filter.

2. Spherical Target with Rod Clutter

Proceeding along the same lines as for the development of the sphere clutter in the prior section, let us now replace it with rod clutter. Using the approximate transfer function expression of the rod (see expression (170)) with that of the target sphere, one can form the ratio $F(j\omega)$ as

$$F(j\omega) = \frac{1}{2\sqrt{k}K}\left(\frac{T_1}{T_r}\right)\frac{[(j\omega+\alpha_o)^2 + \beta_r^2]}{(j\omega + \alpha_1)^2} \qquad (190)$$

the conditions are the same regarding the excitation and the band-limiting as for the prior section as it is apparent from expression (190) that time impulses are going to occur.

The inverse transform of (190) convolved with the filter's band-limiting γ gives

$$\gamma\epsilon^{-\gamma t} * f(t) = \frac{1}{2\sqrt{k}K}\left(\frac{T_1}{T_r}\right)\left[\gamma\epsilon^{-\gamma t} + 2(\alpha_o-\alpha_1)\epsilon^{-\alpha_1 t} + [\beta_r^2 + (\alpha_o-\alpha_1)^2]t\epsilon^{-\alpha_1 t}\right] \qquad (191)$$

Performing next the operation implied by expression (183) gives

$$\frac{S_o^2(t=t_o)}{C_o^2} = \frac{\gamma}{2K^2 k}\left(\frac{T_1}{T_2}\right)^2 \qquad (192)$$

155

This result has the same form as for the spherical clutter which is that the output signal to clutter power ratio is proportional to the filter's bandwidth. If the analysis were continued to determine the enhancement for impulse excitation, the result will be the same as for the spheres. We may then conclude that this filter arrangement is also not good for clutter rejection.

The reason that these two filters have not performed well is that their signal and clutter pole structures are similar. In the following case of plate clutter, this situation will improve.

3. Spherical Targets with Plate Clutter

The impulse excitation conditions will be changed in this case from the prior ones due to the derivative scattering nature of the plate clutter. Although it will still be impulse-like, its shape will be triangular, having a base dimension in time of 2τ and a crest amplitude of unity. Another difference is that the band-limiting filter of Figure 63 will be removed.

Applying the normalized plate transfer function of expression 30 and that of the target sphere to $F(j\omega)$ gives

$$F(j\omega) = \frac{\pi T_1}{\sqrt{k}\, T_2^2} \frac{[j\omega + \alpha_2]}{[j\omega + \alpha_1]^2} \tag{193}$$

where

$$\alpha_2 = \frac{\pi}{T_2} \quad \text{and} \quad \alpha_1 = \frac{1}{1.25\, T_1} \tag{194}$$

Here we see that there are more poles than zeros in the function; hence, the output is finite.

Transforming $F(j\omega)$ to a time function gives

$$f(t) = \frac{\pi\, T_1}{\sqrt{k}\, T_2^2}\left[\varepsilon^{-\alpha_1 t} + (\alpha_2 - \alpha_1)t\varepsilon^{-\alpha_1 t}\right] \qquad (195)$$

The power signal to noise ratio then follows from expression (183) as

$$\frac{S_o^2(\text{Max})}{\overline{C_o^2}} = \frac{\pi^4}{2kT_1}\left(\frac{T_1}{T_2}\right)^6\left[1 + \frac{1}{(1.25\pi)^2}\left(\frac{T_2}{T_1}\right)^2\right] \qquad (196)$$

This is a very encouraging result over the prior two clutter conditions. What is more, this is essentially the same value (for $T_1 \gg T_2$) for the double integrator followed by a matched filter case of section E.2.b (see equation 169). This is the type of result one enjoys, as it confirms the prior filter as being optimal-like.

Consider now the output to input signal to clutter enhancement. The input target signal for the triangular unit amplitude pulse is

$$S_i(\text{Max}) = T_1/2 \qquad (197)$$

The average power clutter may be obtained as per expression (186) after developing $C_i(t)$ using the normalized plate impulse expression of 32 and the triangular pulse. The result is then obtained as

$$\overline{C_i^2} = 2\left(\frac{2}{\pi}\right)^2 \frac{kT_2^4}{\tau} \qquad (198)$$

The input signal to clutter ratio is then

$$\frac{S_i^2(\text{Max})}{\overline{C_i^2}} = \frac{\pi^2}{2}\left(\frac{\tau}{T_1}\right)\frac{1}{kT_1}\left(\frac{T_1}{T_2}\right)^4 \qquad (199)$$

157

The output to input enhancement follows as

$$\frac{S_o^2 (\text{Max})}{\overline{c_o^2}} \bigg/ \frac{S_i^2 (\text{Max})}{\overline{c_i^2}} = \pi^2 \left(\frac{T_2}{T}\right)\left(\frac{T_1}{T_2}\right)^3 \left[1 + \frac{1}{(1.25\pi)^2}\left(\frac{T_2}{T_1}\right)^2\right] \qquad (200)$$

which is very good. Notice that as a multiplier there is the ratio T_2/τ which is the plate's propagation time across its face to the pulse width of the interrogating pulse. This is certainly one of the best clutter rejection filters along with the double integrator matched filter. The same result will be obtained for the enhancement for the other filter too.

We have shown to this point that the best practical filter arrangement is that of Figure 61. Let us now determine the enhancement it provides for a rain clutter condition which will be the subject of the next major section.

G. CLUTTER REJECTION OF RAIN

The performance of an impulse radar system may be degraded in part by the effects of precipitation. The total effect is twofold.

First, there is a scattering effect related to the cross sectional area displayed by the mass of raindrops to the impinging electromagnetic fields.

Secondly, there is the absorption of energy which can be associated with the body of precipitation acting as a conducting medium through which both the scattered target and rain associated electric fields must propagate. We shall take these two effects into consideration when determining the signal to clutter enhancement that may be obtained by the filter of Figure 61.

Some of the statistics obtained during a literature search on rain are as follows.

For a rate of rainfall of 2 millimeters per hour, which would be classed as a "moderate" rain, there would be on the average about 60 drops per cubic

meter in the air above the ground having diameters between 1 and 2 milli-

meters, but only one drop in every 20 cubic meters with diameter greater than

3 millimeters. In the very heavy rain associated with thunderstorms, there

might, on occasions, be as many as 500 to 1000 drops per cubic meter with

diameters between 1 and 2 millimeters and one or two per cubic meter as large

as 5 millimeters in diameter.

We shall begin the investigation by determining the expected attenuation

as a function of frequency through rain.

1. Attenuation of Electromagnetic Waves through Precipitation

Figure 64 shows the expected one way attenuation through various rates of

rainfall as provided by Skolnik (see Reference 11) for a range of frequencies

of from one to ten centimeters of wavelength. Since we are interested in the

attenuation over a broader frequency for impulse application, this required

the extension of the above figure. Considering the physics of the propagation

of an electromagnetic wave through a lossy medium, the attenuation process

may be described as

$$e_o(x,j\omega) = e_1(0,j\omega)\epsilon^{-\zeta(j\omega)x} \qquad (201)$$

where x represents the distance propagated from the source point in kilometers,

$\zeta(j\omega)$ represents the attenuation as a function of frequency, and e_o and e_1 the

fields at x and at the source, respectively. This functional character also

appears in the re-plot of Figure 64, as shown in Figure 65.

Since we are interested in a worst case condition, the expression for the

heavy rain of 40 millimeters/hour was determined to be

$$e_o(x,j\omega) = e_o(x,0)\epsilon^{-(5.26\times10^{-11} f)^{3.33} x} \qquad (202)$$

where the factor f is the frequency in hertz.

159

RAINFALL ATTENUATION, dB/km (ONE WAY)

WAVELENGTH, cm
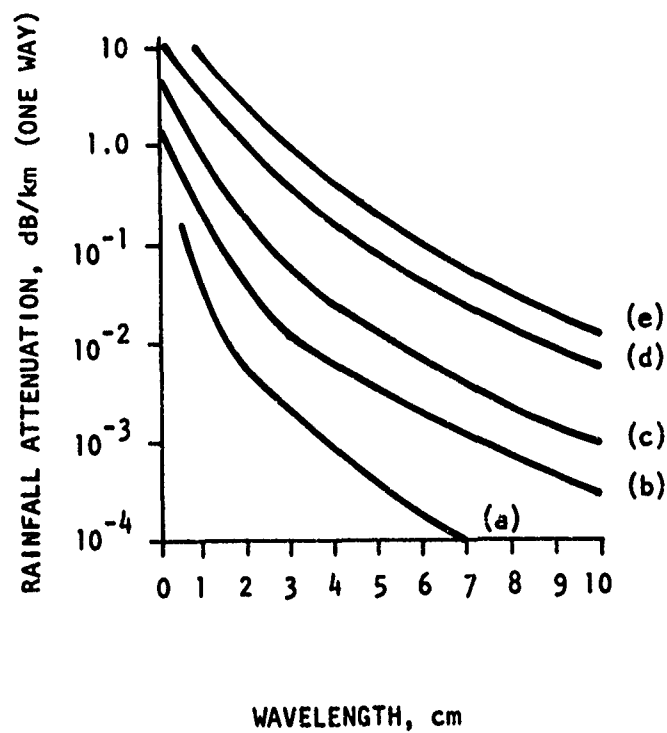
(a) Drizzle - 0.25 mm/hr
(b) Light Rain - 1 mm/hr
(c) Moderate Rain - 4 mm/hr
(d) Heavy Rain - 16 mm/hr
(e) Excessive Rain - 40 mm/hr

Figure 64.   One-way Attenuation (dB/km) in Rain at a Temperature of 18°C
             (Reference 11)

160
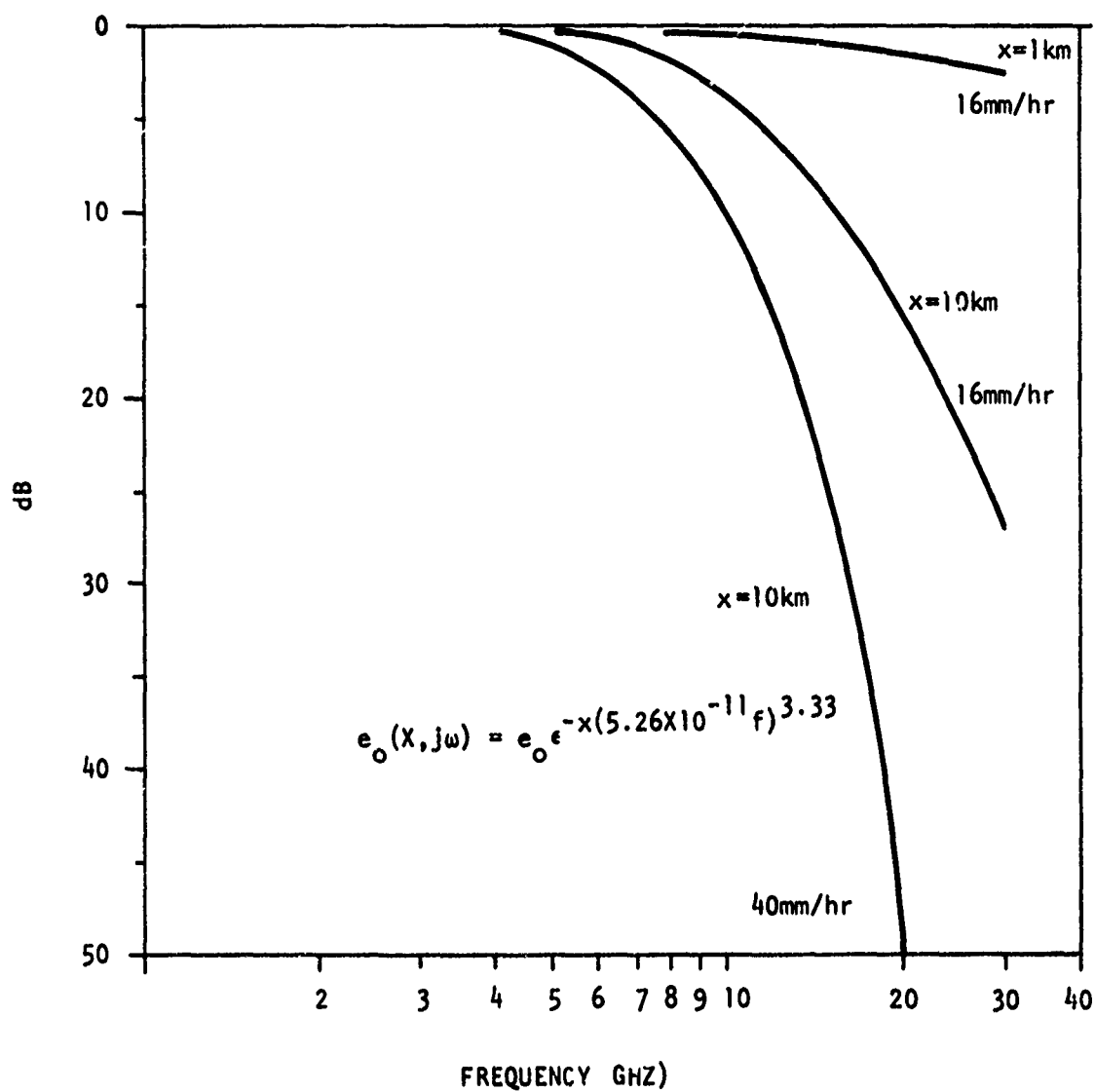
Figure 65. One Way EM Field Attenuation Through Rain Due to Absorption
for Two Ranges and Two Rainfall Rates

161

The above expression will be applied later to the signal to clutter enhancement problem to be investigated.

2. Scattering From Precipitation

Skolnik identifies a parameter Z which he associates with the reflectivity of randomly spaced particles within a given volume. This reflectivity is the summation of the backscatter cross sections of all the particles within the volume. When the backscattering particles are spheres such as rain, and are small with respect to the excitation wave length so that the Rayleigh approximation can be used, then

$$Z = \sum_{i=1}^{n} d_i^6 \tag{203}$$

where d is the particle diameter in millimeters and n is the number of particles. We will be using expression (203) to determine the number of rain drops there are in a given volume for heavy rain (see Reference 13).

Now Z is a meterological parameter that depends only on particle size distribution and concentration. It is desirable to relate it to the precipitation rate "r". Marshall-Palmer have done this (see Reference 12), where they have empirically derived the relationship

$$Z = 200 \, r^{1.6} \tag{204}$$

which they have found accurate to within ±50 percent in most stratiform-type rainfall distributions found in nature where the rate is between 0.5 to 70 millimeters per hour.

Equating expressions (203) and (204) and assuming an average rain drop size d in a given volume gives the relationship

$$n = \frac{200 \, r^{1.6}}{d^6} \quad \text{per cubic meter} \tag{205}$$

162

Let us now determine the number of rain drops in a cubic meter for the heavy rain rate of 40 millimeters/hour for drop sizes of approximately two millimeters. The drop sizes were mentioned in the introduction of this major section as being typical for heavy rain. The number per cubic meter is then calculated to be 1,140 particles, which is in the range of values indicated earlier.

Now that we have established the number of particles, we must next investigate the expected scattering response of these dielectric spheres of diameter d=2 millimeters. Although the literature gives the radar cross section of dielectric spheres, it generally treats them in the Rayleigh region for radar applications. For the purpose of our investigation, we shall modify our scattering models such that their Rayleigh regions have the same value as for dielectric spheres; however, the total description will go beyond this region in our model. In effect, we are seeking a scaling factor to account for the dielectric aspect of the particle sphere. The reason for this model is to bound the frequency response of the dielectric sphere rather than allowing it to continue on to infinity in Rayleigh fashion as the frequency is increased.

Skolnik gives the Rayleigh cross-sectional scattering of a dielectric sphere as (see Reference 13)

$$\sigma_r = \frac{\pi^5}{\lambda^4} |K|^2 d^6 \qquad (206)$$

where λ is the wavelength and $|K|^2$ is the dielectric constant factor which has a mean value of 0.917. Let us now determine the cross-sectional scattering in the Rayleigh region of the model B sphere approximation of Figure 20.

163

Its transfer function is

$$\Delta_s(j\omega) = \frac{T_{1/2}(j\omega)^2 \left[1 + \epsilon^{-j\omega\,2.5T_1}\right]}{(j\omega)^2 + \beta_1^2}$$
(207)

Taking this function in the limit as ω approaches low frequencies gives

$$\Delta_s(j\omega) = \frac{T_1(j\omega)^2}{\beta_1^2} = \left(\frac{2.5}{\pi}\right)^2 T_1^3\,(j\omega)^2$$
(208)

Applying next the definition of radar cross-section (expression 10), the d/c value for T_1 and ω in terms of λ gives

$$\sigma_s = \frac{16\,\pi^5\,d^6}{\lambda^4}$$
(209)

Comparing this cross section with the one given for a dielectric sphere of (206) indicates that the model has 16 times the effective cross section. This amounts to decreasing the transfer function (207) by a factor of four in order to represent a water drop.

With the attenuation expansion of the prior section, for rain absorption and a wide banded frequency model, and the number of drops for heavy rain per unit volume, we are now prepared to perform a calculation to determine the performance of the prewhitened matched filter in rain.

3. Signal to Clutter Calculation of a Spherical Target in Rain

This investigation indicates that the filter that gives the best signal to clutter ratio for a spherical target in spherical clutter is the pre-whitening matched filter combination of Figure 61. We shall now determine the volume that can be range gated before the quantity of rain within that volume causes the signal to clutter power ratio to approach 20 db or less. This 20 db level is the minimum level many radars require in order to function

effectively.

Since the pre-whitening double integrating portion of the filter causes the frequency response to diminish as $1/\omega^2$, it can be stated that the attenuation discussed under sub-section "1" will have more of an effect on the clutter than it will on spherical targets of interest. The reason can be seen by referring to Figure 63 and noticing that cutoff effects begin in the vicinity of 10 gigahertz for heavy rain and a one way distance of 10 kilometers. The $1/\omega^2$ effect will have certainly reduced the target scattered spectrum appreciably before this cut-off frequency. Hence, ignoring the attenuation effects will provide a conservative answer in terms of the volume that can be scanned. As it will be shown, the volume will still be immense.

Let us assume for the sake of determining a conservative maximum cross-sectional area that may be radar-like excited by a single impulse, that we have prior knowledge as to where the spherical target is in space and know its diameter d_1. We have shown, at various times, that for an impulse excitation, the scattered duration of a sphere is $2.5T_1$, where T_1 is d_1/C. Let us then adjust the range gate such that we only observe over this interval. There is a subtle point here that bears emphasis and that is that although the sphere occupies d_1 length in the range gate, the observation is over the space interval of $2.5d$; hence, the clutter over this interval must be considered. See the discussion under this chapter, section B.2.a for multiple clutter. It is also assumed that the number of clutter responses per range gate is the same meaning that any clutter entering from the prior range gate is balanced out by the number that is not recorded in this gate that will appear in the next one.

The expression for the pre-whitened matched filter adjusted to account for the dielectric clutter by reducing T_2 by a factor of four is from

165

expression (159)

$$\frac{s_o^2(\text{Max})}{\overline{c_o^2}} = \frac{16\pi^2}{2.5T_1 k}\left(\frac{d_1}{d_2}\right)^6 \tag{210}$$

Now, if "k" is the total number N of clutter particles observed over the time $2.5T_1$, it may be expressed as

$$k = \frac{N}{2.5T_1} \tag{211}$$

But N is determined by the volume density "n" and the volume interrogated. The range gate volume may be expressed as

$$V = 2.5d_1 A \tag{212}$$

where A is the cross-sectional area. The total number N of clutters is then nV. It follows that applying this result to (211) gives

$$k = \frac{2.5 \, d_1 \, An}{2.5 \, T_1} \tag{213}$$

Applying (213) to (210) and solving for A gives

$$A = \frac{16\pi^2}{2.5 \, d_1 \, n}\left(\frac{d_1}{d_2}\right)^6 \frac{\overline{c_o^2}}{s_o^2(\text{Max})} \quad \text{square meters} \tag{214}$$

We may now calculate the cross-sectional area that a radar beam can impulse interrogate to seek a one meter diameter sphere during a heavy rain and still have a signal to clutter ratio of 20 db (a factor of 100). The heavy rain of 40 millimeters per hour was shown to consist of 1000 drops of 2 millimeters in diameter. Then

$$A = \frac{16\pi^2}{2.5(1)(10^3)}\left(\frac{1}{2\times10^{-3}}\right)^6 \frac{1}{100} = 1 \times 10^{13} \, m^2 \tag{215}$$

a rather impressive area.

Now, if we wish to determine the range in meters that this area, formed

into a conical beam, would create, the relationship is from basic principles.

$$R = \frac{114.6}{\theta} \sqrt{\frac{A}{\pi}} \qquad (216)$$

where R is the range in meters and θ is the beam width in degrees. Applying

the value for area obtained above gives a range for one and a half degree

beam width of 146 million meters. This very large number indicates that one

has a large degree of freedom in terms not only of the choice of the sampling

range gate interval but also in the beam width and the target sizes to be

examined.

Let us next look at a golf ball size metal sphere for the same above con-

ditions. Consider d_1=4 centimeters. The resultant area A can be shown to be

1 megameter square or, for the same beam width, project this area at 146

kilometers of range.

We have demonstrated that the pre-whitened matched filter combination

does indeed provide a high degree of clutter rejection for a high density

rain environment.

This completes the investigation for selecting a filter that provides a

high degree of clutter rejection. We shall next concentrate on the discrimi-

nation problem.

WAVEFORM DISCRIMINATION AND GEOMETRY IDENTIFICATION

A. GENERAL CONSIDERATIONS

This section treats the problem of discriminating or sorting waveforms by class for the eventual identification of a target geometry. The major assumption here is that the waveform which enters the discriminator package is indeed a product of backscatter from the target of interest and therefore is not corrupted by the effects of clutter or noise.

It has been shown in earlier sections of this report that certain types of clutter can be adequately preprocessed out of the signal path by applying suitable filtering to the total input waveform prior to its entry into the discriminator package. Therefore, the pure or non-corrupted signal assumption is considered to be a reasonable one.

It was indicated earlier in the discussion on waveform approximation that geometries of the same general class but of different shapes can possess the same backscatter waveform when interrogated and viewed from a particular aspect angle. One example is the backscatter from the general class of cylinders of equal length viewed end-on. In this case, all cylinders of equal cross-sectional area but of different cross-sectional geometry will possess the same backscatter waveform.

This means that for the purpose of identification at one particular aspect angle the returned waveform does not necessarily uniquely identify the target geometry. It does, however, identify the target class. In order to uniquely identify a target object, such as the cylinder in question, the target

would require interrogation at more than one angle with respect to the target, since depth-geometry (area) variation has been shown to be a primary factor in forming at least the optical portion of a backscattered waveform. A determination of uniqueness for waveform-geometry pairs is outside the limits of this discussion, however. It will be assumed here that a backscatter waveform uniquely defines an abstract geometrical class rather than a particular geometry which must be identified. This uniqueness criterion will be deferred for later investigation.

A number of methods are presently available for classifying data. Among them are correlation methods and the pattern recognition technique, which will both be discussed in this section.

First, however, let us discuss the general philosophy of sorting or classification. The problem of classification of data is a classical problem and all solutions require the same basic elements, whether the solution is by correlation or even simple amplitude measurements.

Any data set which must be judged can be divided first into n separate measurements, which are represented by an n dimensional vector in what is called observation space. The ith measurement expresses a particular property of the total measurement of the event, and each particular coordinate of the vector has associated with it a numerical value which corresponds to the amount of each individual property which the event measurement contains. A set of events which belong to the same class correspond to a single point in observation space only if all events are exactly the same. In the more realistic case where measurements of the events in the same class are only similar but not

equal, the points corresponding to the individual events in observation space correspond to an ensemble of points scattered within some region of the space. A set of points from a given class might be expected to form a cluster in the n-dimensional space in the sense that distances between members of the same class are smaller than those between points which belong to different classes.

A simple illustration of this concept in two dimensional space is given in Figure 66, where the ensemble of points A represents different samples of class A, and those labeled B represent samples of class B. The m and n represent m_{th} and n_{th} data measurements and d represents a metric.

The measurement technique to be utilized which provides the greatest distance between observation points belonging to different classes while providing the least distance between points belonging to the same class is the prime consideration in most sorting systems (see Reference 14).

The concept of automatic sorting is presently being utilized in automatic character recognition and voice recognition and decoding devices. In the case of the character device, the problem is simplified because the input is restricted to a finite number of characters which are of a given size. This means essentially that the universe of possible character decisions is known a priori. Returning to the observation space concept, a known universe of decisions allows the construction of an optimal transformation in observation space which forces the situation that points belonging to the same class are brought closer together and points belonging to different classes are further apart. This general concept of closeness is essential for comparing waveforms and will be considered in a study of a number of metrics in this section.
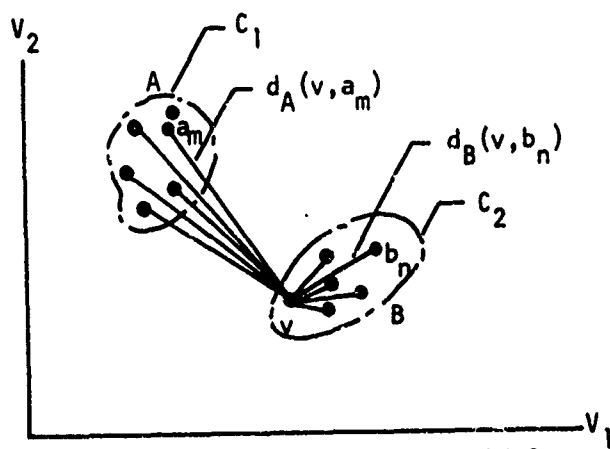
MEMBERS OF 'A' LIE WITHIN C_1,
THOSE OF 'B' LIE WITHIN C_2.

(see Reference 14)

BDM-W-72-094

Figure 66.   Clustering of Sample Points in Classes in Observation Space

Measurement of closeness in any system implies that the vector components comprising the observation point or region corresponding to the classes of interest have been defined. In one sense, definition of the class vectors implies the definition of a library of typical functions which are each defined by a finite number of points. The output of the distance measuring process in most systems corresponds to a scalar magnitude which is compared using an amplitude categorizing process.

The final step in the decision-making process is a logic step based on comparison of a threshold value, determined from previous measurements, and the discriminator output amplitude.

Figure 67 indicates the generalized sifting or discriminator package described in this section.

B. PATTERN RECOGNITION

Pattern Recognition is a general concept framework which is used to organize the classification process. Its value in the problem at hand is that it allows an overview of the problem and a framework for the solution.

The Pattern Recognition process consists of two steps; learning how to categorize the class in which a particular group of objects belong, and of deciding whether a new event belongs to the category or not. In terms of the discussion in the opening remarks, the learning process consists of defining the region of similarity in observation space. Recognition, on the other hand, consists of examining each new input and identifying the name of the region of the space in which the input is contained. In the character recognition problem the region can be rigorously defined and suitable transformations of observation space made such that regions of commonality and intersection are minimized,
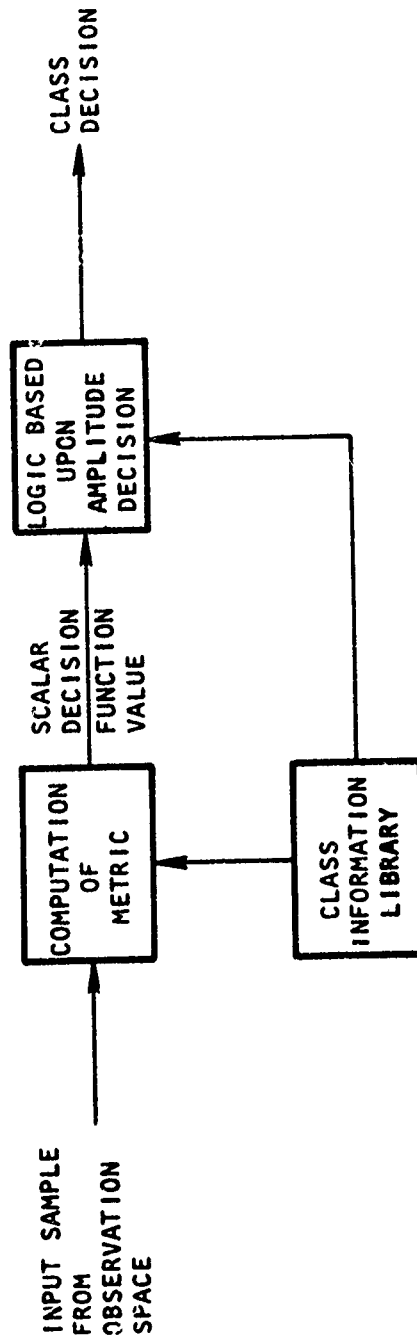
Figure 67. A Generalized Discriminator Package

174

simply because the problem is completely defined. In the problem where the set of possible decision sets is not closed, as in the general geometry identification problem, the concept of defining decision functions and their optimization is not wholly applicable.

Another concept useful to the theory and application of pattern recognition is the consideration of methods which exploit the dissimilarities that exist between the different classes of interest. This, of course, takes advantage of the situation that most characteristics of like sets will be similar, thus resulting hopefully in less computational effort and/or storage capability in the case of a positive identification. Methods which exploit class differences are sometimes termed discriminant techniques because they emphasize properties which allow discrimination between classes.

On the other hand, the use of discriminant functions is considered inferior to the use of likelihood ratios, which are based upon an a priori knowledge of class difference. This is clear, since the decision function approach uses less information on which to base its decisions.

The pattern recognition approach can most easily be understood by citing an example of its use. Many uses are found in the social sciences, where data are generally more difficult to process. In the classification of people into classes, each characteristic, for example height, weight, color, age, etc., is considered as one measurement vector in observation space. Each subject is measured for each characteristic and his measurement vector is plotted as a point representing the tip of a vector in n dimensional observation space. Only those characteristics are measured which the experimenter wishes to use to partition the space. Partitioning is done by encircling the regions representing the class of interest and finding these points enclosed by the solid in the space.

Let us attempt to apply the pattern recognition concept to the impulse signature problem. The raw data which we wish to classify is in the form of an electric field or voltage waveform which is a function of real time. This waveform must be transformed by some as yet undefined process in such a manner that it is represented by a vector in observation space; more specifically in n - dimensional observation space, when the partitioning in general will be more definative as n goes to infinity.

Consider the signature for a moment as an ensemble of points spaced in time, each of which is a measurement of some abstract characteristic of the target. Figure 68 illustrates this concept. The partitioning is simply a sampling of the signature, and the optimum number of samples necessary to completely characterize a function is given by the sampling theorem of information theory.

It was shown earlier in Chapter II that members of the same class but of different sizes are merely altered in magnitude and duration. This characteristic immediately suggests that some type of size normalization should precede the characterization process. Since stretching the input signature waveform cannot easily be done, it is recommended that the input be fitted with a suitable numerical procedure as it enters the discrimination section. Then measure a size-related characteristic of the input waveform and proceed to generate or reconstruct a replica of the signature normalized to and based upon a given class size stored in the memory unit of the discriminator package. Or for the purposes of both computational and time economy, the waveforms of the function library could be initially fitted to allow analytical "stretching" transformations during the identification procedure. This would eliminate the curve fit operation but would still require the generation of a family of class-related waveforms.

176
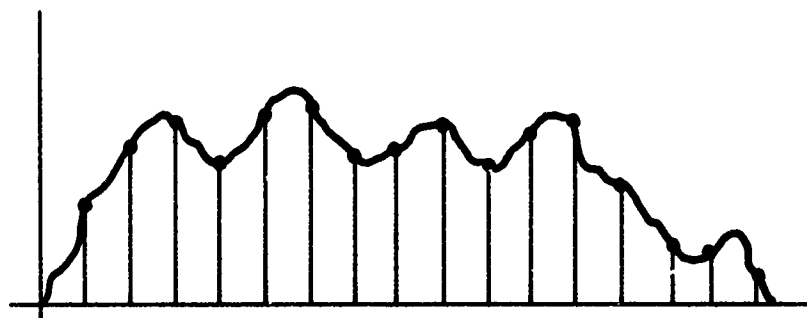
BDM-W-72-094

Figure 68. Partitioning the Signature

C.   SIZE DISCRIMINATION

Consider the problem situation where an input waveform of the form shown in Figure 69(a) impinges upon a processor in which is stored a waveform as shown in Figure 69(b). Clearly, the form is similar, but a point-by-point examination will not identify the points as being equal, since very few points directly correspond, and a cross-correlation will not identify the functions as being of the same class since the cross-correlation would be less than the decision value directed by the autocorrelation of Figure 69(b).

The second function is, from the previous discussion, simply related to the first through a sizing parameter. It then becomes clear that in order to process functions having varying sizes in such a manner that a standard functional library can be used requires a size normalization process.

Let us assume that the sphere's response data is stored as its second integral, parameterized to reflect the size related information. The stored function generator would take the form (see expression 20) indicated in Figure 70.

A similar parameterized waveform for the second integral square plate waveform takes the form indicated in Figure 71.

The parameter K can be readily determined from a given input waveform by simply measuring its maximum value. Having ascertained the size parameterization constant K, the various waveforms in the storage library can be generated to correspond to the size of the target object in question. The size detection and normalization scheme is indicated in Figure 72.

178
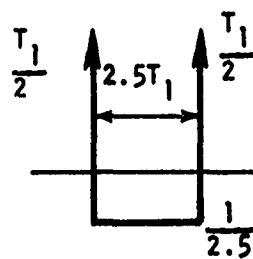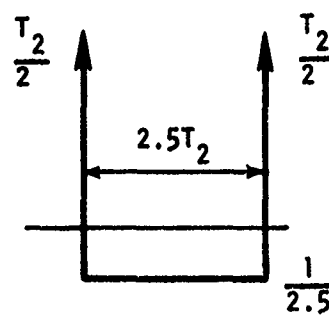
BDM-W-72-094

Figure 69.   Impinging and Stored Waveforms Related to Objects of the Same
            Class But of a Different Size

179

$$K \sin \frac{\pi}{5K} \quad \text{for } 0 \leq t \leq 5K$$

$$0 \text{ for } t \geq 5K$$
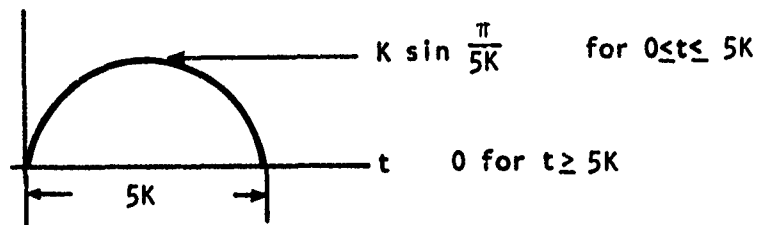
Figure 70. Parameterized Library Waveform for Second Integral of Sphere

$$K\varepsilon^{-\sqrt{\frac{\pi}{K}}\, t}$$
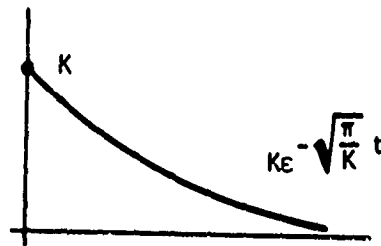
BDM-W-72-094

Figure 71. Parameterized Library Waveform for Second Integral Square Plate
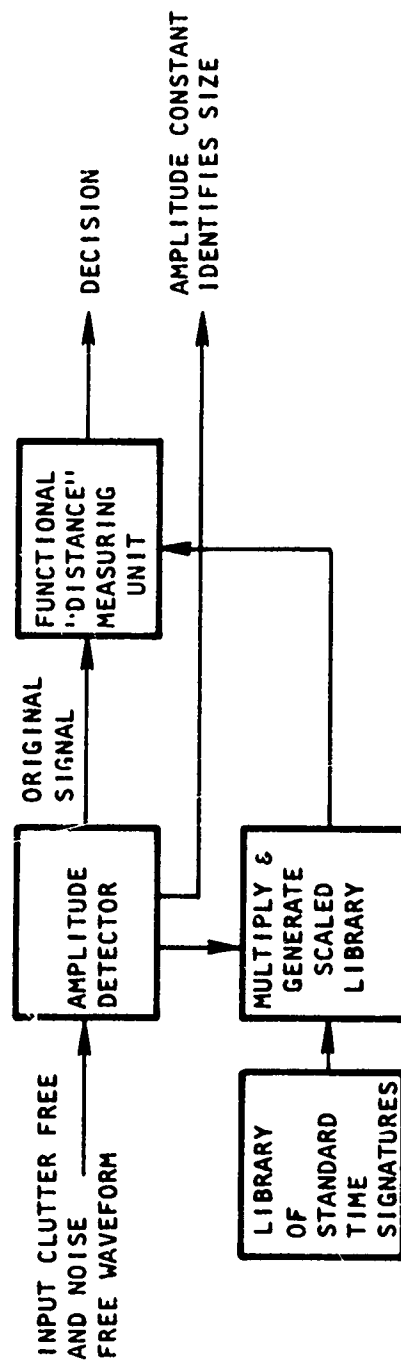
Figure 72. Size Detection, Normalization and Generation Package

BDM-W-72-094

D. MEASURING CLOSENESS OF FUNCTIONS

1. Cross-Correlation

    a. General

    The cross-correlation operation is useful in situations where the input function has been properly size normalized to allow comparison with a predetermined autocorrelation or threshold value. In this section three geometries and their cross and autocorrelations will be investigated to determine the effectiveness of the correlation technique for discriminating the waveforms of geometry classes. Here it is assumed that the size of the input object has not been normalized. Because of the smoothing which integration produces, an integrator and a low-pass filter step have been applied to the input waveforms to produce the following transformed yet unique signature waveforms.

    The value of the correlator output is proportional not only to the value from the correlator integral operation on the two functions of interest but it is also directly proportional to the leading constants of the respective functions in the correlation. This means that the correlator output is size magnitude related. Let us investigate the values which result from both auto and cross-correlations of the three functional forms indicated in Figure 73. (These waveforms have been normalized by removing the $\frac{c}{4r}$ term.)

    First, an explanation of the symbols and assumptions to be used is in order. The correlations will be defined by the integral operation indicated in Figure 74.

    The first subscript denotes the type of signal inputted and the second denotes the type of stored waveform with which it is being correlated. PS, for example, denotes that a decaying exponential caused by a plate scatterer

183

(a) SPHERE

Equation for sphere: $\bar{I}_s^2 \frac{1.25}{\pi}$ and $\frac{1.25}{\pi} T^2 \left(\sin \frac{\pi t}{5T_s} + \frac{\sin \pi (t - 2.5 T_s)}{5 T_s} \right)$; dimensions $1.25T$ and $2.5T$.

(b) PLATE

$\frac{T^2}{\pi}$; $\frac{2T_p^2}{\pi} \varepsilon^{-\alpha_p t}$

$$- \frac{\varepsilon^{-\gamma t} \sin \beta_R t \; cT_R}{4\beta_R r \left[\ln \frac{2l}{a} - 1 \right]}$$
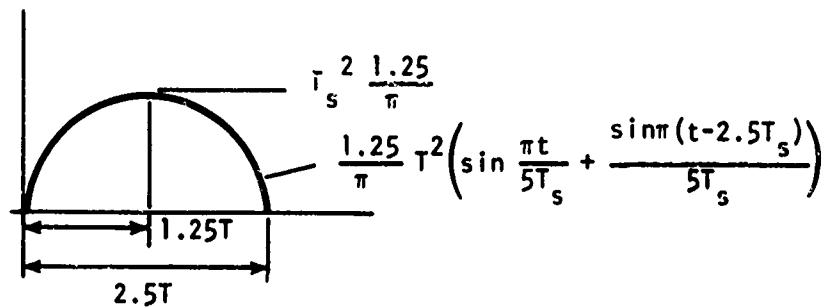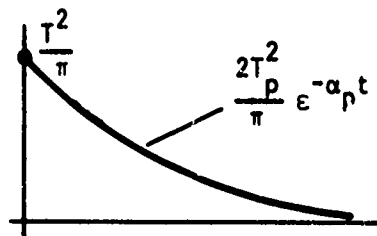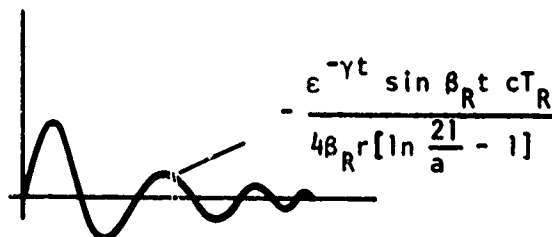
(c) ROD

BDM-W-72-094

Figure 73. Defining Signatures Used in This Section

184

$$\phi_{12}(\tau) = \int_{-\infty}^{+\infty} f_1(t) \, f_2(t-\tau) dt$$

SECOND SUBSCRIPT DENOTES STORED FUNCTION

FIRST SUBSCRIPT DENOTES INPUT FUNCTION

Figure 74. Explanation of Symbols and Assumptions

185

is impinging upon a system which has stored in its library a semi-sinusoid denoting a sphere. ϕ_{ss} denotes an autocorrelation of the sphere's response. Another assumption which will be used is that the leading constants in the expressions for sphere, plate, and rod integral responses can be written as K_s, K_p, and K_r respectively when they are being used in the stored or filter functions. The leading constant is the frequency independent portion of the backscatter expression. Here, for example, K_s denotes the value $\dfrac{T_s c}{8r}$. This simplification will become valuable later in the discussion.

Because amplitude detection is generally used in discrimination problems, it is of interest to determine the maximum values of the auto and cross-correlations.

The autocorrelations are : for a sphere,

$$\phi_{ss} \text{ (Max)} = \frac{125}{64} \quad \frac{T_s^5}{\pi^2} \quad \frac{c^2}{16r^2} \tag{217}$$

or, assuming the stored magnitude given only by K_s,

$$\phi_{ss} \text{ (Max)} = \frac{cK_s}{4r} \quad \frac{25}{16} \quad \frac{T_s^3}{\pi} \tag{218}$$

and, for a plate,

$$\phi_{pp} \text{ (Max)} = \frac{c^2}{8r^2} \quad \frac{T_p^4}{2\alpha_p \pi^2} \tag{219}$$

or, assuming the stored magnitude given only by K_p,

$$\phi_{pp} \text{ (Max)} = \frac{cK_p}{2r} \quad \frac{T_p^2}{\pi 2\alpha_p} \tag{220}$$

186

and, for a rod,

$$\phi_{rr} \, (\text{Max}) = \left[\frac{c^2 T_r^4}{16 r^2 \pi^2 \left[\ell n \, \frac{2\ell}{a} - 1 \right]^2} \right] \left[\frac{1}{4} \right] \left[\frac{1}{\alpha_r} - \frac{\alpha_r}{\alpha_r^2 + \beta_r^2} \right] \qquad (221)$$

or, assuming the stored magnitude given only by K_r,

$$\phi_{rr} \, (\text{Max}) = \frac{c K_r}{4r} \quad \frac{T_r^2}{\pi} \cdot \frac{1}{\left[\ell n \, \frac{2\ell}{a} - 1 \right]} \quad \left[\frac{1}{4} \right] \left[\frac{1}{\alpha_r} - \frac{\alpha_r}{\alpha_r^2 + \beta_r^2} \right]$$

Assume a filter with an input response like that of the square plate, $K_p \epsilon^{-\alpha_p t}$, with a rod's impulse response

$$\epsilon^{-\alpha_r t} \sin \beta_r t \; c T_r \bigg/ 4 \beta_r \left[\ell n \, \frac{2\ell}{a} - 1 \right] \qquad (222)$$

as defined by expression (222) impinging upon it. The cross-correlation output has the form of

$$\phi_{rp}(\tau) = \frac{K_p T_r^2}{\pi \left[\ell n \, \frac{2\ell}{a} - 1 \right]} \quad \frac{c}{4r} \quad \frac{\epsilon^{-\alpha_p \tau} \beta_r}{\left(\alpha_p + \alpha_r \right)^2 + \beta_r^2} \qquad \tau \leq 0. \qquad (223)$$

The maximum value occurs at $\tau = 0$ and has the value

$$\phi_{rp} \, (\text{Max}) = \frac{K_p T_r^2}{\pi \left[\ell n \, \frac{2\ell}{a} - 1 \right]} \quad \frac{c}{4r} \quad \frac{\beta_r}{\left(\alpha_p + \alpha_r \right)^2 + \beta_r^2} \qquad (\tau = 0) \qquad (224)$$

187

Corresponding output values for other waveform combinations are

$$\phi_{pr}(\tau) = \frac{2K_r T_p^2}{\pi} \frac{c}{4r} \frac{\varepsilon^{-\alpha_p \tau} \beta_r}{\left(\alpha_p + \alpha_r\right)^2 + \beta_r^2} \qquad (\tau \leq 0) \qquad (225)$$

and

$$\phi_{pr}(Max) = \frac{2K_r T_p^2}{\pi} \frac{c}{4r} \frac{\beta_r}{\left(\alpha_p + \alpha_r\right)^2 + \beta_r^2} \qquad (\tau = 0) \qquad (226)$$

For $\tau \geq 0$,

$$\phi_{rp}(\tau) = \frac{2\varepsilon^{-\alpha_p \tau} K_p T_r^2}{\pi \left[\ln \frac{2\ell}{d} - 1\right]} \frac{c}{4r} \left[\frac{\left[\alpha_p + \alpha_r\right]\sin\beta_p\tau + \beta_r \cos \beta_r\tau}{\left(\alpha_p + \alpha_r\right)^2 + \beta_r^2}\right] \qquad (\tau \geq 0) \qquad (227)$$

$$\phi_{pr}(\tau) = \varepsilon^{-\alpha_p \tau} \frac{2K_r T_p^2}{\pi} \frac{c}{4r} \left[\frac{\left[\alpha_p + \gamma_r\right]\sin\beta_p\tau + \beta_r \cos \beta_r\tau}{\left(\alpha_p + \alpha_r\right)^2 + \beta_r^2}\right] \qquad (\tau \geq 0) \qquad (228)$$

Now assume a filter with a response like that of the sphere,

$$K_s \left[\sin \beta_s t \, u(t) + \sin \beta_s(t - 2.5T_s) \, u(t - 2.5T_s)\right], \qquad (229)$$

with the plate's backscatter waveform impinging upon it. The graphical form of the cross-correlation for $\tau \leq 0$ is indicated in Figure 75, and the cross-correlation expressions in this region are

$$\phi_{ps} = K_s \frac{2T_p^2}{\pi} \frac{\varepsilon^{\alpha_p \tau}}{\alpha_p^2 + \beta_s^2} \left[\beta_s \varepsilon^{-\alpha_p 2.5T_s} + \beta_s\right] \qquad (\tau \leq 0) \qquad (230)$$

188
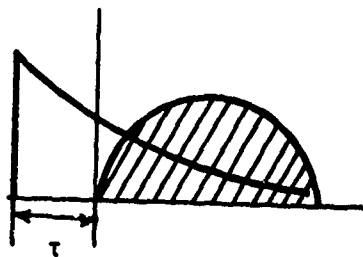
BDM–W–72–094

Figure 75. Sphere-Plate Cross-Correlation for $\tau \leq 0$

and

$$\phi_{sp} = K_p \frac{1.25T_s^{\,2}}{\pi} \frac{\epsilon^{\alpha_p \tau}}{\alpha_p^{\,2} + \beta_s^{\,2}} \left[\beta_s \epsilon^{-\alpha_p 2.5T_s} + \beta_s \right] \qquad (\tau \le 0) \qquad (231)$$

For $0 \le \tau \le 2.5T_s$, the cross-correlation is indicated in Figure 76. The expressions for the cross-correlation in this region are

$$\phi_{ps} = K_s \frac{T_p^{\,2}}{\pi} \frac{2\epsilon^{\alpha_p \tau}}{\alpha_p^{\,2} + \beta_s^{\,2}} \left[\beta_s \epsilon^{-2.5\alpha_p T_s} + \epsilon^{\alpha_p \tau} (\alpha_p \sin \beta_s \tau + \beta_s \cos \beta_s \tau) \right]$$

$$(232)$$

and

$$\phi_{sp} = K_p \frac{1.25T_s^{\,2}}{\pi} \frac{\epsilon^{\alpha_p \tau}}{\alpha_p^{\,2} + \beta_s^{\,2}} \left[\beta_s \epsilon^{-2.5\alpha_p T_s} + \epsilon^{\alpha_p \tau} (\alpha_p \sin \beta_s \tau + \beta_s \cos \beta_s \tau) \right]$$

$$(233)$$

For $\tau > 2.5T_s$, $\phi_{sp} = \phi_{ps} = 0$

Envisioned for a discrimination scheme utilizing cross-correlation is the system indicated in Figure 77. The decision threshold chosen for this exercise is the auto-correlation of the backscatter waveform of interest. Of interest, then, is the degree of discrimination or enhancement which the cross-correlation technique provides for the geometries which are being treated in this exercise.

Because the functional form of ϕ_{sp} and ϕ_{ps} is rather simple, let us look at these functions in greater depth to investigate for discrimination characteristics associated with the correlation function.

Since the generalized decision process is based upon a decision threshold, it became necessary to determine the maximum value for ϕ_{sp} and ϕ_{ps}. This was done by the usual calculus procedures, and the results are indicated in Figure 78. This figure indicates the value of τ as a function of the β_s/α_p

190
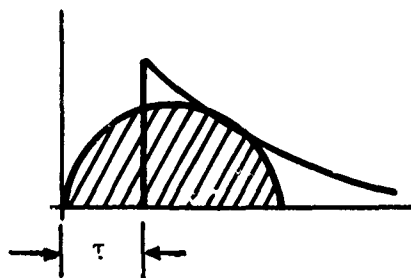
BDM-W-72-094

Figure 76. Sphere-Plate Cross-Correlation for $0 \leq \tau \leq 2.5T_s$
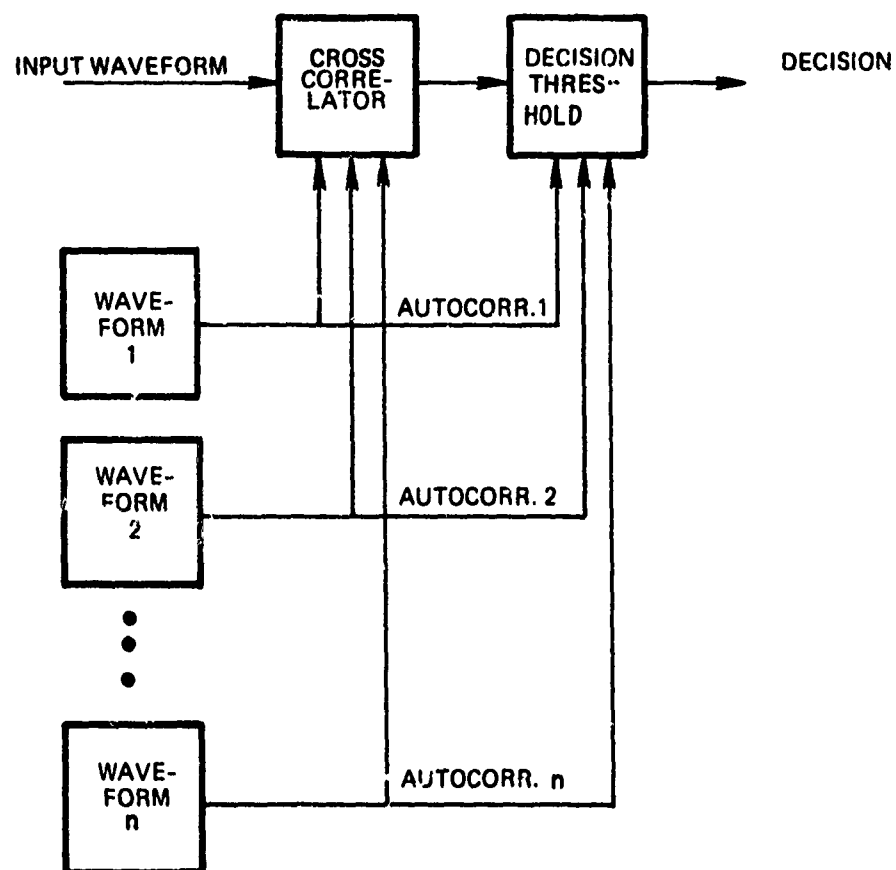
BDM-W-72-094

Figure 77. Discrimination System Utilizing Cross-Correlation
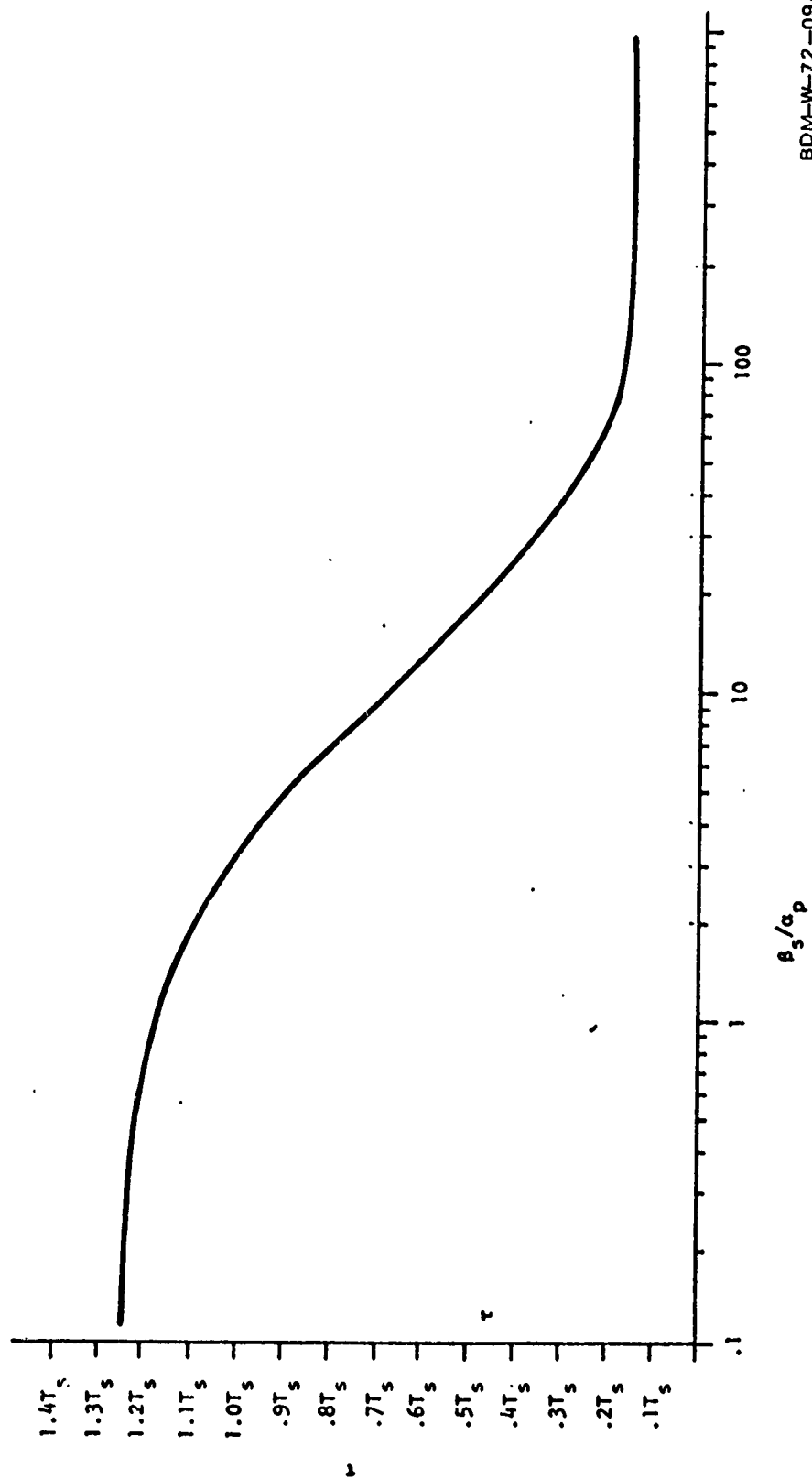
Figure 78. Values of τ For Which ϕ_{sp} and ϕ_{ps} Have a Maximum in the Interval $0 < \tau < 2.5T_s$

BDM-W-72-094

193

(size) ratio for which the maximum cross-correlation occurs. From this curve, the expressions for the correlation functions were evaluated.

Figure 79 displays the ϕ_{ss}/ϕ_{ps} and ϕ_{pp}/ϕ_{sp} ratios as functions of the sphere diameter to plate side ratio d/ℓ.

A number of conclusions regarding the use of correlation as a discriminant can be made by studying the figure. Note, for example, that for one d/ℓ ratio, both ratios are equal and thus no discrimination can be attained. On the other hand, as the d/ℓ ratio becomes greater or less than this value, the ability to discriminate becomes greater. For example, with a d/ℓ ratio of one, the ϕ_{ss}/ϕ_{ps} ratio is 2.7; whereas the ϕ_{pp}/ϕ_{sp} ratio is 0.8, a ratio of discrimination of 3.4. When the d/ℓ ratio rises to 1.5, the respective ratios are 8.5, 0.34, and 25. In general, then, this exercise indicates that the correlation technique is a useful one for purposes of discrimination, but that it exhibits one major shortcoming: There is a range about a size ratio value where very little discrimination is expected.

An extension of this technique can be made to an n class system. In that situation, the plot equivalent to that of Figure 79 would be in an (n-1) space. In that case, an examination of the n correlation ratios would necessarily identify the target. Again, however, there would exist a space of size ratios (equivalent to the point indicated previously in two-space) for which little or no discrimination would be possible.

b. Transformations on the Correlation Function

Having found correlation to be a valuable tool, the exploration of transformations on the correlation integral was felt to be a valuable exercise. Specifically, here we will investigate the form

194
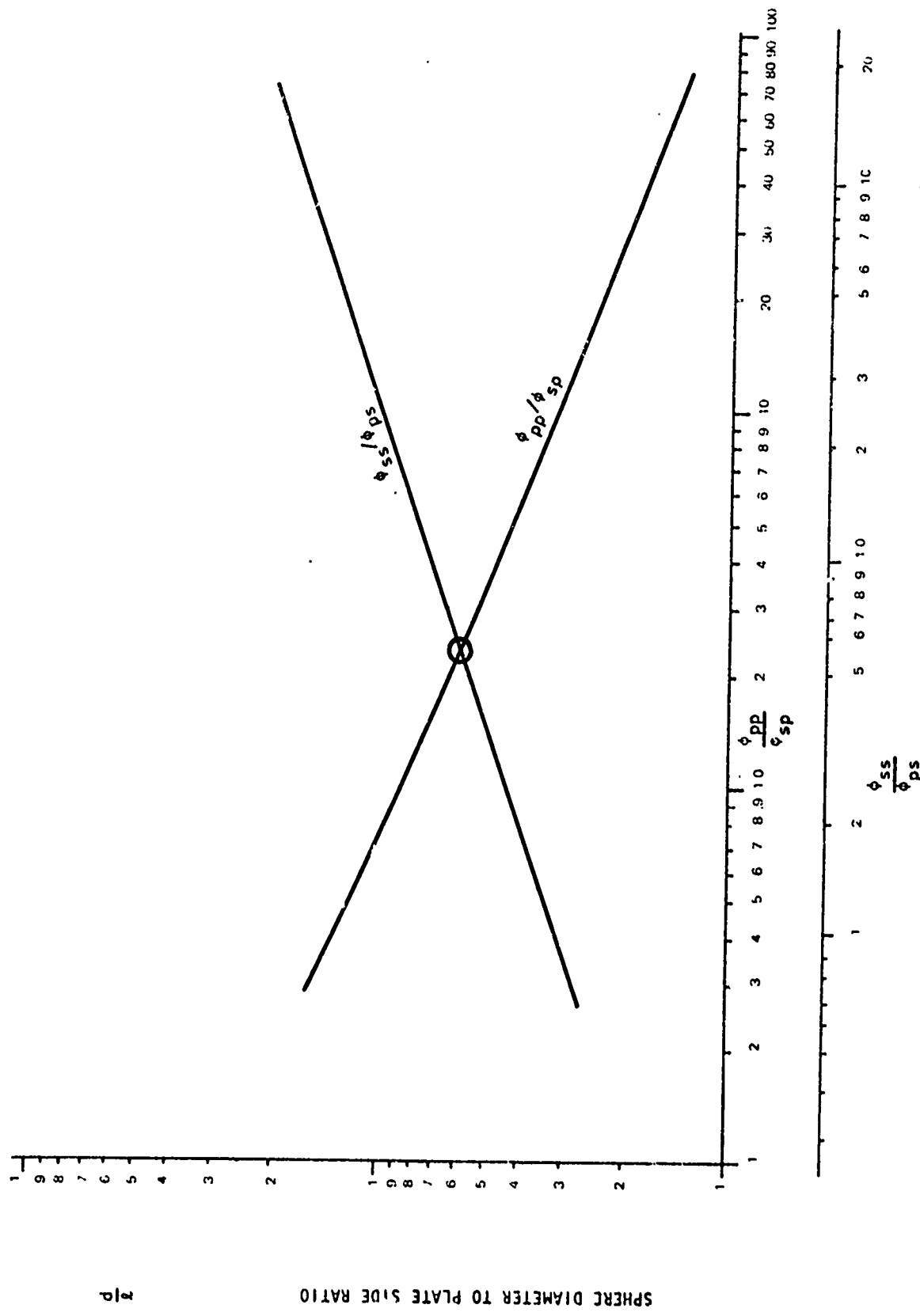
Figure 79. Ratios of Autocorrelations of Unit Sphere and Plate to Cross-Correlation of Plate and Unit Sphere as a Function of Sphere Diameter to Plate Side Ratio

$$\phi_{12}(\tau) = \int_{-\infty}^{+\infty} \left[f_1(t) \, f_2(t - \tau) \right]^n \, dt \qquad (234)$$

and its discrimination function through an exercise letting n = 2 and where f_1 and f_2 are the familiar sphere and plate double integral waveforms.

Carrying out the operation, the cross-correlation can be written,

$$\phi_{sp}(\tau) = \left[\frac{1.25 T_s^2}{\pi} \right]^2 \left[\frac{T_p^2}{\pi} \right]^2 \frac{4}{2(K^2+1)\beta_s} \left\{ \frac{1 - \varepsilon^{-\frac{K\pi}{1.25 T_s}(\tau - 2.5 T_s)}}{2K} \right.$$

$$\left. + \left(K \sin \frac{\pi\tau}{2.5 T_s} + \cos \frac{\pi\tau}{2.5 T_s} \right) \sin \frac{\pi\tau}{2.5 T_s} \right\} \quad 0 \leq \tau \leq 2.5T \qquad (235)$$

where $K = \dfrac{\alpha_p}{\beta_s}$.

Again, because it is of interest to utilize a threshold or maximum amplitude device for decision making, it is necessary to find the maximum value of ϕ_{sp}. In the size ratio range of interest, the maximum cross-correlation occurs in the $0 < \tau < 2.5 T_s$ range. The maximum value of expression (235) was calculated in a manner similar to that described in the previous section.

The autocorrelations again maximize for a value of $\tau = 0$, and have values of

$$\phi_{ss}(\text{Max}) = \frac{3\pi}{8\beta} \cdot \left(\frac{1.25 T_s^2}{\pi} \right)^4 = .0235 T_s^9 \qquad (236)$$

and

$$\phi_{pp}(\text{Max}) = \frac{T_p^8}{\alpha_p \pi^4} = .00818 T_p^9 \qquad (237)$$

196

The ratios

$$\left. \frac{\phi_{ss}(\tau^2)}{\phi_{ps}(\tau^2)} \right|_{Max} \quad \text{and} \quad \left. \frac{\phi_{pp}(\tau^2)}{\phi_{sp}(\tau^2)} \right|_{Max} \quad \quad (238))$$

are plotted in Figure 80 for comparison with the similar ratios determined
by the conventional correlation integral. Again the values of the correlation
ratios are equal for a particular size ratio and they diverge as the size
ratio becomes either greater or smaller than the critical value. For par-
ticular ranges of the values of $\frac{d}{\ell}$ the values of the discriminate function are
more divergent using this method than in the conventional case, thus providing
a high degree of discrimination ability. For example, for the $\frac{d}{\ell}$ ratio of 0.16,
the ϕ_{pp2}/ϕ_{sp2} ratio is 3.6×10^3 and the ϕ_{ss2}/ϕ_{ps2} ratio is 3.25×10^{-3}, a
discriminant ratio of 1.1×10^6. This compares with a discriminant ratio of
4.22×10^3 with the correlation technique reported in the previous section. In
the region where d/ℓ is 1.5, the higher order process yields a discriminant
ratio of only 2.48, which compares unfavorably with that of 25 found by the
previous method. This indicates that neither technique is optimal over the
full d/ℓ range, but rather that each is best used over a particular range if
high discrimination potentials are desired.

2. Area Differences

Investigating the correlation process reveals that the basic distance
measuring technique upon which it is based is the simple Euclidean metric,
for this type of problem simply involves measuring the absolute distance between
points of two functions having equal abscissas. More generally, it is a
transformation which may be considered as a summing of the individual metrics
under an equal weighting. In general, when correlation is used, problems
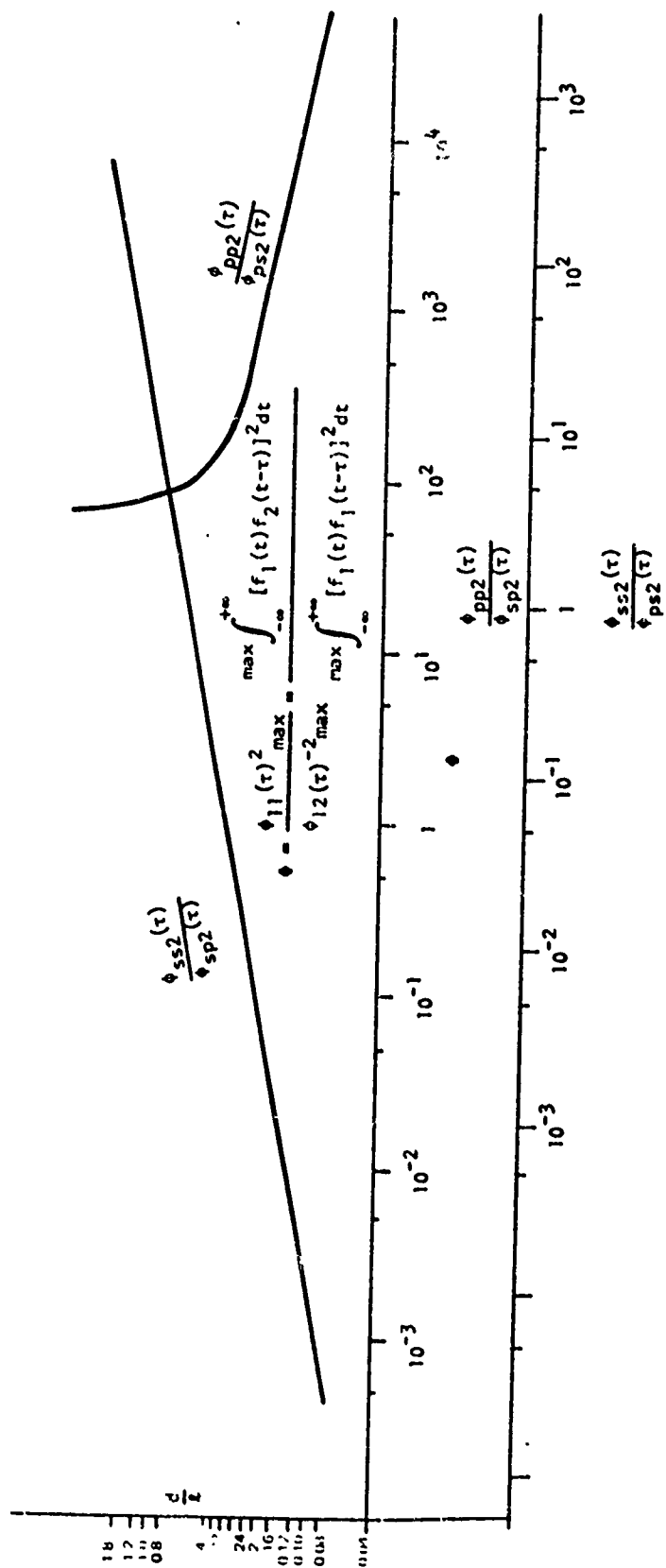
Figure 80. The Parameter φ (As Defined Above) Versus the Sphere-Plate Size Ratio d/ℓ

BDM-W-72-094

198

INPUT WAVEFORM
$f_i(t)$
SIZE
(NORMALIZED)

$f_i(t) - f_n(t)$

ABSOLUTE
VALUE
$\left| f_i(t) - f_n(t) \right|$

INTEGRATOR
$\int \left| f_i(t) - f_n(t) \right| dt$

NULL
DETECTOR

SEQUENTIAL
SWITCH

DECISION
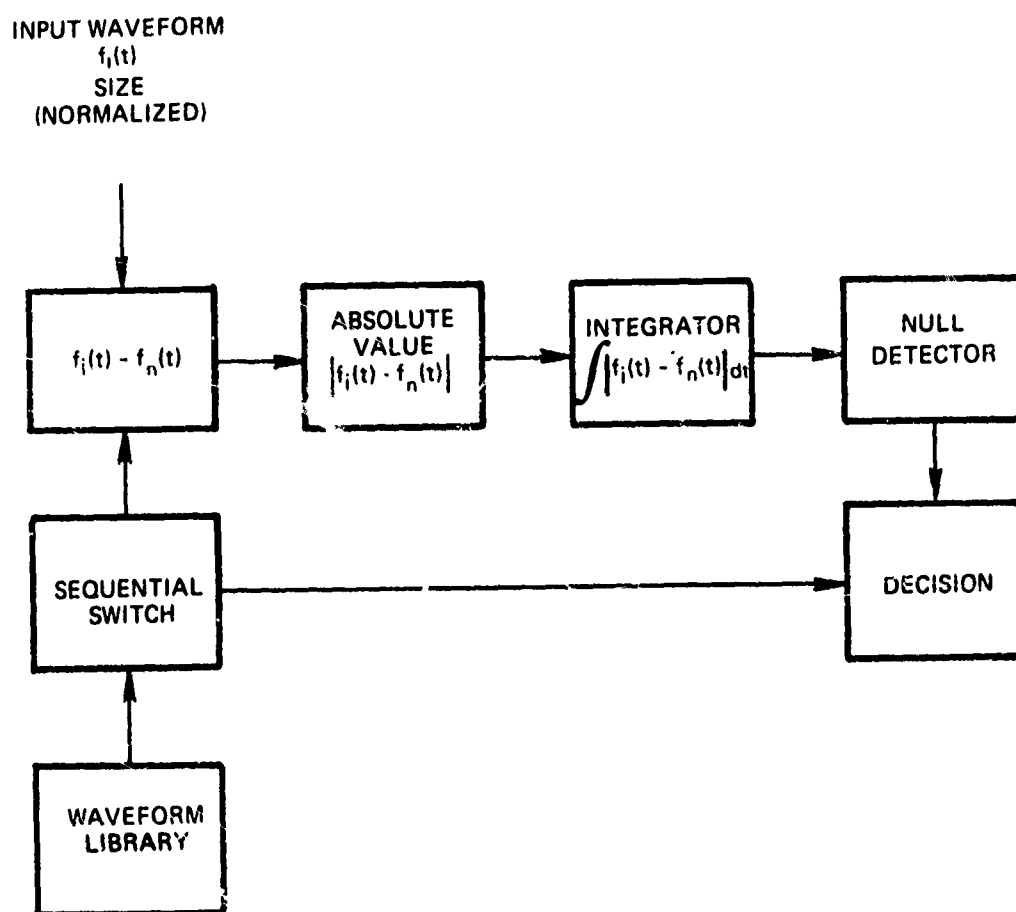
WAVEFORM
LIBRARY

BDM-W-72-094

Figure 81. Area Difference Integral Waveform Identification Scheme

SPHERE

PLATE

2.5T$_s$
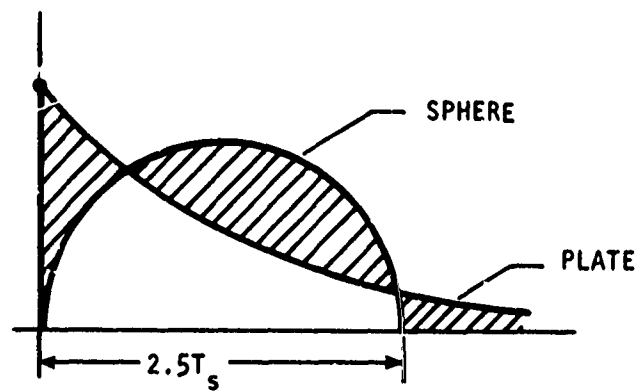
BDM-W-72-094

Figure 82. The Area Difference for a Sphere-Plate Discriminator

The cross-hatched region is the area difference between the two functions and is a measure of their similarity or dissimilarity, since only a matched condition will produce a zero area difference.

Figure 83 is a plot of the integrator output as a function of the plate length to sphere diameter ratio (the waveform for one of which would be stored in a recognition situation). Note that while in a recognition status the output of the integrator would be a null, the area difference in the plate-sphere situation exhibits a lower limit. The null provides positive identification of waveform similarity, since the only constraint upon the identification decision is the degree of deviation from a null which the designer allows in the decision criteria. As the similarity of waveforms from different classes becomes greater, the allowed deviation from the absolute null value will require tightening. This is equivalent to reducing the intersect regions of presently overlapping sets by simply reducing their volume.

A technique which may be used to facilitate decision making may be to transform the decision function in an advantageous manner. For example, decision functions may be transformed by reciprocating or antilog transformations. Two integral differences could be quite close together, but first reciprocating and then taking the inverse logarithm will produce transform discriminant values which will allow a greater ability to select the match function because a small difference is amplified by the transformation.

One advantage of this scheme is that it does not require a complex implementation package. Only a size normalization, a trigger to initiate processing, a function generator, and a null [range] detector are required to produce a waveform recognition package.
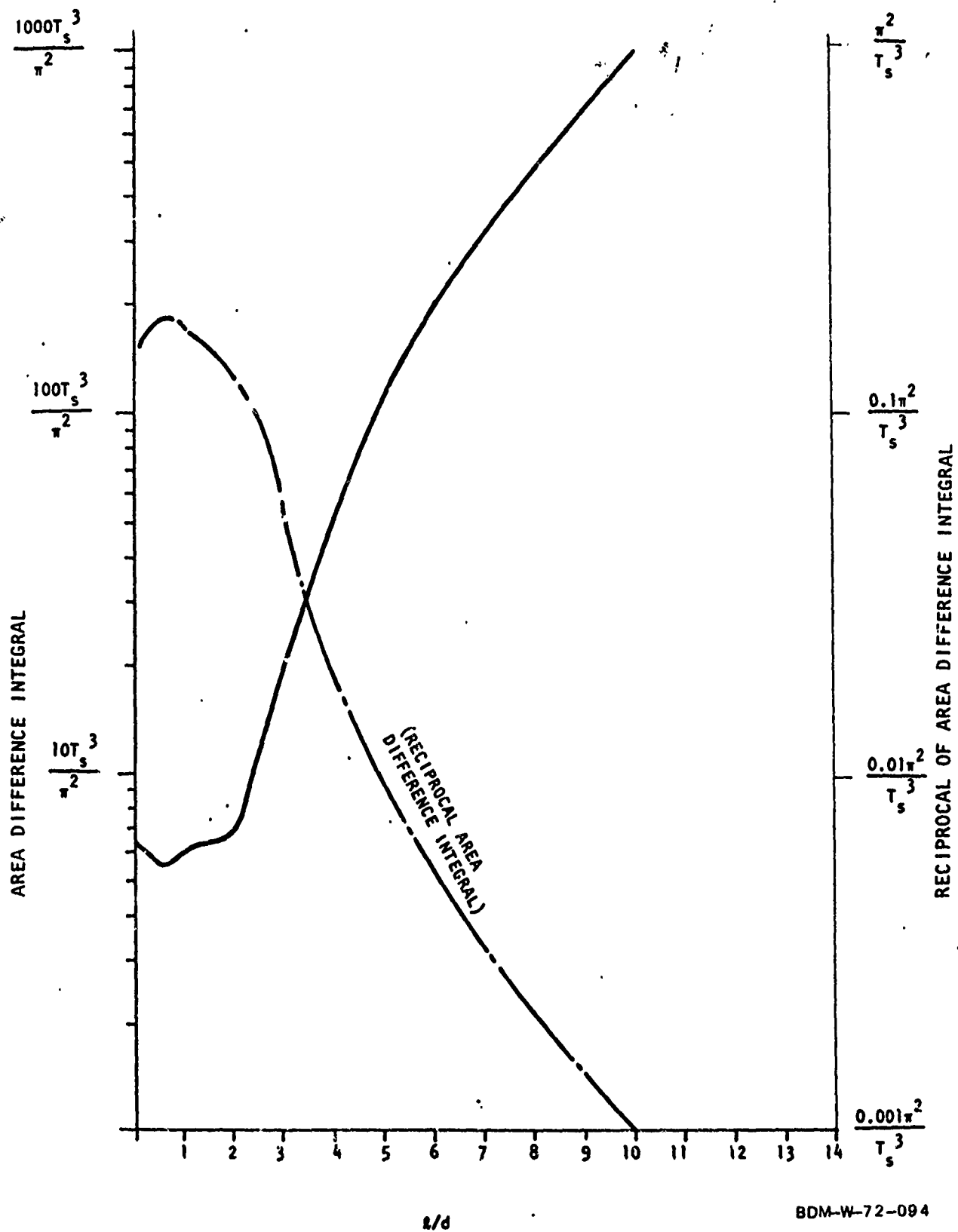
Figure 83. Plate/Sphere Area Difference Integral

BDM-W-72-094

202

3 Weighting Functions

a. General

Weighting has a number of uses in measuring closeness between points and sets of points. In the two methods treated thus far, similarity was treated in terms of transformations based directly upon the Euclidean metric or mean square distance. The method of measuring distance was not further treated or specified but rather left as a generalized distance concept because there are many metric forms, only one of which is the Euclidean form.

In some cases, however, it is desirable to weight some of the measurement data more heavily than other of the data, depending upon the degree of its contribution in defining the class of the subject of interest. A key to understanding this concept is the term "feature weighting," which serves particularly well in exemplifying the use of the weighting function in the problem at hand.

Suppose that there exist n classes, each of which is defined by a waveform which exists exclusively between the limits $0 \leq \tau \leq T_i$. Suppose in addition, that all are the same or similar with the exception of a region of Δ width between $t_1 \leq t \leq t_2$ as shown in Figure 84.

With an a priori knowledge of the nature of these waveforms, it would be desirable to heavily weight the data in the region $t_1 \leq t \leq t_2$ and less heavily weight the data outside the region. This is clear and in keeping with the philosophy initially discussed in this chapter, since it indeed exploits the dissimilarities in samples of different classes while similar regions of the functions play only a small role in determining similarity.

$f_1(t)$

Δ

$f_2(t)$

$f_3(t)$

t_1 t_2

0        $t \longrightarrow$ T_1
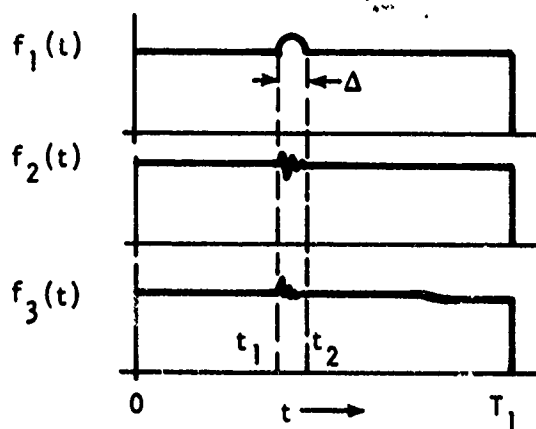
BDM-W-72-094

Figure 84. n Classes Determined by Similar Functions Find Feature
Weighting Advantageous

204

One type of metric which has been used earlier in this chapter is the Euclidean form

$$d(a,b) = |a-b| \qquad (239)$$

or

$$d(a,b) = \sqrt{\sum_{n=1}^{N} (a_n - b_n)^2} \qquad (240)$$

A form of weighting which is often used is the one described by the metric

$$d(a,b) = \sqrt{\sum_{n=1}^{N} W_N^2 (a_n - b_n)^2} \qquad (241)$$

where W_n is the weighting function.

A more complex form is the functional weighting

$$d(a,b) = f(|a-b|). \qquad (242)$$

A good example of the functional weighting is the exponential weighting indicated by the expression

$$d(a,b) = K \exp\left(-\gamma \sqrt{\sum_{n=1}^{N} (a_n - b_n)^2}\right) \qquad (243)$$

b. Distribution Weighting

Not all waveshapes emanating from the same object class are necessarily the same. However, certain portions of the waveforms are more alike than others, and these are the portions which characterize the waveform as belonging to that particular class. Consider defining a class and performing experiments in which each element of the class is illuminated with the impulse waveform. One could expect to find a distribution of return signatures as indicated in Figure 85.

205

$f(t)$

MEAN VALUE
SIGNATURE

t ⟶
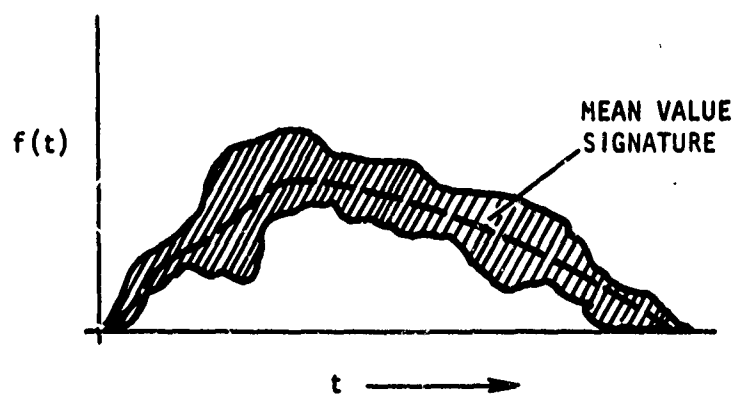
BDM-W-72-094

Figure 85.   Return Signatures in a Distribution About a Mean

The mean value of the distribution can be determined and it as well as a standard deviation from the mean at each point are indicated in the figure. One step simpler is the situation where the deviation from the mean of the experimentally determined signatures is not a function of t. Consider the situation where the signatures are distributed Gaussian about the mean value function. This is a reasonable assumption since many natural phenomena distribute Gaussian. Figure 86 indicates the Gaussian distributed signature pattern. A suggested weighting scheme which heavily weights signature characteristics of a similar nature and the converse is to weight an unknown input function with the value of the distribution for that point in time. Consider an input function $f_1(t)$, to determine whether or not it belongs to the class defined by the distribution defined in the figure. The discriminant function is given by expression (244)

$$d = \sum_{n=1}^{N} \exp \left[-\alpha \left| f_{mn}(t) - f_{1n}(t) \right| \right] \tag{244}$$

The value of α is dependent upon the distribution and is determined experimentally. In the region a - b the weighting would be equal to 1, a full weighting, and in other regions the weighting would be less, depending upon the value of $\exp[-|(x_1-x)|]$ at that point. The selection of the threshold value for d at which a class identification is made is based principally upon the types of class waveforms which all of the classes exhibit, as well as their similarity. When two or more classes are similar, regions in observation space may overlap, thus creating set intersects which result in identification of a waveform as belonging to more than one class. This situation can be alleviated by either increasing the discrimination thresholds of the intersecting functions or by

207
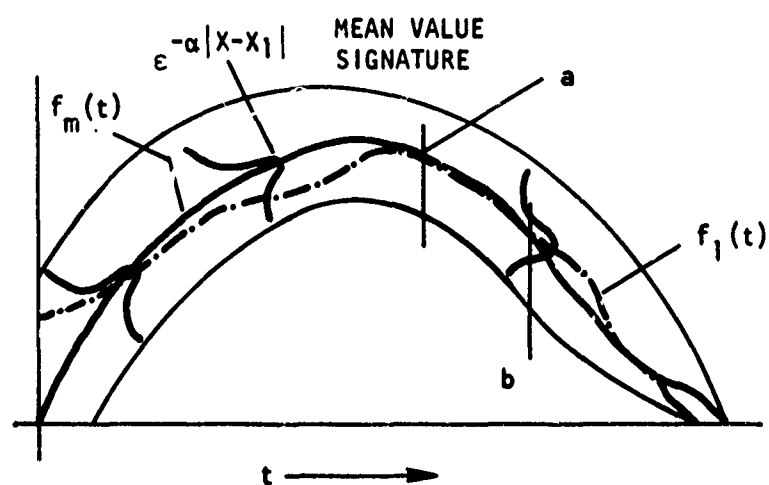
Figure 86. Class Signatures Distributed Gaussian About a Mean Value Function

adjusting the weighting with the constraint that the number of correct identi-
fications be maximized.

4. The Decision Template Concept

The latter work with distribution function weighting suggests the
construction of a mathematical template which may be used to compute a dis-
criminant function. A very simple scheme is to assign a weight of one
[recognition] to a partition value if it lies within the template region
and zero [no recognition] to the partition value when it lies outside the
template region. Here again the decision threshold value selection is based
wholly upon the similarity of waveforms belonging to classes other than the
one of interest.

It was desired to develop a system which would identify a waveform
given that the input sample had no deviations from the waveform stored in the
library. It was also desired that the value of the discriminant function be
as large as possible when the recognition state was met and as small as
possible when any other state was met.

A suggested scheme is a decision template like that described above
and implemented by an exponential transformation. The exponential transfor-
mation of expression

$$d_1 = \sum_{n=1}^{N} \exp^{-\alpha|f_1(t) - f_2(t)|} \tag{245}$$

is a metric much like the one discussed in the section on distribution weighting,
but here there is no distribution and α controls the allowed width of the
decision template. The discriminant function will have the form indicated in
expression (242). It is desired that since the input is an exact replica of
one of the waveforms stored in the function library, that the template width

209

be made δ wide [a line width] to just accommodate the function itself. This can be done by letting the value of α in the exponential become a large number. Figure 87 illustrates the decision template.

When α is a large value, only those Euclidean distances which are zero will make a contribution to the discriminant function, since in effect, those points which lie exactly on the curve will contribute a value of one and those not lying on the curve will contribute a value of zero. Any other function will be assigned a value of one only at the points of intersection while the replica will be assigned a value of one at all points for which it is sampled. The value of α is dependent upon the implementation of the system. Specifically, a finite template width must be constructed to accommodate nonlinearities in the system which would force an exact replica impinging upon the system to deviate from the stored waveform when it is measured.

As an example of the use of this concept to generate discriminant function values, the plate and sphere impulse waveforms, normalized to produce equal amplitudes, were used in a scheme having n partition values. Either of the waveforms could play the role of the impinging waveform. Assuming that the replica is impinging for either waveform; the output value would be computed as n for either curve, since a value of 1 would be assigned at each partition point. Again it must be cautioned that size normalization must precede this process and further that sampling must be over a time width at least equal to the width of the library waveform for this process to be successful. Figure 88(a) shows the two functions of interest in this section, and Figure 88(b) shows a plot of their difference magnitude.

ALL OTHER FUNCTIONS

δ WIDE

FUNCTION OF INTEREST

f(t)

t ⟶
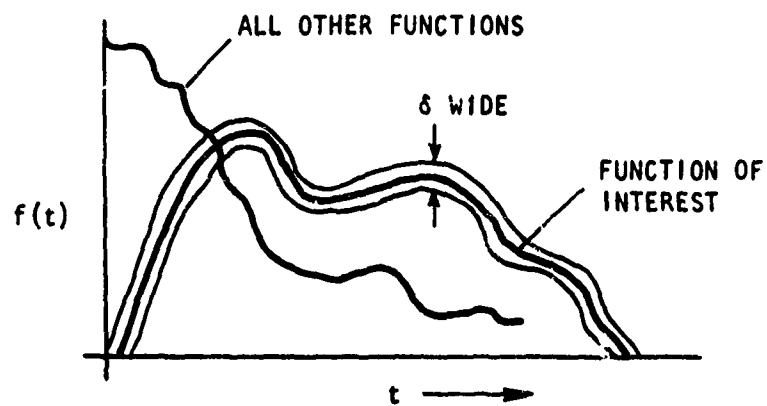
BDM-W-72-094

Figure 87. The δ Width Decision Template for Non-Distributed Functions

211
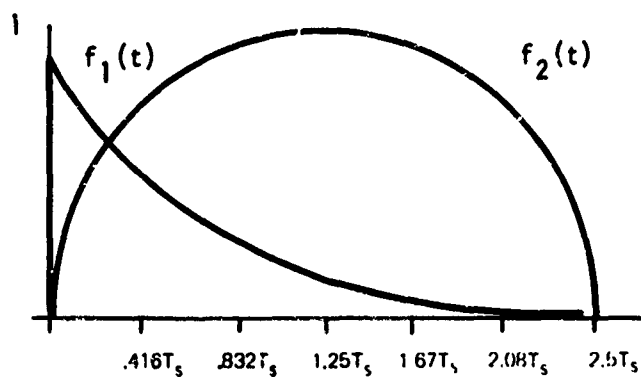
(a) NORMALIZED SPHERE
    AND PLATE WAVEFORMS
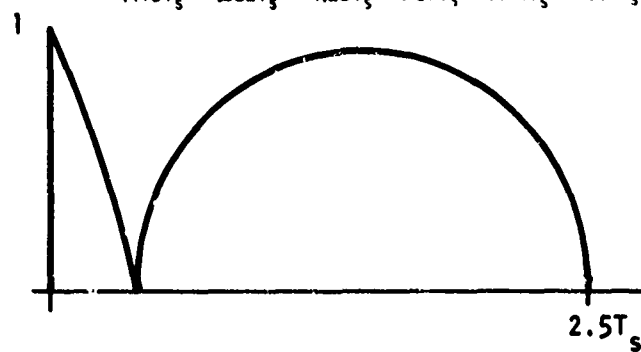
(b) $|f_1(t) - f_2(t)|$

BDM-W-72-094

Figure 88. Sphere and Plate Waveforms and Their Difference Magnitude

212

The variable N was assigned values of 31 and 61 and the variable
α, reflecting the width of the decision template was assigned arbitrary
values of 10, 20 and 40. Not only the discriminant of expression (245) but
also the discriminant

$$d_2 = \sum_{n=1} \exp\left[-(f_1(t) - f_2(t))^2\right] \qquad (246)$$

indicated in expression (246) was investigated for corresponding output values
with these two functions.

The discriminant values were computed as follows:

	f_1/f_2	f_1/f_1 or f_2/f_2	Discriminant Ratio
(n=31; α=10)	$d_1 = 6.306$	$d_1 = 31$	4.93
(n=31; α=20)	$d_1 = 4.502$	$d_1 = 31$	6.9
(n=31; α=10)	$d_2 = 2.380$	$d_2 = 61$	13
(n=31; α=20)	$d_2 = 1.475$	$d_2 = 61$	21.1
(n=61; α=10)	$d_2 = 4.492$	$d_2 = 61$	13.5
(n=61; α=20)	$d_2 = 2.491$	$d_2 = 61$	24.5
(n=61; α=40)	$d_2 = 1.549$	$d_2 = 61$	39.4

Bearing in mind the construction of this technique, the combination
of highest value of both n and α is seen to be most advantageous since it
maximizes the Discriminant Ratio.

Since increasing the value of n was seen to be advantageous, a continuous measure was felt applicable. Here the discriminant is defined by expression

$$d = \int_{o}^{2.5T_s} \epsilon^{-\alpha \left[\left| \epsilon^{-\alpha}p^{\tau} - \sin \beta_s \tau \right| \right]} dt \qquad (247)$$

The integral was solved graphically based upon the data indicated in Figure 89. Here the area under the envelopes represents the discriminant function. Again the matched case is simply solved but the discriminant value here is

$$\int_{o}^{2.5T_s} \epsilon^{0} dt = 2.5T_s \qquad (248)$$

For the unmatched case the discriminant values were calculated for the continuous sampling as

f_1/f_2	Discriminant Ratio
$d(=10) = 0.17T_s$	14.7
$d(=20) = 0.0729T_s$	34.3
$d(=40) = 0.0425T_s$	58.8

The discriminant ratio is defined as the ratio of the matched discriminant value (here a constant $= 2.5T_s$) to the unmatched discriminant value. The most advantageous case is the one for which $\alpha = 40$, the highest discriminant ratio. It is conceivable that as $\alpha \to \infty$, $d(\alpha=\infty) \to 0$, and the Discriminant Ratio will go to infinity. But the value of α must be selected

214

$$W_2 = \varepsilon^{-\alpha}|f_1(t) - f_2(t)|$$

$$\text{DISCRIMINANT} = \int_0^{2.5T_s} \varepsilon^{-\alpha}|f_1(t) - f_2(t)|_{dt}$$
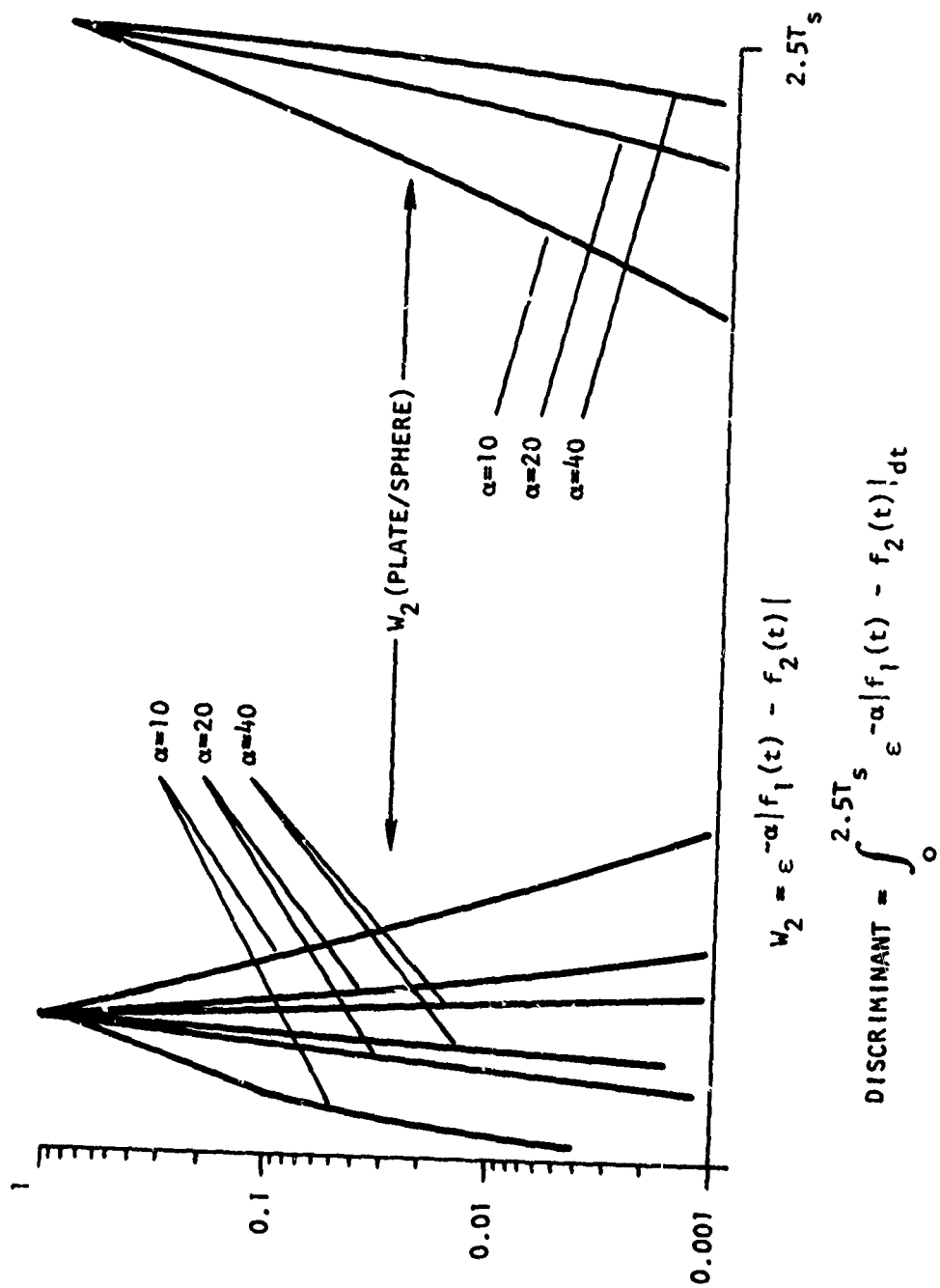
Figure 89. Exponentially Weighted Sphere/Plate Metric for Computation of Discriminant Function

BDM-W-72-094

215

based upon the quality of the implementation system and the degree of replication of the waveform of interest to the stored waveform. As in previous cases, the limitations upon the lower value of the discriminant threshold are a function of the specific classes which will be treated in the system and of their similarity. These are decisions which the designer must make based upon the expected system inputs. If the expected inputs are unknown with exception to the one of interest, the safest course is to raise the threshold until the point is reached for which incorrect classifications are being made. The result is that the choice of the discrimination function threshold is dependent upon the statistics of the problem and therefore cannot be chosen or dictated without specific knowledge of the problem at hand.

5. Summary

This section of the report has addressed the problem of geometry identification through classification of the backscattered waveform. One of the assumptions upon which this study has been made is that the backscatter is unique for each geometry class. As has been shown in Section II, the backscatter is physically dependent only upon area and depth relationships, but not necessarily the total geometrical configuration. This however, is a problem involving multiple interrogation by radar sites removed from one another with respect to aspect angle and must be addressed as a separate problem.

This study has indicated first that the object size must either be known or that size normalization procedures must be implemented prior to the identification process.

216

A thorough search of the current literature in the area of pattern recognition and waveshape identification, along with the study of a number of techniques for determining metrics, were carried out. These studies revealed that the basic concept of recognition of waveshape necessarily requires a system of the form indicated in Figure 72. This system incorporates a function library, a size normalization (if a size range is desired), a distance measuring unit, and a decision unit. Most decision functions are implemented by comparing the length of the decision function vector with a predetermined threshold value. The problem which remains, however, is how does one best measure the distance between two functions which represent two different geometry classes.

Two rather easily implemented techniques based upon cross-correlation were advanced. These studies indicated that a sphere and a plate can be identified based upon threshold values, but that there is a size ratio range where discrimination is not possible.

Another simple technique which was investigated is the area differences technique. With this technique it was shown that a sphere and plate could be differentiated and that there exists a size ratio where the discriminant function assumes a minimum value not equal to zero.

In a further investigation the concept of feature weighting was studied. This technique is particularly applicable to problems where the classes are defined by waveshapes which are somewhat similar with exception to a portion of the waveform where features play a decisive role in discrimination. It is for this reason that the decisive portion of the waveform is heavily weighted in the decision process and, conversely, the somewhat similar portion of the waveform is weighted less heavily.

217

In studying the weighting process, several metrics were discovered which allow distance measurement based upon probabilities of decisiveness of various portions of the waveform. This in turn lead to the formation of the concept of the decision template, which was shown to allow a very accurate decision based upon the nulling process. Here the decision threshold is the null, and the process is limited only by the clutter rejection technique and the quality of the class definition in the waveshape library. Theoretically, if the target function is known using this technique it will be identified, since the output will be a null, and otherwise the output will be finite value. In no case can a particular measurement technique be classified as optimum or "the best one can do" simply because the nature of the problem of optimization constrains the technique.

CHAPTER V

RESULTS AND RECOMMENDATIONS

This chapter will provide an overview of the results of this study followed by a series of briefs on areas for future study.

A.   SUMMARY OF RESULTS

This report is divided into three chapters, each of which concerns itself with a single aspect of the detection and discrimination problem.

In Chapter II the backscatter waveshapes of three basic geometrical configurations were developed. These shapes are: the sphere, the thin flat plate, and the long thin rod. Because the sphere has been studied in great detail and is well documented in the literature, this shape and its waveform served as a firm foundation for postulating simplified waveshapes. Starting with the work of Kennaugh and Moffett (see References 3, 4, and 5), it was shown that the impulse response of the sphere can be approximated quite well by several simple and mathematically tenable models. One of these models is the form

$$\delta_s(t) = \frac{c}{4r}\left[\frac{T}{2}\,\delta(t) + \frac{T}{2}\,\delta(t-2.5T) - \frac{1}{2.5}\,u(t) + \frac{1}{2.5}\,u(t-2.5T)\right] \qquad (249)$$

(where $T = d/c$ is the target dimension to velocity ratio and "r" is the observation distance) which became quite useful in later work. Another model which is not only quite useful in work involving filter analysis but is also verified quite well by experimental work is the form

$$\delta_s(t) = \frac{c}{4r}\left[\frac{T}{2}\,\delta(t) + \frac{T}{2}\,\delta(t-2.5T) - \frac{\pi}{5}\,u(t)\,\sin\frac{2\pi}{5T}\,t - \frac{\pi}{5}\,u(t-2.5T)\,\sin\frac{2\pi}{5T}\,(t-2.5T)\right]$$

$$(250)$$

Another sphere backscatter impulse response approximation which was found to be particularly useful in frequency domain filter analysis was the form

$$\delta_s(t) = \frac{c}{4r}\left(\frac{T}{2}\right)\left[\delta(t) - \frac{1}{1.25T}\varepsilon^{-\frac{t}{1.25T}}\left(2 - \frac{t}{1.25T}\right)\right] \tag{251}$$

The flat plate scattering of dimension "ℓ" was determined by two methods. A first approximation, which is based upon the methods of Kennaugh and Moffett, resulted in a model of the form

$$\delta_p(t) = \frac{\ell^2}{2\pi cr}\frac{d}{dt}\delta(t) \tag{252}$$

An extension of this model led to an expression which more closely approximates experimentally experimental work in which BDM has participated. This model postulates a time waveshape of the form

$$\delta_p(t) = \frac{\ell^2}{2\pi cr}\left[\frac{d}{dt}\delta(t) - \alpha\delta(t) + \alpha^2\varepsilon^{-\alpha t}\right] \tag{253}$$

The thin rod was modeled by studying the impulse of a thin monopole antenna absorbing and reradiating energy in space. Its transfer function was developed and shown to be

$$\Delta_r(j\omega) = \frac{KT_r(j\omega)^2}{(j\omega+\alpha_o)^2 + \beta_r^2} \tag{254}$$

where K is a constant, T_r is ℓ/c, α_o its damping constant and β_r its resonant frequency.

In Chapter III several filter configurations were investigated for their signal-to-clutter enhancement capabilities. The orthogonal filter was advanced as a filter which, although it is not a practical configuration, theoretically can produce an infinite signal-to-noise output ratio. The Lee correlation

220

technique is another technique which was advanced for informational purposes. With this technique, a clutter waveform can be removed from the target waveform and an infinite signal-to-clutter ratio will be seen at the filter output so long as the clutter is moving randomly with respect to the target.

The white noise matched filter configuration was studied for its enhancement of the signal-to-clutter ratio for a target in the presence of clutter. For a target sphere and spherical clutter with impulsive interrogation, the output signal-to-clutter ratio was found to be (the 1 subscript relates to the target and 2 to the clutter)

$$\frac{S_o(max)}{C_o(max)} = 2\left(\frac{T_1}{T_2}\right) \tag{255}$$

or a power S/C ratio proportional to the square of the sphere diameters. However, only a factor of four in enhancement between input and output power ratios can be had with this configuration. With the same filter configuration but with a finite pulse width interrogator, the filter enhancement in output to input signal-to-clutter power ratio was found to be

$$\frac{S_o^2(max)/\overline{C_o^2}}{S_i^2(max)/\overline{C_i^2}} = 3.54\left(\frac{T_1}{T_2}\right)^2 \tag{256}$$

The relationship shows that the enhancement increases with the second power of the sphere and clutter diameters.

Multiple clutter objects were investigated to ascertain the effect upon the composite backscatter waveform of placing many objects with various spacings in height and depth in the same range cell. It was found that spheres, to possess unique waveforms in time, must be displaced at least 1.25d between centers in depth. Placing several similar objects of the same

221

size exactly in the same range from the radar unit and in the same range cell will add to form a composite waveform with the original period and the composite amplitude. It was found that the maximum matched filter output resulting from multiple sphere targets placed one behind the other in a line will possess a backscatter waveform which will be limited in amplitude to four times the amplitude of that produced by one sphere's backscatter waveform.

In the case of randomly spaced spherical clutter surrounding a large spherical target, the output-to-input signal-to-clutter power enhancement with the white noise matched filter configuration was found to be

$$\frac{S_o^2(max)/\overline{C_o^2}}{S_i^2(max)/\overline{C_i^2}} = 0.92 \left(\frac{T_1}{T_2}\right)^2 \tag{257}$$

which is again proportional to the ratio of their diameters squared.

The low pass filter was advanced as possible means for taking advantage of the fact that clutter might have a peculiar frequency domain character. With the configuration described in this report, which was composed of a low pass filter preceded by an integrator, the power output-to-input signal-to-noise enhancement was found to be

$$\left[\frac{S_o(max)/C_i(max)}{S_i(max)/C_i(max)}\right]^2 = \frac{\beta_1}{\gamma} \left[\frac{T_1}{T_2}\right]^2 \tag{258}$$

where β_1 is a parameter of the target and γ is the cutoff frequency of the filter. It is possible to preserve the target waveform's shape by making the $\frac{\beta_1}{\gamma}$ ratio less than 0.1. This characteristic is of possible interest.

A multipole low pass filter was designed by adding a second stage to the single pole configuration. This effort resulted in a greater enhancement of the output-to-input signal-to-clutter ratio.

A bandpass filter was next considered. The full filter configuration was an integrator followed by a band pass filter. Of interest here was the ability of the filter to discriminate between a sphere and a plate of approximately the same size. It was found that the output signal-to-clutter ratio for a sphere target and plate clutter is on the order of 1.0 for the equal cross sectional area case.

Since prior results indicated that a low pass filter scheme tends to enhance clutter rejection, combinations of low-pass and matched filters were then investigated. For the configuration composed of a matched filter preceded by an integrator, the sphere target-plate clutter situation resulted in an output signal-to-clutter power ratio

$$\left[\frac{S_o(max)}{C_o(max)}\right]^2 = \frac{(2.5)^6}{64} \pi^2 \left(\frac{T_1}{T_2}\right)^4 \tag{259}$$

With a spherical target and spherical clutter the same output power ratio is

$$\left[\frac{S_o(max)}{C_o(max)}\right]^2 = \frac{\pi^2}{4} \left[\frac{T_1}{T_2}\right]^4 \left[1 - \left(\frac{T_2}{T_1}\right)^2\right]^2 \tag{260}$$

Comparing the expression for spheres to the sphere-plate result suggests that this filter is better for plate than sphere clutter.

Considered next was a configuration composed of a double integrator followed by a matched filter. With both a spherical target and spherical clutter, the output signal-to-clutter power ratio was determined as

$$\left[\frac{S_o(max)}{C_o(max)}\right]^2 = \frac{\pi^2}{16} \left(\frac{T_1}{T_2}\right)^6 \tag{261}$$

This result proved to be rather encouraging, since it represented the largest signal-to-clutter ratio obtained for targets and clutter of the same

223

configuration.

In the special case where "K" random clutterers per range gate sampling time were considered with this filter configuration, the output signal-to-clutter power ratio was found to be

$$\frac{S_o^2(max)}{\overline{C_o^2}} = \frac{\pi^2}{2.5} \frac{1}{kT_1} \left(\frac{T_1}{T_2}\right)^6 \tag{262}$$

It was also shown that the filter enhancement ability is a function of its interrogating waveshape.

With the same filter configuration but with a spherical target and plate clutter, the corresponding output signal-to-clutter power ratio for "k" randomly spaced plates in the range gate has the form

$$\frac{S_o^2(max)}{\overline{C_o^2}} = \frac{\pi^4}{2.5T_1 k} \left(\frac{T_1}{T_2}\right)^6 \tag{263}$$

which is π^2 or approximately ten times greater than for the sphere on sphere case. Because of the high enhancement capabilities of this configuration, it was found to be the best for the case where the target object is larger than the clutter object.

The optimum filter configuration, which is essentially a "prewhitening" filter followed by a matched filter was considered next.

In the treatment of a spherical target amidst spherical clutter it was found that there is no clutter rejection enhancement between the output and input signal-to-clutter power ratio. In reality, there can be, however, and that depends upon the form of the input signal-to-clutter ratio.

In the case of rod shaped clutter and a spherical target, again the filter did not perform well. The reason that the filter does not perform well,

however, is that the signal and clutter pole structures are similar.

In the case of a spherical target immersed in plate clutter, the output-to-input power signal-to-clutter ratio is

$$\frac{\frac{S_o^2(max)}{\overline{C_o^2}}}{\frac{S_i^2(max)}{\overline{C_i^2}}} = \pi^2 \left(\frac{T_2}{\tau}\right)\left(\frac{T_1}{T_2}\right)^3 \left[1 + \frac{1}{(1.25\pi)^2}\left(\frac{T_2}{T_1}\right)^2\right] \qquad (264)$$

This enhancement figure is very good and compares quite favorably with the configuration described previously, that of a double integrator followed by a matched filter.

Rain was studied as a practical clutter medium. The case of excessively heavy rainfall and its raindrop size and density was studied to determine a realistic clutter situation. This information was used with the prewhitened matched filter to achieve a quite good output signal-to-noise power ratio of

$$\frac{S_o^2(max)}{\overline{C_o^2}} = \frac{16\pi^2}{2.5T_1 k}\left(\frac{d_1}{d_2}\right)^6 \qquad (265)$$

where "k" is the total number "N" of clutter particles observed over the time $2.5T_1$. The cross-sectional area was calculated which one might be able to observe in space with the high clutter environment with a given deterioration of the signal-to-clutter ratio. It was found, as an example, that with a signal-to-clutter ratio of only 20 dB, a golf ball sized target could be identified in a heavy rain environment at a range of up to 146 Km with this prewhitened matched filter.

In Chapter IV, the problem of identifying a given object by its geometry class from its impulse waveform was investigated. It was determined that the problem could be essentially formulated as a pattern recognition problem. One of the points of interest in this section is the problem related to object

225

size and the backscatter waveform. It was shown to be a relatively easy matter to build a system which could incorporate the ability to discriminate between objects of the same object class and of a different size.

Next, a number of schemes were developed to measure distance between functions. Essentially, the classification problem when classifying waveforms is a distance measuring process. The cross-correlation operation was used, along with the autocorrelation value as a means of measuring the metric. It was shown that the technique is valuable and is capable of a high discrimination ratio, but the discrimination ratio is a function of the sizes of the waveforms stored in the function library.

The concept of feature weighting was described. This is particularly valuable in cases where large portions of waveforms of differing classes are similar, but the marked differences appear only as a fine grain feature area.

The area difference integral was shown to also be a valuable tool for measuring the metric between function representative of two different classes. Its value is that the function is positively identified, because upon positive identification state the discriminant transforms into a null or zero state.

Finally, the discriminants associated with the pattern template concept were investigated. This is a very interesting technique and the discriminant can best be described by

$$d = \int_{0}^{t_o} e^{-\alpha |f_1(t) - f_2(t)|} dt \tag{266}$$

where α is a large number.

In this method, a limiting value is outputted for the discriminant when the waveform like the one stored in the system impinges upon its input.

226

Otherwise, a small output or one equal to zero, as shown in the exercises, is outputted for the discriminant value.

B. RECOMMENDED AREAS OF POSSIBLE FUTURE STUDY

The following paragraphs will briefly list areas of possible future study.

1. Experimental Verification of Performance of Best Filter Determined in This Study

This study showed that the filter that provided the best signal-to-clutter enhancement was a matched filter preceded by a double integrator. It is recommended that the predicted performance be confirmed by laboratory experiments. This could be accomplished by obtaining an off-the-shelf random noise generator and applying its output to a filter that produces time responses that represent the impulse scattering response of clutter objects of interest. This output then becomes the random spaced time response of clutter objects as might be observed by an impulse excitation of clutter objects in space.

The clutter rejection filter described above would then be assembled and tested for the above input with and without the presence of a desired target signal. Tests could then be performed which could include varying the amplitude and spacing of the clutter (along with its shape) and observing the filter's output performance.

This could be followed by varying the occurrence of the target signal and its shape to confirm its detectability.

At the satisfactory completion of these laboratory tests, the next step would be to use this filter arrangement in conjunction with an impulse radar and determine the signal-to-clutter rejection that can be achieved in various small clutter environments such as rain with various targets present.

227

2. **Overall Impulse Radar Performance Study for Clutter Rejection using the Derived Filters of this Study**

Knowledge and experience is currently available as a result of RADC-funded contracts and other work such that an entire signal processing study could be performed on an impulse radar. It is recommended that impulse radars, as currently configured, be analyzed in conjunction with the filters determined in this study in order to assess their application for clutter rejection and detection. An obvious consideration is that the impulse radar does not generate a single impulse (since it cannot transmit dc) but it transmits either a monocycle or its derivative. This study centered on a pure impulse excitation. It should be determined what effect the change in waveshape has on the filter performance or if an additional modification is required.

This study should also consider the practical limitations imposed by the radar's parameters such as the antenna, transmitter, and receiver bandwidth, and other characteristics. Further work should also be undertaken to determine environmental effects upon the spectral content of the impulse output signal. Particularly important are the effects of the earth (groundscatter and absorption), weather, and of radiators and absorbers of EM in the path between the antenna and the target. Normal receiver and antenna noise should also be considered.

3. **Cataloging Impulse Scattered Wave Shapes in Order to Construct Discriminator Decision Functions**

For indications which will become helpful in designing an appropriate decision function for various geometries, a number of various objects having the same general characteristics and geometry should be irradiated as targets to determine the deviation from a mean value function. This mean value and

deviation could then be used as a standard decision function for further work in the area of target geometry identification. This investigation would also point up the target characteristics which give rise to variations in the fine grain structural variations in the backscattered time-waveshape.

Because the impulse radar time waveshape is indicative only of area size and depth variations, it is not a sufficient indicator of the geometry of a three-dimensional object, especially that of a complex object. It is of interest to investigate possible schemes for further enhancing or interrogating the target return in order to obtain a complete indication of the geometry of interest.

Therefore, a study item should be to determine the effect in scatter transform space of rotating the geometry of the scatterer in real three-dimensional space. It is suggested that a number of objects--rod, plate, and oblate spheroid--be studied by slowly rotating them a few degrees and recording the time-waveshape as a function of their angle. Then develop a technique to incorporate this rotation in the processor.

In terms of theoretical analyses, it is suggested that an investigation be made of the discrimination potential of polarization of the receive and transmit antennas. This is best investigated by looking at the electromagnetic equations with sufficient boundary condition dependent upon the scatter geometry.

Further extensions of the waveform identification and pattern recognition work should be studied in order to determine the optimal transformation which provides the decision function for arbitrary input functions.

4. Backscattering and Target Identification Studies

In the area of target identification, the rotation study suggested earlier could be applied to a system utilizing multiple interrogators and a correlation scheme to analyze the backscatter from a number of points. This system would allow a decision of the three-dimensional geometry of the target.

Further work should be done to provide a more sophisticated scheme for predicting the waveshapes backscattered from complex, multifaceted geometries. While the work of Cosgriff is helpful in determining the waveshape of simple geometries, it incorporates a degree of unsophistication which makes it difficult to theoretically predict backscatter from objects having many surfaces and boundaries.

Moving objects require additional receiver processing. Methods particularly suited to the impulse radar technique, and related necessarily to the range gating problem, should be investigated to determine how to best solve the clutter/identification/translation/rotation problem associated with the moving target.

Experimental work should be undertaken to determine the specific effects of dielectric constant upon the cross-section of an object. Theoretical data is available on dielectric constant variation of a sphere's cross-section, but this should be verified experimentally. Preliminary indications, gleaned from the literature, indicate perterbations in the cross-sections across the band. In addition, other geometries' dielectric dependence should be seriously investigated.

230

REFERENCES

1. Weil, H., M. L. Barasch and T. A. Kaplan. <u>Scattering of Electromagnetic Waves by Spheres</u>, University of Michigan Research Institute Report 2255-20-7, July 1956.

2. Stratton, J. A. <u>Electromagnetic Theory</u>, McGraw Hill, 1941.

3. Kennaugh, E. M. and R. L. Cosgriff. "The Use of Impulse Response in Electromagnetic Scattering Problems", 1958 IRE National Convention Record, pt. 1, pp. 72-77.

4. Kennaugh, E. M. and D. L. Moffatt. "Transient and Impulse Response Approximations", Proceedings of the IEEE, 53, 8, August 1965, pp. 893-901.

5. Kennaugh, E. M. and D. L. Moffatt. "The Axial Echo Area of a Perfectly Conducting Prolate Spheroid", IEEE Transactions on Antennas and Propagation, Vol. AP-13, pp. 401-409, May 1965.

6. (DELETED)

7. (DELETED)

8. Zadeh, L. A. and J. R. Ragazzini. "Optimum Filters for the Detection of Signals in Noise", Proceedings of the IRE, 40, 1123-1131.

9. Thomas, J. B. <u>An Introduction to Statistical Communication Theory</u>, Wiley, New York, 1969.

10. Lee, Y. W. <u>Statistical Theory of Communications</u>, Wiley, New York, 1960, pp. 303-312.

11. Skolnik, M. I. <u>Introduction to Radar Systems</u>, McGraw-Hill, New York, 1962, pp. 543-544.

12. Marshall, J. S. and W. Palmer. "Measurement of Rainfall by Radar", J. Met., 4, p. 186.

13. Skolnik, M. I. <u>Radar Handbook</u>, McGraw-Hill, New York, 1970, p. 24-21 and pp. 24-30 and 24-31.

14. Sebestyen, George Sr. <u>Decision Making Processes in Pattern Recognition</u>, Macmillan, 1962.